CHAPTER 1
Introduction to the Theory of Incompressible Inviscid Flows*

Thomas Y. Hou
Applied and Computational Mathematics, Caltech,
Pasadena, USA.
E-mail: hou@acm.caltech.edu

Xinwei Yu
Department of Mathematics, UCLA,
Los Angeles, USA.
E-mail: xinweiyu@math.ucla.edu

Abstract

In this chapter, we consider the 3D incompressible Euler equations. We present classical and recent results on the issue of global existence/finite-time singularity. We also introduce the theories of lower dimensional model equations of the 3D Euler equations and the vortex patch problem.

1 Introduction

The goal of these lecture notes is to introduce to the readers classical results as well as recent developments in the theory of 3D incompressible Euler equations. We will focus on the global existence/finite time singularity issue. We will start with the basic properties of the incompressible fluid flows, and then discuss the local and global well-posedness of the incompressible Euler equations. Of particular interest is the global existence or possible finite time blow-up of the 3D incompressible Euler equation. This is one of the most outstanding open problems in the past century. Here, we carefully examine the nature of the nonlinear vortex stretching term for the 3D Euler equation as well as several model problems for the 3D Euler equation. We put extra effort in taking into account the local geometrical properties and possible depletion of nonlinearity. By going through the nonlinear analysis of various fluid models,

*The first author is partly supported by a NSF grant DMS-0713670 and a FRG grant DMS-0353838. The second author is partly supported by a NSF grant DMS-0354488.

we can gain valuable insights into the fluid dynamic prolems being studied. Through the analysis, we can also learn how various functional analysis and PDE techniques are being used for realistic applications, and what are their strengths and limitations. We especially emphasize the interplay between the physical and geometric properties of the fluid flows and modern nonlinear PDE techniques. By going through these analyses systematically, we can have a good understanding of the state of the art of nonlinear PDE methods and their applications to fluid dynamics problems.

This chapter is organized as follows:

1. Introduction
2. Derivation and Exact Solutions
3. Local Well-posedness of the 3D Euler Equation
4. The BKM Blow-up Criterion
5. Recent Global Existence Results
6. Lower Dimensional Models for the 3D Euler Equation
7. Vortex Patch

2 Derivation and Exact Solutions

2.1 Derivation of the Euler Equations

The equation that governs the evolution of inviscid and incompressible flow is the Euler equation. Here we first derive the 3D Euler equation briefly. For more detailed derivations, the readers should consult other text books in fluid mechanics, such as Chorin-Marsden [12], Lamb [31], Marchioro-Pulvirenti [36], or Lopes Filho-Nussenzveig Lopes-Zheng [33].

We consider a domain Ω which is filled with a fluid, such as water. In classical continuum mechanics, the fluid can be seen as consisting of infinitesimal particles. At each time t, each particle has a one to one correspondence to the coordinates $x = (x_1, x_2, x_3) \in \Omega$. The fluid can be described by its density ρ, velocity $\mathbf{u} = (u_1, u_2, u_3)$ and pressure p at each such point $x \in \Omega$. Under the above assumptions, we can denote the position of any particle at time t by $X(\alpha, t)$ which starts at the position $\alpha \in \Omega$ at $t = 0$. Its evolution is governed by the following differential equation:

$$\begin{aligned} \frac{dX(\alpha,t)}{dt} &= \mathbf{u}(X(\alpha,t),t), \\ X(\alpha,0) &= \alpha. \end{aligned} \tag{2.1}$$

To study the dynamics of the fluid, we must establish relations between ρ, $\mathbf{u}$ and p. We do this by considering two basic mechanical rules: the conservation of mass, and the conservation of momentum.

The *conservation of mass* claims that, for any fixed region $W \subseteq \Omega$ which doesn't change with time,

$$\frac{d}{dt}\int_W \rho(x,t)\ dx = -\int_{\partial W} \rho(x,t)\mathbf{u}(x,t)\cdot\mathbf{n}(x,t)\ d\sigma \tag{2.2}$$

for all time t, where $\mathbf{n}(x,t)$ is the outer unit normal vector to ∂W, and $d\sigma$ is the area unit on ∂W. Using the Gauss theorem we arrive at

$$\frac{d}{dt}\int_W \rho(x,t)\ dx = -\int_W \nabla\cdot(\rho(x,t)\mathbf{u}(x,t))\ dx$$

which implies

$$\int_w (\rho_t + \nabla\cdot(\rho\mathbf{u}))\ dx = 0.$$

If we assume the continuity of the integrand $\rho_t + \nabla\cdot(\rho\mathbf{u})$, by the arbitrariness of W, we get

$$\rho_t + \nabla\cdot(\rho\mathbf{u}) = 0. \tag{2.3}$$

Since otherwise, there would be a point x_0 such that the integrand is not 0. Without loss of generality, we assume $(\rho_t + \nabla\cdot(\rho\mathbf{u}))(x_0) > 0$. Then by continuity, there is $r > 0$ such that $\rho_t + \nabla\cdot(\rho\mathbf{u}) > 0$ for any $x \in B(x_0, r)$. This leads to a contradiction by taking we take $W = B(x_0, r)$. Equation (2.3) is called the *continuity equation*.

Let J be the determinant of the Jacobian matrix, $\frac{\partial X}{\partial \alpha}$. It can ben proved by direct calculations (the reader should try to prove this as an exercise, see also Chorin-Marsden [12]) that

$$\frac{dJ}{dt} = (\nabla\cdot\mathbf{u})J, \quad J(0) = 1.$$

We assume that the flow is incompressible. Incompressibility implies that the flow is volume preserving. Using the above equation one can show that the velocity is divergence-free, i.e.

$$\nabla\cdot\mathbf{u} = 0 \tag{2.4}$$

In this case, we have the determinant of the Jacobian matrix, J, to be identically equal to one, i.e $J \equiv 1$. If the initial density is constant, i.e. $\rho(x,0) \equiv \rho_0$, equation (2.3) implies that density is constant globally, i.e.

$$\rho(x,t) \equiv \rho_0.$$

Remark 2.1. -

1. The above derivation of the mass conservation equation is under the assumption that ρ, $\mathbf{u}$ and ∂W are all smooth enough, e.g., C^1.
2. One can also derive (2.3) in a Lagrangian way, i.e., by considering an evolving region Ω_t that is a collection of particles. See e.g. Lopes Filho-Nussenzveig Lopes-Zheng [33].
3. Yet another way is through the variational formulation. See e.g. Marchioro-Pulvirenti [36].

The *conservation of momentum* means

$$\frac{d}{dt}\int_{\Omega_t} \rho\mathbf{u}\ dx = \mathbf{F}(\Omega_t)\ , \tag{2.5}$$

where $\mathbf{F}(\Omega_t)$ is the force acting on Ω_t. Here $\Omega_t \equiv \cup_{\alpha\in\Omega_0} X(\alpha,t)$ for some $\Omega_0 \subseteq \Omega$ is a collection of particles that is carried by the flow. We first assume that the interaction in the fluid is local, i.e., all the forces between points inside Ω_t cancel each other by Newton's third law. This assumption implies

$$\mathbf{F}(\Omega_t) = \int_{\partial\Omega_t} \mathbf{f}\ d\sigma$$

for some $\mathbf{f}$. Our second assumption is that the fluid is ideal, which means that $\mathbf{f} = -p\mathbf{n}$, where $\mathbf{n}$ is the unit outer normal to $\partial\Omega_t$. Now the momentum relation becomes

$$\frac{d}{dt}\int_{\Omega_t} \rho\mathbf{u}\ dx = \int_{\partial\Omega_t} -p\mathbf{n}\ d\sigma = -\int_{\Omega_t} \nabla p\ dx\ ,$$

where the second equality follows from the Gauss theorem

$$\int_{\Omega} \partial_i f\ dx = \int_{\partial\Omega} f n_i\ d\sigma.$$

To derive a pointwise equation similar to (2.3), we need to put the $\frac{d}{dt}$ inside the integration in the term

$$\frac{d}{dt}\int_{\Omega_t} \rho\mathbf{u}\ dx.$$

Note that since $\Omega_t = X(\Omega_0, t)$ depends on t, it is not the same as

$$\int_{\Omega_t} (\rho\mathbf{u})_t\ dx.$$

Instead of naïvely putting the differentiation inside, we proceed as follows. We first change variables from the Eulerian variable x to the Lagrangian variable α. Since the flow is incompressible, the determinant of the Jacobian matrix is equal to one, i.e., $det(X_\alpha) = 1$. Thus we have

$$\begin{aligned}
\frac{d}{dt}\int_{\Omega_t} \rho\mathbf{u}\, dx &= \frac{d}{dt}\int_{\Omega_0} \rho(X(\alpha,t),t)\mathbf{u}(X(\alpha,t),t)\, d\alpha \\
&= \int_{\Omega_0} \frac{d}{dt}\rho(X,t)\mathbf{u}(X,t) + \rho(X,t)\frac{d}{dt}\mathbf{u}(X,t)\, d\alpha \\
&= \int_{\Omega_0} (\rho_t + \mathbf{u}\cdot\nabla\rho)\,\mathbf{u} + \rho\,(\mathbf{u}_t + \mathbf{u}\cdot\nabla\mathbf{u})\, d\alpha \\
&= \int_{\Omega_0} \rho(\mathbf{u}_t + \mathbf{u}\cdot\nabla\mathbf{u})\, d\alpha \\
&= \int_{\Omega_t} \rho(\mathbf{u}_t + \mathbf{u}\cdot\nabla\mathbf{u})\, dx.
\end{aligned}$$

where the first equality follows from the fact that the flow map $\alpha \mapsto X(\alpha, t)$ is one-to-one and has Jacobian 1, and the fourth equality follows from (2.3) and the incompressibility condition. Now we have

$$\int_{\Omega_t} \rho(\mathbf{u}_t + \mathbf{u}\cdot\nabla\mathbf{u})\, dx = -\int_{\Omega_t} \nabla p\, dx.$$

Finally, by the arbitrariness of Ω_t, we get

$$\rho(\mathbf{u}_t + \mathbf{u}\cdot\nabla\mathbf{u}) = -\nabla p. \tag{2.6}$$

by an argument that is similar to the one leading to (2.3). (2.6) is the *balance of momentum*.

If we further assume that the flow has constant initial density, then we have $\rho(x,t) \equiv \rho_0$, and equation (2.6) is equivalent to:

$$\mathbf{u}_t + \mathbf{u}\cdot\nabla\mathbf{u} = -\nabla p$$

where p is the "rescaled" pressure p/ρ_0.

Under these assumptions, we obatin the 3D Euler equation as follows:

$$\begin{aligned}
\mathbf{u}_t + \mathbf{u}\cdot\nabla\mathbf{u} &= -\nabla p, \qquad (2.7)\\
\nabla\cdot\mathbf{u} &= 0.
\end{aligned}$$

In the remaining part of this lecture note, we will focus on (2.7).

2.2 The Vorticity-Stream function formulation

2.2.1 Vorticity

We consider the Taylor expansion of the velocity $\mathbf{u}(x,t)$ at some point x.

$$\begin{aligned}\mathbf{u}(x+h,t) &= \mathbf{u}(x,t) + \nabla\mathbf{u}\cdot h + O(h^2)\\ &= \mathbf{u}(x,t) + \frac{\nabla\mathbf{u}+\nabla\mathbf{u}^t}{2}h + \frac{\nabla\mathbf{u}-\nabla\mathbf{u}^t}{2}h + O(h^2)\\ &\equiv \mathbf{u}(x,t) + S(x,t)h + \Omega(x,t)h + O(h^2).\end{aligned}$$

where S is symmetric and Ω is anti-symmetric. In 3D, it's easy to see that there is a vector ω such that

$$\Omega(x,t)h = \frac{1}{2}\omega(x,t)\times h.$$

This implies that locally, the flow is rotating around an axis $\xi(x,t) \equiv \frac{\omega(x,t)}{|\omega(x,t)|}$. The vector field $\omega(x,t)$ is called "vorticity". And it is easy to check that

$$\omega(x,t) = \nabla\times\mathbf{u}(x,t).$$

2.2.2 Vorticity-Stream function formulation

By taking $\nabla\times$ on both sides of the 3D Euler equation (2.7), we have

$$\omega_t + \mathbf{u}\cdot\nabla\omega = \omega\cdot\nabla\mathbf{u} = S\cdot\omega. \tag{2.8}$$

which is the vorticity formulation. The last equality follows from the fact that

$$\Omega\cdot\omega = \frac{1}{2}\omega\times\omega\equiv 0,$$

since by definition we have

$$\frac{1}{2}\omega\times h \equiv \Omega\cdot h$$

for any vector h. Now there are two unknowns ω and $\mathbf{u}$, so we have to find the relation between them to close the system. This relation is the so-called Biot-Savart law.

$$\mathbf{u}(x) = \frac{1}{4\pi}\int_{\mathbb{R}^3}\frac{x-y}{|x-y|^3}\times\omega(y)\,dy. \tag{2.9}$$

Note that we need $u(x)$ to vanish at ∞ for the above formula to hold. To derive the Biot-Savart law, first define a vector valued function Ψ, called "stream function", such that

$$-\triangle\Psi = \omega.$$

Now it is easy to check that

$$\mathbf{u} = \nabla \times \Psi$$

satisfies

$$\nabla \times \mathbf{u} = \omega.$$

(Hint: Use the identity

$$-\nabla \times (\nabla \times) + \nabla(\nabla \cdot) = \triangle,$$

and then try to show

$$\|\nabla(\nabla \cdot \Psi)\|_{L^2}^2 = 0$$

using the same identity. Details are left as exercises. Or see Bertozzi-Majda [35]).

Now the Biot-Savart law (2.9) follows from the formula

$$\Psi = \frac{1}{4\pi} \int \frac{1}{|x-y|} \omega(y)\, dy,$$

where $\frac{1}{4\pi}\frac{1}{|x|}$ is the fundamental solution for the Poisson equation

$$-\triangle u = f$$

in 3D.

Besides (2.8), another important form of the vorticity evolution is the "stretching formula".

$$\omega(X(\alpha,t),t) = \nabla_\alpha X(\alpha,t)\omega_0(\alpha) \tag{2.10}$$

where $\omega_0(\alpha) = \omega(X(\alpha,0),0) = \omega(\alpha,0)$, and X is defined by (2.1). To prove it, just differentiate both sides with respect to time, which yields

$$\begin{aligned} \omega_t + \mathbf{u} \cdot \nabla\omega &= \nabla_\alpha \mathbf{u}(X(\alpha,t),t)\omega_0(\alpha) \\ &= \nabla\mathbf{u} \cdot (\nabla_\alpha X \cdot \omega_0) \\ &= \nabla\mathbf{u} \cdot \omega(x,t), \end{aligned}$$

which is just (2.8). One catch: this "proof" actually uses the uniqueness of the solution to the system (2.8), (2.9).

For the convenience of future references, we will denote the differentiation in time along the Lagrangian trajectory as $\frac{D}{Dt}$, which has the property:

$$\frac{D}{Dt} w = w_t + \mathbf{u} \cdot \nabla w.$$

$\frac{D}{Dt}$ is also called material derivative.

2.2.3 2D Euler equations

In some physical cases, such as the flow passing around a cylinder with infinite length, we can assume that $u_3 \equiv 0$ and $\mathbf{u}, p$ depend on x_1, x_2 only. In this case, the Euler equations (2.7) remains the same form, but the vorticity-stream function form reduces to

$$\omega_t + \mathbf{u} \cdot \nabla \omega = 0 \tag{2.11}$$

and

$$\mathbf{u}(x) = \frac{1}{2\pi} \int \frac{(x-y)^{\perp}}{|x-y|^2} \omega(y)\ dy \tag{2.12}$$

where ω is a short-hand for ω_3.

One important difference between 2D and 3D Euler equations is that, the right hand side is 0 in (2.11), which means the vorticity is conserved along Lagrangian trajectory pathes. This point can be illustrated more clearly by looking at the "stretching formula" in 2D, which is

$$\omega(X(\alpha, t), t) = \omega_0(\alpha). \tag{2.13}$$

This difference plays an important role in the theory of 2D Euler equations, which is far more complete than its 3D counterpart.

2.3 Conserved Quantities

2.3.1 Local conserved quantities

First we consider those quantities that are carried by a collection of flow particles.

Let C_0 be a closed curve in $\mathbb{R}^3$. We define

$$C_t = \cup_{\alpha \in C_0} X(\alpha, t).$$

and the circulation

$$\Gamma_{C_t} \equiv \oint_{C_t} \mathbf{u} \cdot ds.$$

Theorem 2.2. *(Kelvin's Circulation Theorem).* $\Gamma_{C_t} \equiv \Gamma_{C_0}$.

Proof. We first prove the following.

$$\frac{d}{dt} \int_{C_t} \mathbf{u} \cdot ds = \int_{C_t} \frac{D\mathbf{u}}{Dt} \cdot ds.$$

To prove it, let $\alpha(\beta)$ be a parametrization of the loop C_0, with $0 \le \beta \le 1$. Then C_t is parametrized as $X(\alpha(\beta), t)$. Thus

$$\begin{aligned}\frac{d}{dt}\int_{C_t} \mathbf{u}\cdot ds &= \frac{d}{dt}\int_0^1 \mathbf{u}(X(\alpha(\beta),t),t)\cdot \frac{\partial}{\partial\beta}X(\alpha(\beta),t)\ d\beta \\ &= \int_0^1 \frac{D\mathbf{u}}{Dt}(X(\alpha(\beta),t),t)\cdot \frac{\partial}{\partial\beta}X(\alpha(\beta),t)\ d\beta \\ &\quad + \int_0^1 \mathbf{u}(X(\alpha(\beta),t),t)\cdot \frac{\partial}{\partial\beta}\mathbf{u}(X(\alpha(\beta),t),t)\ d\beta\end{aligned}$$

where we have used the relation

$$\frac{\partial X}{\partial t}(\alpha,t) = \mathbf{u}(X(\alpha,t),t).$$

Note that the first term is just

$$\int_{C_t} \frac{D\mathbf{u}}{Dt}\cdot ds,$$

we just need to show that the second term is 0. This is easy, since we have

$$\int_0^1 \mathbf{u}\cdot\frac{\partial}{\partial\beta}\mathbf{u}\ ds = \frac{1}{2}\int_0^1 \frac{\partial}{\partial\beta}(\mathbf{u}\cdot\mathbf{u})\ \ ds = 0,$$

which follows from the fact that C_t is a close loop.

Now we prove the circulation theorem. We have

$$\frac{d}{dt}\int_{C_t} \mathbf{u}\cdot ds = \int_{C_t}\frac{D\mathbf{u}}{Dt}\cdot ds = -\int_{C_t}\nabla p\cdot ds = -\int_{C_t} p_s ds = 0$$

since C_t is closed. Thus ends the proof. □

Next let C_0 be a general curve and $C_t = X(C_0, t)$. Then as long as the flow is still regular, C_t is still a curve in $\mathbb{R}^3$. C_t is called a vortex line if the following is satisfied

$$C_0 \text{ is tangent to } \omega_0(\alpha) \text{ at any } \alpha \in C_0. \qquad (2.14)$$

One can verify that as long as (2.14) is satisfied, the same tangency condition is satisfied at every moment t, i.e.,

$$C_t \text{ is tangent to } \omega(x,t) \text{ at any } x \in C_t.$$

A collection of vortex lines is called a "vortex tube". One readily sees that vorticity is always tangent to the side surface of a vortex tube.

The above properties make vortex tube/line very important objects in the theories/numerical simulations/physical experiments of the 3D Euler equation, as we will reveal later in this lecture note.

2.3.2 Global conserved quantities

The most well-known global conserved quantities are the following (we will indicate the dimension and region/manifold, $\mathbb{T}^d$ stands for d-dimensional periodic torus):

1. The integral of velocity. ($\mathbb{R}^d$ and $\mathbb{T}^d$, $d = 2, 3$).

$$\frac{d}{dt}\int \mathbf{u}\ dx = 0.$$

2. Kinetic energy. ($\mathbb{R}^d$, $\mathbb{T}^d$, smooth bounded domain, $d = 2, 3$).

$$\frac{d}{dt}\int |\mathbf{u}|^2\ dx = 0.$$

Remark 2.3. In the $\mathbb{R}^d$ case, caution must be taken. We actually need that the kinetic energy $\int |\mathbf{u}|^2\ dx$ to be finite. In 3D this requirement is reasonable, while in 2D it is not.

3. Center of vorticity. ($\mathbb{R}^2$, if $\mathbf{u}\omega$ decays fast enough at ∞).

$$\bar{x} = \int_{\mathbb{R}^2} x\omega\ dx = \text{const.}$$

4. Moment of inertia. ($\mathbb{R}^2$, if $\mathbf{u}\omega$ decays fast enough at ∞).

$$I = \int_{\mathbb{R}^2} |x|^2\,\omega\ dx = \text{const.}$$

5. Functions of vorticity. ($d = 2$).

$$\int_{\Omega_t} f(\omega)\ dx = \int_{\Omega_0} f(\omega_0)\ d\alpha$$

for any measurable f and material domain Ω_t. In particular, we see that the L^p norm of ω is conserved for $1 \le p \le \infty$.

6. Other quantities.

$$\int_{\mathbb{R}^3} x \times \omega\ dx$$

$$\int_{\mathbb{R}^3} x \times (x \times \omega)\ dx;$$

helicity

$$\int_{\mathbb{R}^3} \mathbf{u}\cdot\omega\ dx;$$

and spirality

$$\omega\cdot\gamma$$

where $\gamma = \mathbf{u} + \nabla\phi$ with ϕ solving

$$\frac{D}{Dt}\phi = -|\mathbf{u}|^2/2 + p.$$

This quantity is conserved along particle trajectories.

2.4 Special Flows

2.4.1 Axisymmetric Flow

In this subsection we introduce the axisymmetric flow, i.e., when written in cylindrical coordinates $x_1 = r\cos\theta$, $x_2 = r\sin\theta$ and $x_3 = z$, the velocity u and the pressure p depend only on r and z. Unlike the 2D Euler equations, this particular flow retains some 3D characters and is often referred to as the $2\frac{1}{2}$-D equations.

We introduce the cylindrical frame of reference:

$$\begin{aligned} e_r &= (\cos\theta, \sin\theta, 0) \\ e_\theta &= (-\sin\theta, \cos\theta, 0) \\ e_z &= (0, 0, 1). \end{aligned}$$

and can easily rewrite the 3D Euler equations in the new frame, with $\mathbf{u} = \mathbf{u}(r, z)$ and $p = p(r, z)$, as

$$\mathbf{u}_t + (\mathbf{u}\cdot\tilde{\nabla})\mathbf{u} + B = -\tilde{\nabla}p \tag{2.15}$$

where

$$\tilde{\nabla} = (\partial_r, 0, \partial_z)$$

and

$$B = \frac{u^\theta}{r}(-u^\theta, u^r, 0).$$

We leave the details (which can be found in e.g. Lopes Filho-Nussenzveig Lopes-Zheng [33]) for this system to the reader as exercises.

1. Derive equations (2.15).
2. Prove that, in the moving frame (e_r, e_θ, e_z), we have

$$\begin{aligned} \omega &= \omega^r e_r + \omega^\theta e_\theta + \omega^z e_z \\ &\equiv \left(-\partial_z u^\theta\right) e_r + \left(\partial_z u^r - \partial_r u^z\right) e_\theta + \left(\partial_r u^\theta + \frac{u^\theta}{r}\right) e_z. \end{aligned}$$

3. When $u^\theta \equiv 0$, (2.15) becomes axisymmetric flows without swirl. Prove that the equations are

$$\begin{aligned} \left(\partial_t + \mathbf{u}\cdot\tilde{\nabla}\right)\mathbf{u} &= -\tilde{\nabla}p \\ \tilde{\nabla}\cdot(r\mathbf{u}) &= 0 \end{aligned} \tag{2.16}$$

Furthermore, one can reduce the equation into the $r-z$ plane which is 2D. Prove that the equation for ω^θ (note that $\omega^r = \omega^z = 0$) is

$$(\partial_t + \mathbf{u} \cdot \nabla) \left(\frac{\omega^\theta}{r} \right) = 0.$$

2.4.2 Radially (circularly) symmetric flow

In the 2D case. We consider $\omega_0 \equiv \omega_0(r)$ which is circularly symmetric. Then by exploring the invariance of the Laplacian we easily see that ψ defined by

$$-\triangle \psi = \omega_0$$

is also a circularly symmetric function. Thus

$$\mathbf{u} = \nabla^\perp \psi$$

is always tangent to the contours $\omega_0 \equiv$const. One can easily verify that

$$\omega \equiv \omega_0, \mathbf{u} \equiv \mathbf{u}_0$$

is a steady solution for the 2D Euler equations. The velocity is explicitly given as

$$\mathbf{u} = \frac{x^\perp}{r^2} \int_0^r s\omega(s)\ ds, \tag{2.17}$$

where $r = |x|$. These stationary solutions are called Rankine vortices. The reader can try to derive the "radial_symmetric_biot_savart law" (2.17) as an exercise (Hint: it is easier to start from the stream function Ψ).

Now consider the special case, where ω_0 is supported in $B_R \equiv \{x \mid |x| \leq R\}$, with $\int_{B_R} \omega_0 = 0$. Then it is easy to see that $\mathbf{u}$ is also supported in B_R. Such a vortex is called a confined eddy. The importance of this observation can be seen from the following property:

The superposition of two disjoint confined eddies is still a solution.

This gives us a way to construct very complicated exact solutions to the 2D Euler equations.

2.4.3 Jets and Strains

Let $D(t)$ be any family of symmetric and trace-free matrices that smoothly depends on t, and let ω solves

$$\frac{d\omega}{dt} = D(t)\omega$$
$$\omega(0) = \omega_0.$$

We introduce

$$\mathbf{u} = \frac{1}{2}\omega \times x + D(t)x.$$

It is easy to check that we can define p such that $\mathbf{u}$ solves the 3D Euler equations in the whole space. One thing that worths noting is that, the velocity we defined above is growing unboundedly at ∞ and is thus non-physical.

It is illustrating to study some special cases.

1. Jet. Take $\omega_0 = 0$ thus $\omega \equiv 0$. Note that we can write $D(t)$ to be diagonal:

$$D(t) = \begin{bmatrix} -\gamma_1 & 0 & 0 \\ 0 & -\gamma_2 & 0 \\ 0 & 0 & \gamma_1 + \gamma_2 \end{bmatrix}$$

   and get

$$\mathbf{u} = (-\gamma_1 x_1, -\gamma_2 x_2, (\gamma_1 + \gamma_2)x_3).$$

2. Swirling jet. We take $\omega_0 = (0, 0, a)$ and get

$$\omega = (0, 0, ae^{(\gamma_1+\gamma_2)t}),$$

   and

$$\mathbf{u} = \left(-\gamma_1 x_1 - \frac{1}{2}a(t)x_2, -\gamma_2 x_2 + \frac{1}{2}a(t)x_1, (\gamma_1 + \gamma_2)\, x_3\right).$$

3. Strain. We take $\omega_0 = 0$ and $\gamma_1 = -\gamma_2 = \gamma$.

$$\mathbf{u} = (-\gamma x_1, \gamma x_2, 0)\,.$$

3 Local Well-Posedness of the 3D Euler Equation

First we consider the local well-posedness for classical solutions. By classical solutions we mean solutions such that (2.7) holds in the classical sense, i.e., all the derivatives are in the classical sense, the multiplications are pointwise, and the equalities hold everywhere. Our main goal in this section is to prove the following:

Theorem 3.1. *If the initial velocity* $\mathbf{u}_0 \in H^m \cap C^2$ *for some* $m > 2 + d/2$, *then there is* $T > 0$ *such that there is a unique solution* $\mathbf{u} \in H^m \cap C^2$ *in* $[0, T]$.

To do this, we use the standard technique of mollifiers. In short, we approximate (2.7) by a sequence of equations that can be shown to admit global smooth solutions, and then establish the local in time existence by taking limit.

3.1 Analytical preparations

3.1.1 Sobolev spaces

The Sobolev spaces $H^k, k \in \mathbb{Z}, k \geq 0$ is defined as

$$H^k(\mathbb{R}^d) = \left\{ f(x) \mid \sum_{|\alpha| \leq k} \|\partial^\alpha f\|_{L^2}^2 < \infty \right\}$$

where α is a multi-index $\alpha = (\alpha_1, \alpha_2, \ldots, \alpha_d)$. $|\alpha| \equiv \sum \alpha_i$ and $\partial^\alpha \equiv \frac{\partial^{|\alpha|}}{\partial x_1^{\alpha_1} \cdots \partial x_d^{\alpha_d}}$. H^k is a Banach space with norm

$$\|f\|_{H^k} = \left(\sum_{|\alpha| \leq k} \|\partial^\alpha f\|_{L^2}^2 \right)^{1/2} .$$

If we consider the Fourier transform of f, we have

$$\|f\|_{H^k} = \left(\sum_{|\alpha| \leq k} \left\| \xi^\alpha \hat{f} \right\|_{L^2}^2 \right)^{1/2}$$

where $\xi^\alpha \equiv \xi_1^{\alpha_1} \cdots \xi_d^{\alpha_d}$. Now by some simple algebra we can obtain the following equivalent norm

$$\|f\|_{H^k} \sim \left\| \langle \xi \rangle^k \hat{f} \right\|_{L^2} \sim \left\| (1 - \triangle)^{k/2} f \right\|_{L^2}$$

where $\langle \xi \rangle \equiv (1 + |\xi|^2)^{1/2}$, and $\triangle$ is the Laplacian.

The point in writing the H^k norm this way is that, now we can take k to be any real number instead of non-negative integers. Usually, when k is not an integer, we replace it by s.

The following theorem is used extensively in PDE researches.

Theorem 3.2. *The space $C_0^\infty(\mathbb{R}^d)$ is dense in $H^s(\mathbb{R}^d)$.*

The most important property of the Sobolev spaces is the embedding theorems. We will not prove these theorems here, interested readers can look up the proof in e.g. Adams [1], which is a classic and not very hard to read.

Before introducing the theorems, we first recall what "embedding" means. Consider two Banach spaces X and Y, with norms $\|\cdot\|_X$ and $\|\cdot\|_Y$. Assume that there is a third space Z which is dense in both X and Y. We say X is embedded in Y, if there is a constant C such that

$$\|\cdot\|_Y \leq C \|\cdot\|_X .$$

This means that all the elements in X is also in Y. Furthermore, we say X is compactly embedded in Y, if X is embedded in Y, and any bounded subset of X (in the X norm) is precompact in Y (with respect to the Y norm). That is, if $\{x_n\} \subset X$ is uniformly bounded, then there is a subsequence which is Cauchy in Y. We denote embedding by $\hookrightarrow$.

Theorem 3.3. *(Embeddings for H^s). Let $H^s(\mathbb{R}^d)$ be the Sobolev space. We have*

$$H^{s+k} \hookrightarrow C^k$$

for all $s > d/2$ and $k \in \mathbb{Z}$, nonnegative.

3.1.2 Hodge decomposition and the Leray projection

We denote by $H^s(\mathbb{R}^d)$ the Sobolev spaces, and let $V^s \subset H^s(\mathbb{R}^d; \mathbb{R}^d)$ be the subspace of divergence-free vector fields.

Lemma 3.4. *(Hodge decomposition). Let $\mathbf{u}$ be a vector field with components in $L^2(\mathbb{R}^d)$. There exists a unique decomposition $\mathbf{u} = \mathbf{u}_1 + \mathbf{u}_2$, where $\mathbf{u}_1$ is divergence-free and $\mathbf{u}_2$ is a gradient. Furthermore $\mathbf{u}_1$ and $\mathbf{u}_2$ are orthogonal in L^2. We denote by P the projection $L^2(\mathbb{R}^d; \mathbb{R}^d) \mapsto V^0$ which maps $\mathbf{u}$ to $\mathbf{u}_1$, then P commutes with derivatives, convolution and is also a map from H^s to V^s.*

Proof. First we solve

$$\triangle \phi = \nabla \cdot \mathbf{u}$$

Thus

$$\phi = \triangle^{-1}(\nabla \cdot \mathbf{u}) + H$$

where H is a harmonic function and $\triangle^{-1}$ is the convolution with the Green's function of the Laplacian in $\mathbb{R}^d$. Now define

$$\mathbf{u}_2 = \nabla \phi = (\nabla^2 \triangle^{-1}) \cdot \mathbf{u} + \nabla H$$

By going to the Fourier space, it is easy to see that the first term is in L^2. To make $\mathbf{u}_2 \in L^2$, we must have $\nabla H \in L^2$, which means it must vanish at ∞. But since each entry of ∇H is harmonic, we see that this implies that $\nabla H \equiv 0$.

Now we have

$$P = \left(I - \nabla^2 \triangle^{-1}\right) \cdot . \tag{3.1}$$

It is easy to check the commutativity properties. □

This operator P is often referred to as the *Leray projection operator*.

3.1.3 The Aubin-Lions Lemma

For evolution PDEs, generally one can not treat time and space as equal, so one need compactness results that has different requirement in space and time. A standard result is the Aubin-Lions lemma.

First we prove a technical lemma. Let $X \hookrightarrow Y \hookrightarrow Z$ be Banach spaces that have embedding relations as indicated. Recall that $X \hookrightarrow Y$ is compact means that for any $\{f_n\}$ that is uniformly bounded in X, there is a subsequence that is convergent in the norm of Y.

Lemma 3.5. *Assume that $X \hookrightarrow Y$ is compact. then for every $\eta > 0$ there exists a constant $C_\eta > 0$ such that*

$$\|v\|_Y \le \eta \|v\|_X + C_\eta \|v\|_Z$$

for every $v \in X$.

Proof. The proof is standard. We prove by contradiction. Assume there is a $\eta > 0$ and a sequence $\{v^n\} \subset X$ such that

$$\|v^n\|_Y > \eta \|v^n\|_X + n \|v^n\|_Z ,$$

then by taking $w^n \equiv v^n / \|v^n\|_X$ we see that the same inequality holds for w^n. Now w^n is bounded in X, which means there is a subsequence, still denote as w^n, such that

$$w^n \to w \in Y$$

in Y. Note that $\|w^n\|_Y \le C\|w^n\|_X \le C$ by the embedding assumption and the fact that $\|w^n\|_X = 1$. Now divide both sides of the equation for w^n by n, we have

$$w^n \to 0 \text{ in } Z.$$

But on the other hand, we have

$$w^n \to w \neq 0$$

in Y and thus we have a contradiction, since the embedding, convergence in Y to some limit implies convergence in Z to the same limit. □

Lemma 3.6. *(Aubin-Lions). Suppose that $X \hookrightarrow Y$ is compact. Let $T > 0$. Let $\{u^n\}$ be a bounded sequence in $L^\infty([0,T];X)$. Suppose this sequence is equicontinuous as Z-valued functions defined on $[0,T]$. Then the same sequence is precompact in $C([0,T];Y)$.*

Proof. First, it follows directly from Lemma 3.5 that each u^n is in $C([0,T];Y)$. Second, by the conditions in the Lemma we see that we can use the Arzela-Ascoli lemma on $C([0,T];Z)$ and see that u^n is precompact in it. Finally, still by Lemma 3.5 we see that u^n is precompact in $C([0,T],Y)$. □

Remark 3.7. A comparison with the Arzela-Ascoli lemma in analysis is helpful. There we basically have a sequence that is uniformly bounded and equicontinuous in $C\left([0,T],Y\right)$ for some Y. Here the boundedness condition, which is usually easier to establish, is strengthened, while the harder condition equicontinuity is weakened.

3.1.4 Calculus Inequalities

Let u and v be in $H^m(\mathbb{R}^d)$ with $m \in \mathbb{N}$.

Lemma 3.8. -

1. *If u and v are bounded and continuous then there exists a constant $C > 0$ such that*

$$\|uv\|_{H^m} \leq C\left(\|u\|_{L^\infty}\|D^m v\|_{L^2} + \|v\|_{L^\infty}\|D^m u\|_{L^2}\right).$$

2. *If u, v and ∇u are bounded and continuous then there exists a constant $C > 0$ such that*

$$\sum_{0\leq|\alpha|\leq m}\|D^\alpha(uv) - uD^\alpha v\|_{L^2} \leq C\left(\|\nabla u\|_{L^\infty}\left\|D^{m-1}v\right\|_{L^2} + \|v\|_{L^\infty}\|D^m u\|_{L^2}\right).$$

Proof. First we prove 1. It is enough to prove that

$$\left\|D^\alpha u D^\beta v\right\|_{L^2} \leq C\left(\|u\|_{L^\infty}\|D^m v\|_{L^2} + \|v\|_{L^\infty}\|D^m u\|_{L^2}\right)$$

where in the RHS (right hand side) we actually define

$$\|D^m v\|^2_{L^2} = \sum_{|\alpha|=m}\|D^\alpha v\|^2_{L^2},$$

while in the LHS (left hand side) α, β are multi-indices with $|\alpha|+|\beta| = m$.

We illustrate the idea of the proof by considering the scalar case. We estimate

$$\|u'v'\|_{L^2} = \left(\int\left(u'v'\right)^2\,dx\right)^{1/2}$$

where $\alpha = \beta = 1$ and $m = 2$. By Hölder's inequality, we have

$$\|u'v'\|_{L^2} \leq \|u'\|_{L^4}\|v'\|_{L^4}.$$

Next we establish the Gagliardo-Nirenberg inequality

$$\left\|D^i u\right\|_{L^{2r/i}} \leq c_r\|u\|^{1-i/r}_{L^\infty}\|D^r u\|^{i/r}_0$$

with $0 \leq i \leq r$. In our case, $i = 1, r = 2$, the Gagliardo-Nirenberg inequality reduces to

$$\|u'\|_{L^4} \leq c\|u\|^{1/2}_{L^\infty}\|u''\|^{1/2}_0. \tag{3.2}$$

The proof is easy. We have

$$\begin{aligned}
\|u'\|_{L^4}^4 &= \int (u')^4 \; dx \\
&= \int (u')^3 \; du \\
&\leq c \left| \int u \, (u')^2 \, u'' \; dx \right| \\
&\leq c \left| \int u^2 \, (u'')^2 \; dx \right|^{1/2} \left| \int (u')^4 \; dx \right|^{1/2} \\
&\leq c \, \|u\|_{L^\infty} \, \|u''\|_{L^2} \, \|u'\|_{L^4}^2 \, .
\end{aligned}$$

which proves (3.2).

Now we have

$$\|u'v'\|_{L^2} \leq c \, \|u\|_{L^\infty}^{1/2} \, \|u''\|_{L^2}^{1/2} \, \|v\|_{L^\infty}^{1/2} \, \|v''\|_{L^2}^{1/2} \, .$$

By using Young's inequality

$$ab \leq \frac{a^p}{p} + \frac{b^q}{q}$$

where $p, q > 0$ with $\frac{1}{p} + \frac{1}{q} = 1$ we finish the proof.

The general cases of 1 and 2 are left as exercises. □

3.1.5 Gronwall's inequality

In dealing with evolution equations, we need to estimate various quantities. In doing so we often end up with inequalities like

$$X(t) \leq a(t) + \int_0^t b(s) X(s) \; ds$$

where $X(t)$ is the non-negative quantity we need to estimate, and $a(t), b(t) \geq 0$ with $a(t)$ differentiable. The trick in getting an estimate for X is the following. We also assume that everything is continuous.

Fix $\varepsilon > 0$, let $Y^\varepsilon(t)$ satisfy

$$Y^\varepsilon(t) = a(t) + \varepsilon + \int_0^t b(s) Y^\varepsilon(s) \; ds,$$

then it is easy to see that $Y^\varepsilon(t)$ is differentiable, and satisfies

$$\begin{aligned}
\left(Y^\varepsilon\right)'(t) &= a'(t) + b(t) Y^\varepsilon(t) \\
Y^\varepsilon(0) &= a(0) + \varepsilon
\end{aligned}$$

which gives

$$Y^\varepsilon(t) = (a(0)+\varepsilon)\, e^{\int_0^t b(s)\ ds} + \int_0^t a'(s) e^{\int_s^t b(\tau)\ d\tau}\ ds.$$

Now by arbitrariness of ε we get what we need, as long as we have

$$X(t) \le Y^\varepsilon(t)$$

for any $\varepsilon > 0$. To show this, consider $W \equiv Y^\varepsilon - X$, which satisfies

$$\begin{aligned} &W(t) \ge \varepsilon + \int_0^t b(s)W(s)\ ds \\ &W(0) = \varepsilon > 0. \end{aligned}$$

By the continuity of W and the condition $b(s) \ge 0$ it is easy to see that $W(t) \ge \varepsilon$ for all $t > 0$. Thus we proved the following lemma.

Lemma 3.9. *(Grönwall's lemma.) If $X(t), a(t), b(t) \ge 0$ are continuous, $a(t)$ differentiable, with*

$$X(t) \le a(t) + \int_0^t b(s)X(s)\ ds,$$

then we can estimate $X(t)$ by

$$X(t) \le a(0)e^{\int_0^t b(s)\ ds} + \int_0^t a'(s)e^{\int_s^t b(\tau)\ d\tau}\ ds.$$

3.2 Properties of mollifiers

Definition 3.10. Let $\rho \in C_0^\infty(\mathbb{R}^d)$ be any radial function, i.e., $\rho(x)$ depends only on $|x|$. We choose $\rho \ge 0$ with $\int_{\mathbb{R}^d} \rho\ dx = 1$. For any $\varepsilon > 0$, define

$$\rho_\varepsilon(x) = \varepsilon^{-d}\rho(x/\varepsilon).$$

Then we call the family $\{\rho_\varepsilon\}$ a family of mollifiers.

In the following, we will denote

$$M^\varepsilon f = (\rho_\varepsilon * f)(x).$$

for any function f.

Next we develop some main properties of the mollification operator M^ε.

Lemma 3.11. *. For any function f such that $M^\varepsilon f$ is well-defined, we have*

1. *$M^\varepsilon f$ is smooth, i.e., C^∞.*
2. *For all $f \in C^0(\mathbb{R}^d)$, we have $M^\varepsilon f \to f$ uniformly on any compact set Ω, and*
$$\|M^\varepsilon f\|_{L^\infty} \le \|f\|_{L^\infty}.$$
3. *$M^\varepsilon D^\alpha = D^\alpha M^\varepsilon$ for any multi-index α.*
4. *For all $f \in L^p$, $g \in L^q$ with $1/p + 1/q = 1$,*
$$\int_{\mathbb{R}^d} (M^\varepsilon f)\, g \, dx = \int_{\mathbb{R}^d} f \,(M^\varepsilon g)\, dx.$$
5. *For all $f \in H^s(\mathbb{R}^d)$, $M^\varepsilon f$ converges to f in H^s and the rate of convergence in the H^{s-1} norm is $O(\varepsilon)$.*
6. *For all $f \in H^s(\mathbb{R}^d)$, $k \in \mathbb{Z}^+ \cup \{0\}$, and $\varepsilon > 0$, we have*
$$\|M^\varepsilon f\|_{s+k} \le \frac{c_{sk}}{\varepsilon^k} \|f\|_s\,,$$
$$\left\|M^\varepsilon D^k f\right\|_{L^\infty} \le \frac{c_k}{\varepsilon^{d/2+k}} \|f\|_{L^2}\,.$$

Proof. 1–4 are easy and omitted. Interested readers can try to prove them or check Bertozzi-Majda [35]. To prove 5 and 6, it is important to know the representation of M^ε in the Fourier space:

$$\widehat{M^\varepsilon f}(\xi) = \hat{\rho}(\varepsilon\xi) f(\xi).$$

Note that by construction

$$\hat{\rho}(0) = \int \rho \, dx = 1.$$

As $\varepsilon \to 0$, for any ξ, we have

$$\hat{\rho}(\varepsilon\xi) \sim 1 + O(\varepsilon).$$

It is clear now that why we can expect $M^\varepsilon f \to f$ at all.

Another key factor in proving 5 and 6 is the Fourier side characterization of $H^s(\mathbb{R}^d)$. Recall that

$$\left|\widehat{\nabla f}(\xi)\right| = c\,|\xi| \left|\hat{f}(\xi)\right|$$

where c depends on the definition of Fourier transforms, e.g., if we define

$$\hat{f}(\xi) = \int e^{-i\xi\cdot x} f(x) \, dx$$

then $c = 1$. The particular value of c is not important here. In the following, we will just take $c = 1$. Now $f \in H^s$ is equivalent to

$$\langle \xi \rangle^s \hat{f}(\xi) \in L^2$$

where $\langle \xi \rangle \equiv \left(1 + |\xi|^2\right)^{1/2}$.

With the above understanding, 5 and 6 are easy to prove. For example, we prove the second estimate in 6. For any multi-index α with $|\alpha| = k$, we have

$$\begin{aligned}
|(M^\varepsilon D^\alpha f)(x)| &= c \left| \int e^{i\xi\cdot x} \hat{\rho}(\varepsilon\xi) \xi^\alpha \hat{f}(\xi) \, d\xi \right| \\
&\le c \int_{\mathbb{R}^d} |\hat{\rho}(\varepsilon\xi)| \, |\xi|^k \left| \hat{f}(\xi) \right| \, d\xi \\
&\lesssim \|f\|_{L^2} \left(\int_{\mathbb{R}^d} |\hat{\rho}(\varepsilon\xi)|^2 \, |\xi|^{2k} \, d\xi \right)^{1/2} \\
&= \|f\|_{L^2} \left(\int_{\mathbb{R}^d} |\hat{\rho}(\eta)|^2 \, |\eta|^{2k} \, d\eta \right)^{1/2} \varepsilon^{-k-d/2} \\
&\lesssim \varepsilon^{-k-d/2} \|f\|_{L^2}
\end{aligned}$$

where $\eta \equiv \varepsilon\xi$ and note that the integration is over $\mathbb{R}^d$, thus the factor $\varepsilon^{-d/2}$. The integral on $\hat{\rho}$ is bounded since $\rho \in C_0^\infty \subset H^k$ is a fixed function.

The other inequalities in 5 and 6 can be proved similarly and are left to the readers. □

3.3 Global existence of the mollified equation

We consider the mollified equations:

$$\begin{aligned}
\partial_t u^\varepsilon + M^\varepsilon \left(\left((M^\varepsilon u^\varepsilon) \cdot \nabla \right) (M^\varepsilon u^\varepsilon) \right) &= -\nabla p^\varepsilon \\
\nabla \cdot u^\varepsilon &= 0 \\
u^\varepsilon(x, 0) &= u_0(x).
\end{aligned} \tag{3.3}$$

or, by using the Leray projection operator,

$$\begin{aligned}
\partial_t u^\varepsilon + P \left(M^\varepsilon \left(\left((M^\varepsilon u^\varepsilon) \cdot \nabla \right) (M^\varepsilon u^\varepsilon) \right) \right) &= 0, \\
P u^\varepsilon &= u^\varepsilon, \\
u^\varepsilon(x, 0) &= u_0(x).
\end{aligned} \tag{3.4}$$

where u^ε denotes the solution and is not necessarily of the form $M^\varepsilon v$ for some v. We will prove the global existence (i.e., for all time $t \in \mathbb{R}^+$) of the mollified 3D Euler equations. Our strategy is to prove local existence by treating (3.4) as an ODE in some Banach space, and then extend the existence time to ∞. In the following of this section, we will omit the superscipt ε and denote u^ε by u.

Lemma 3.12. *Let $m \in \mathbb{N}$. Then for every $u_0 \in V^m$ and $\varepsilon > 0$ there exists $T^\varepsilon > 0$ and a solution $u^\varepsilon \in C^1([0, T^\varepsilon); V^m)$ to the problem (3.4), or equivalently, (3.3).*

Proof. Let

$$F_\varepsilon(u) = -P\left(M^\varepsilon\left(\left(\left(M^\varepsilon u\right)\cdot\nabla\right)\left(M^\varepsilon u\right)\right)\right).$$

Then (3.4) becomes

$$\frac{du^\varepsilon}{dt} = F_\varepsilon(u^\varepsilon).$$

which is an ODE in a Banach space. The only thing we need to check before applying the Picard iteration to get local in time existence is that

1. $F_\varepsilon : V^m \mapsto V^m$, and
2. F_ε is locally Lipschitz in V^m.

For the first claim, we have the following estimate:

$$\begin{aligned}
\|F_\varepsilon(u)\|_{H^m} &\le \|M^\varepsilon\left(\left(\left(M^\varepsilon u\right)\cdot\nabla\right)\left(M^\varepsilon u\right)\right)\|_{H^m} \\
&\le C\|M^\varepsilon\left(\nabla\cdot\left(M^\varepsilon u\otimes M^\varepsilon u\right)\right)\|_{H^m} \\
&\le \frac{C}{\varepsilon}\|M^\varepsilon u\otimes M^\varepsilon u\|_{H^m} \\
&\le \frac{C}{\varepsilon^{3/2}}\|u\|_{H^m}^2
\end{aligned}$$

where we have used the calculus inequalities (see Lemma 2.1.8) and the following properties of the mollifiers: $\|M^\varepsilon Df\|_{H^m} \le C\|f\|_{H^m}/\varepsilon$, $\|M^\varepsilon u\|_{L^\infty} \le C\|u\|_{H^m}/\varepsilon^{d/2}$, which follows from Lemma 2.1.11(6).

Next we show that F_ε is Lipschitz. Let v_1 and v_2 belong to V^m, then

$$\|F_\varepsilon(v_1) - F_\varepsilon(v_2)\|_{H^m} \le \frac{C}{\varepsilon}\left(\|M^\varepsilon v_1\otimes M^\varepsilon(v_1 - v_2)\|_{H^m} + \|M^\varepsilon v_2\otimes M^\varepsilon(v_1 - v_2)\|_{H^m}\right)$$

by adding and subtracting $M^\varepsilon\left(\left(\left(M^\varepsilon v_1\right)\cdot\nabla\right)\left(M^\varepsilon v_2\right)\right)$. By using the calculus inequality again (Lemma 2.1.8), we can bound the RHS by

$$\frac{C}{\varepsilon^{3/2}}\left(\|v_1\|_{H^m} + \|v_2\|_{H^m}\right)\|v_1 - v_2\|_{H^m} \le C_\epsilon\|v_1 - v_2\|_{H^m}$$

since $\|v_i\|_{H^m}$ (i=1,2) is bounded and ϵ is finite. This proves the local Lipschitz condition of F_ϵ. □

To extend the existence time to infinity we need to show that the Lipschitz constant

$$\frac{C}{\varepsilon^{3/2}}\left(\|v_1\|_{H^m}+\|v_2\|_{H^m}\right)$$

depends only on ε and initial conditions. We only need to show that for any solution u, $\|u\|_{H^m}$ is bounded by the H^m norm of the initial value u_0.

First, by integration by parts, it is easy to see that

$$\|u\|_{L^2}\le\|u_0\|_{L^2}.$$

The remaining is done by the following lemma:

Lemma 3.13. *Let $m\in\mathbb{N}$ and $u\in C^1([0,T);V^m)$ be a solution of the mollified 3D Euler equations (3.4). Then*

$$\|u\|_{H^m}\le\|u_0\|_{H^m}\,e^{C\int_0^t\|\nabla M^\varepsilon u\|_{L^\infty}\,dt}$$

Proof. Let α be a multi-index, with $|\alpha|\le m$. Applying D^α to both sides of (3.3), multiplying them by $D^\alpha u$ and integrate, we have

$$\begin{aligned}\frac{1}{2}\frac{d}{dt}\int|D^\alpha u|^2\,dx&=-\int D^\alpha u\cdot\left(M^\varepsilon D^\alpha\left(\left((M^\varepsilon u)\cdot\nabla\right)(M^\varepsilon u)\right)\right)\\&=-\int D^\alpha M^\varepsilon u\cdot D^\alpha\left(\left((M^\varepsilon u)\cdot\nabla\right)(M^\varepsilon u)\right)\,dx\\&=-\int D^\alpha M^\varepsilon u\cdot D^\alpha\left(\left((M^\varepsilon u)\cdot\nabla\right)(M^\varepsilon u)\right)\\&\quad+\int D^\alpha M^\varepsilon u\cdot\left(\left((M^\varepsilon u)\cdot\nabla\right)D^\alpha M^\varepsilon u\right)\,dx,\end{aligned}$$

where the term involving the pressure vanishes after integrated by parts due to the incompressibility condition, and the last equality comes from the following argument:

$$\int D^\alpha M^\varepsilon u\cdot\left(\left((M^\varepsilon u)\cdot\nabla\right)D^\alpha M^\varepsilon u\right)\,dx=\frac{1}{2}\int(M^\varepsilon u)\cdot\nabla\left(|D^\alpha M^\varepsilon u|^2\right)\,dx=0$$

via integration by parts due to the incompressibility condition.

Now we sum over all $0\le|\alpha|\le m$. Using the calculus inequality, we have

$$\begin{aligned}\frac{d}{dt}\|u\|_{H^m}^2&\le C\|u\|_{H^m}\sum_{|\alpha|\le m}\left\|D^\alpha\left(\left((M^\varepsilon u)\cdot\nabla\right)(M^\varepsilon u)\right)-\left((M^\varepsilon u)\cdot\nabla\right)D^\alpha M^\varepsilon u\right\|_{L^2}\\&\le C\|u\|_{H^m}\left(\|\nabla M^\varepsilon u\|_{L^\infty}\left\|D^{m-1}DM^\varepsilon u\right\|_{L^2}+\|D^mM^\varepsilon u\|_{L^2}\|\nabla M^\varepsilon u\|_{L^\infty}\right)\\&\le C\|\nabla M^\varepsilon u\|_{L^\infty}\|u\|_{H^m}^2.\end{aligned}$$

To finish the proof, we just need to apply the standard Gronwall's inequality from Lemma 3.9. □

3.4 Local existence of the Euler equations

Now we are ready to give the local existence theorem.

Theorem 3.14. *Let $u_0 \in V^m$ for $m \geq 4$. There exists $T_0 = T_0\left(\|u_0\|_{H^m}\right) > 0$ such that for any $T < T_0$, there exists a unique solution $u \in C^1\left([0,T];V^m\right)$ of the 3D incompressible Euler equations with u_0 as initial data.*

Proof. By Lemma 3.13 we have

$$\frac{d}{dt}\|u^\varepsilon\|_{H^m}^2 \leq C\|\nabla M^\varepsilon u^\varepsilon\|_{L^\infty}\|u^\varepsilon\|_{H^m}^2$$

Note that $m \geq 4 > 3/2+1$, by Theorem 3.3, H^m is embedded into C^1, which means $\|\nabla M^\varepsilon u^\varepsilon\|_{L^\infty} \leq \|M^\varepsilon u^\varepsilon\|_{C^1} \lesssim \|M^\varepsilon u^\varepsilon\|_{H^m} \leq \|u^\varepsilon\|_{H^m}$. Thus we have

$$\frac{d}{dt}\|u^\varepsilon\|_{H^m} \leq C\|u^\varepsilon\|_{H^m}^2$$

and the constant C here is independent of ε. Therefore we see that our u^ε is uniformly bounded in $L^\infty\left([0,T];H^m\right)$ by

$$\frac{\|u_0\|_{H^m}}{1-CT\|u_0\|_{H^m}}.$$

for any $T < T_0 \equiv \left(C\|u_0\|_{H^m}\right)^{-1}$. To apply the Lions-Aubin lemma we need to show that u^ε is Lipschitz in t in some larger space, which we take to be H^{m-1}. In fact we have

$$\begin{aligned}
\|\partial_t u\|_{H^{m-1}} &= \|F_\varepsilon(u^\varepsilon)\|_{H^{m-1}} \\
&\leq C\|\nabla\cdot(M^\varepsilon u^\varepsilon \otimes M^\varepsilon u^\varepsilon)\|_{H^{m-1}} \\
&\leq C\|M^\varepsilon u^\varepsilon \otimes M^\varepsilon u^\varepsilon\|_{H^m} \\
&\leq C\|M^\varepsilon u^\varepsilon\|_{L^\infty}\|u^\varepsilon\|_{H^m} \\
&\leq C\|u^\varepsilon\|_{H^m}^2,
\end{aligned}$$

where we have used the calculus inequality (Lemma 2.1.8) and the Sobolev embedding theorem. Thus we see that u^ε is Lipschitz in t wrt H^{m-1}-norm.

We fix $R_k > 0$ and use Lemma 3.6 (The reason we need this step is that we need $H^m \hookrightarrow H^{m-1}$ to be compact, which won't hold for unbounded regions, as can be seen by taking $X = H^1(\mathbb{R})$, $Y = L^2(\mathbb{R})$ and $f_n(x) = f(x-n)$ for some $f \in H^1$. Obviously $\{f_n\}$ is bounded in X but not convergent in Y.) with $X = H^m(B(0,R_k))$, $Y = Z = H^{m-1}(B(0,R_k))$. Taking $R_k \to \infty$ and using a diagonal argument we see that u^ε has a subsequence, which we do not relabel, that is strongly convergent in $C\left([0,T];H^{m-1}_{loc}(\mathbb{R}^3)\right)$. Denote the limit by u.

Moreover, since $m \geq 4 > 3/2+2$, we see that the convergence also holds in $C\left([0,T]\,; C^1_{loc}(\mathbb{R}^3)\right)$.

We rewrite the equation as

$$u^\varepsilon = u_0 + \int_0^t F^\varepsilon(u^\varepsilon)\ ds.$$

It is easy to see that

$$u = u_0 + \int_0^t F(u)\ ds$$

where $F(u) \equiv P(u \cdot \nabla u)$. Thus we have further that

$$u \in C^1\left([0,T]\,; C^1_{loc}(\mathbb{R}^3)\right)$$

which implies that we can legitimately differentiate with respect to t. Now taking d/dt on both side, we see that u satisfies

$$\begin{aligned} u_t + P(u \cdot \nabla u) &= 0 \\ \nabla \cdot u &= 0 \\ u(\cdot, 0) &= u_0 \\ |u| \to 0 \text{ as } |x| &\to \infty. \end{aligned}$$

The final step for existence is to recover the pressure. This follows directly from the Leray decomposition.

Now we show the uniqueness. Suppose that there are two solutions u_1 and u_2, then we immediately have

$$(u_1 - u_2)_t + P\left(u_1 \cdot \nabla u_1 - u_2 \cdot \nabla u_2\right) = 0$$

with $u_1 - u_2 = 0$ at $t = 0$. Multiply to $u_1 - u_2$ and integrate, we can easily derive

$$\frac{d}{dt}\left\|u_1 - u_2\right\|_{L^2}^2 \leq C(\left\|u_1\right\|_{H^m} + \left\|u_2\right\|_{H^m})\left\|u_1 - u_2\right\|_{L^2}^2$$

by the calculus inequalities. Then by using Gronwall's inequality, we see that the only solution is $u_1 - u_2 \equiv 0$. Thus ends the proof for uniqueness. □

4 The BKM Blow-up Criterion

4.1 The Beale-Kato-Majda Criterion

One of the important points that should be noted is that the above existence result is local in time, meaning that the solution may cease to be in H^m (also known as (aka) blow-up) in some finite time. Thus it is important to have some quantities to indicate such a blow-up. One of them is the quantity

$$\int_0^T \|\omega(\cdot, s)\|_{L^\infty} \ ds$$

proposed by T. Beale, T. Kato and A. Majda.

By the same method used in the last section, we can have the following bound:

$$\|u(\cdot, t)\|_{H^m} \leq Ce^{c\int_0^t \|\nabla u\|_{L^\infty} \ ds} \|u_0\|_{H^m} .$$

So it is clear that as long as $\|\nabla u\|_{L^\infty}$ is uniformly bounded in some time interval $(0, T)$, then the solution exists upto T. In fact this is what Ebin, Fischer and Marsden proved in their 1972 paper [23]. Thus the key is to bound $\|\nabla u\|_{L^\infty}$ by $\|\omega\|_{L^\infty}$ at the same time t. Recall the 3D Biot-Savart law

$$u(x) = \int K(x - y)\omega(y) \ dy$$

where $K(z)$ is the matrix kernel

$$K(z) = \frac{1}{|z|^3} \begin{pmatrix} 0 & -z_3 & z_2 \\ z_3 & 0 & -z_1 \\ -z_2 & z_1 & 0 \end{pmatrix}.$$

If we differentiate under the integration formally, we would have

$$\nabla u(x) = \int \nabla K(x - y)\omega(y) \ dy. \tag{4.1}$$

The operator $\nabla K*$ in fact has nice properties. To see this, we recall a theorem from Stein [44], which is also called the Calderon-Zygmund Lemma.

Theorem 4.1. *Let $K \in L^2(\mathbb{R}^d)$. We suppose:*

1. *The Fourier transform of K is essentially bounded*

$$\left|\hat{K}(x)\right| \leq B.$$

2. *K is C^1 outside the origin and*

$$|\nabla K(x)| \leq B/|x|^{d+1}.$$

For $f \in L^1 \cap L^p$, let us set

$$(Tf)(x) = \int_{\mathbb{R}^d} K(x - y)f(y) \ dy.$$

Then there exists a constant A_p, so that

$$\|T(f)\|_p \le A_p \|f\|_p , \quad 1 < p < \infty.$$

One can thus extend T to all of L^p by continuity. The constant A_p depends only on p, B, and the dimension n. In particular, it does not depend on the L^2 norm of K.

The remark following the theorem in Stein [44] claims that the assumption $K \in L^2$ can be safely dropped in practice.

Now it is easy to check that our kernel ∇K satisfies the conditions in the theorem, thus the L^p norm of ∇u is thus bounded by the L^p-norm of ω. But here what we need is a L^∞ bound. The key lies in the following lemma. It will also become clear that the formal differentiation in (4.1) is "almost legitimate".

Lemma 4.2. *Let u and ω be related with the Biot-Savart law, and $u \in H^3(\mathbb{R}^3)$, then*

$$\|\nabla u\|_{L^\infty} \le C \left(1 + \ln^+ \|u\|_{H^3} + \ln^+ \|\omega\|_{L^2}\right) (1 + \|\omega\|_{L^\infty}) . \tag{4.2}$$

Proof. By the Biot-Savart law, $u = K * \omega$, where K is a matrix-valued singular kernel, homogeneous of degree -2, behaves like $O\left(|x|^{-2}\right)$ at ∞. Since $u \in H^3(\mathbb{R}^3)$, we have $\omega \in H^2(\mathbb{R}^3)$ and thus in $C^{0,\gamma}(\mathbb{R}^3)$ for some $0 < \gamma < 1$ by the Sobolev embedding theorems. Now we compute ∇u.

$$\begin{aligned}
\partial_{x_j} u(x) &= \int_{\mathbb{R}^3} K(y) \partial_{x_j} \omega(x-y)\, dy \\
&= -\int_{\mathbb{R}^3} K(y) \partial_{y_j} \omega(x-y)\, dy \\
&= -\lim_{\delta \to 0} \int_{|y| \ge \delta} K(y) \partial_{y_j} \omega(x-y)\, dy \\
&= \lim_{\delta \to 0} \left(\int_{|y| \ge \delta} \partial_{y_j} K(y) \omega(x-y)\, dy - \int_{|y|=\delta} K(y) \omega(x-y) \frac{-y_j}{\delta}\, dy \right) \\
&= pv \int_{\mathbb{R}^3} \partial_{y_j} K(y) \omega(x-y)\, dy + \lim_{\delta \to 0} \int_{|z|=1} K(z) \omega(x - \delta z) z_j\, dz \\
&= pv \int_{\mathbb{R}^3} \partial_{y_j} K(y) \omega(x-y)\, dy + C_j \cdot \omega(x)
\end{aligned}$$

where $C_j = \int_{|z|=1} K(z) z_j\, dz$ is a matrix. Here $pf \int f dx$ stands for principle value integral. Note that we can also write $C_j \cdot \omega$ as $c_j \times \omega$ for some c_j defined as $\int_{|z|=1} \frac{z}{|z|^3} z_j\, dz$. The above computation shows that, for our purpose, it is enough to estimate the formal ∇u as given in (4.1).

Now to estimate $\|\nabla u\|_{L^\infty}$ by ω, we only need to bound the principal value integral

$$pv \int \nabla K(y)\omega(x-y)\ dy.$$

Note that for any $a < b$, we have the important cancellation property

$$\int_{a\le|y|\le b} \nabla K(y)\ dy = 0.$$

Fix $x \in \mathbb{R}^3$ and $0 < \delta < \varepsilon \le R < \infty$, we have

$$\begin{aligned}
\left|\int_{|y|\ge\delta} \nabla K(y)\omega(x-y)\ dy\right| &\le \left|\int_{\delta\le|y|\le\varepsilon} \nabla K(y)\left(\omega(x-y)-\omega(x)\right)\ dy\right| \\
&\quad + \left|\int_{\varepsilon\le|y|\le R} \nabla K(y)\omega(x-y)\ dy\right| \\
&\quad + \left|\int_{|y|\ge R} \nabla K(y)\omega(x-y)\ dy\right| \\
&\le C\|\omega\|_{C^{0,\gamma}} \int_{\delta\le|y|\le\varepsilon} |y|^{\gamma-3}\ dy \\
&\quad + C\|\omega\|_{L^\infty} \int_{\varepsilon\le|y|\le R} |y|^{-3}\ dy \\
&\quad + C\|\omega\|_{L^2} \left(\int_{|y|\ge R} |y|^{-6}\ dy\right)^{1/2} \\
&\le C\|u\|_{H^3}\varepsilon^\gamma + C\|\omega\|_{L^\infty}\ln(R/\varepsilon) + CR^{-3/2}\|\omega\|_{L^2}
\end{aligned}$$

Finally, taking $R^{3/2} = \|\omega\|_{L^2}$, and $\varepsilon = 1$ if $\|u\|_{H^3} \le 1$ and $(\|u\|_{H^3})^{-1/\gamma}$ otherwise, we get the desired estimate. □

The main result is almost straightforward now.

Theorem 4.3. *(Beale, Kato, Majda 1984). Let $u_0 \in V^m$ with $m \ge 4$. Let $u \in C^1([0,T);V^m)$ be a solution of the 3D incompressible Euler equations (2.7) with initial data u_0. Let $\omega = \nabla\times u$ be the associated vorticity. Then T is the maximum time for u to be in the above function class if and only if*

$$\int_0^T \|\omega\|_{L^\infty}\ dt = \infty.$$

Proof. The "if" part is obvious. Since $\int_0^T \|\omega\|_{L^\infty} = \infty$, necessarily $\|\omega\|_{L^\infty} \to \infty$ at $t \to T$. Then $\|u\|_{W^{1,\infty}} \to \infty$ as $t \to T$ and u can not be in V^m for $m \ge 4$ by the embedding theorems.

Now we deal with the "only if" part. First, as we have shown at the beginning of this subsection,

$$\|u\|_{H^m} \leq Ce^{c\int_0^T \|\nabla u\|_{L^\infty}\ dt} \|u_0\|_{H^m}.$$

Furthermore, by applying the same method to the vorticity equation, we can easily derive

$$\|\omega\|_{L^2} \leq \|\omega_0\| e^{C\int_0^t \|\nabla u\|_{L^\infty}\ ds}.$$

Substituting the above two inequalities into (4.2) in Lemma 4.2 gives

$$\|\nabla u\|_{L^\infty} \leq C\left(1 + (1 + \|\omega\|_{L^\infty}) \int_0^T \|\nabla u\|_{L^\infty}\ dt\right)$$

From this we have the estimate

$$\|\nabla u\|_{L^\infty} \leq \|\nabla u_0\|_{L^\infty} e^{C\int_0^T \|\omega\|_{L^\infty}\ dt}$$

by the Grönwall's lemma 3.9. Thus ends the proof. □

Remark 4.4. An immediate result of applying the Beale-Kato-Majda criterion is this. There is no finite-time blow-up in 2D Euler equations.

4.2 Improvements of the BKM Criterion

During the more than 20 years following the BKM criterion, there are several improvements ([7, 8, 9, 42, 43], to name a few). In particular, in Chae [9], the condition of $\int_0^T \|\omega\|_\infty dt = \infty$ is sharpened to

$$\int_0^T \|\tilde{\omega}(t)\|^2_{\dot{B}^0_{\infty,1}}\ dt = \infty.$$

where for any fixed orthonormal frame (e_1, e_2, e_3),

$$\tilde{\omega} = \omega^1 e_1 + \omega^2 e_2$$

is the projection of the vorticity in the plane of $e_1 - e_2$. The Besov space $\dot{B}^0_{\infty,1}$ is defined as f such that

$$\sum_{j\in\mathbb{Z}} \|\varphi_j * f\|_{L^\infty} < \infty,$$

where the Schwarz function $\varphi \in \mathcal{S}$ satisfying

1. $\mathrm{Supp}\hat{\varphi} \subset \left\{\xi \in \mathbb{R}^d \mid \frac{1}{2} \leq |\xi| \leq 2\right\}$, (note this is why we can't take $\varphi \in C_0^\infty$).

2. $\hat{\varphi}(\xi) \geq C > 0$ if $\frac{2}{3} < |\xi| < \frac{3}{2}$.
3. $\sum_{j\in\mathbb{Z}} \hat{\varphi}_j(\xi) = 1$ where $\hat{\varphi}_j = \hat{\varphi}(2^{-j}\xi)$.

We present the main idea of the proof here. The key to the proof is to bound the growth of $\omega^3 \equiv \omega \cdot e_3$ by $\tilde{\omega} = \omega^1 e_1 + \omega^2 e_2$.

Recall that the evolution of ω satisfies

$$\omega_t + u \cdot \nabla \omega = S \cdot \omega$$

where $S = \frac{1}{2}\left(\nabla u + \nabla u^t\right)$. Dot product with e_3, we have

$$\frac{D\left(\omega^3\right)}{Dt} = \omega \cdot S \cdot e_3.$$

Now we estimate the right hand side. We have (since this estimate is independent of time, we omit t)

$$\begin{aligned}
\omega \cdot S \cdot e_3 = &\frac{1}{4\pi} pv \int \frac{\omega(x) \times \omega(x+y)}{|y|^3} \cdot e_3 - 3\frac{y \times \omega(x+y)}{|y|^5} \cdot e_3 \left(y \cdot \omega(x)\right)\, dy \\
= &\frac{1}{4\pi} pv \int \left\{ \frac{\tilde{\omega}(x) \times \tilde{\omega}(x+y)}{|y|^3} \cdot e_3 \right. \\
&-3\frac{y \times \tilde{\omega}(x+y)}{|y|^5} \cdot e_3 y_3 \omega_3(x) \\
&\left. -\, 3\frac{y \times \tilde{\omega}(x+y)}{|y|^5} \cdot e_3 \left(y \cdot \tilde{\omega}(x)\right) \right\} dy \\
= &\tilde{\omega} \cdot \mathcal{P}(\tilde{\omega}) \cdot e_3 + \omega^3 e_3 \cdot \mathcal{P}(\tilde{\omega}) \cdot e_3.
\end{aligned}$$

where $\mathcal{P}$ is the matrix valued singular integral operator defined by

$$\mathcal{P}(\omega) = S = \frac{1}{2}\left(\nabla u + \nabla u^t\right)$$

for ω and u related by the Biot-Savart law. This operator $\mathcal{P}$ is known to be bounded on $\dot{B}^0_{\infty,1}$. This combined with the fact that $\dot{B}^0_{\infty,1} \hookrightarrow L^\infty$ yields

$$\begin{aligned}
\|\omega \cdot S \cdot e_3\|_{L^\infty} &\lesssim \left\|\omega^3\right\|_{L^\infty} \|\mathcal{P}(\tilde{\omega})\|_{L^\infty} + \|\tilde{\omega}\|_{L^\infty} \|\mathcal{P}(\tilde{\omega})\|_{L^\infty} \\
&\leq \left\|\omega^3\right\|_{L^\infty} \|\mathcal{P}(\tilde{\omega})\|_{\dot{B}^0_{\infty,1}} + \|\tilde{\omega}\|_{L^\infty} \|\mathcal{P}(\tilde{\omega})\|_{\dot{B}^0_{\infty,1}} \\
&\lesssim \left\|\omega^3\right\|_{L^\infty} \|\tilde{\omega}\|_{\dot{B}^0_{\infty,1}} + \|\tilde{\omega}\|^2_{\dot{B}^0_{\infty,1}}.
\end{aligned}$$

Then it is easy to get

$$\left\|\omega^3\right\|_{L^\infty} \leq \left(\left\|\omega^3_0\right\|_{L^\infty} + \int_0^t \|\tilde{\omega}\|^2_{\dot{B}^0_{\infty,1}}\, ds\right) \exp\left(C\int_0^t \|\tilde{\omega}(s)\|_{\dot{B}^0_{\infty,1}}\, ds\right)$$

by integrating the equation for ω^3 along one particle trajectory $X(\alpha, t)$, and then applying the Grönwall's lemma.

Finally, using the Cauchy-Schwarz inequality, and the embedding $\dot{B}^0_{\infty,1} \hookrightarrow L^\infty$ again, we have

$$\begin{aligned}\int_0^T \|\omega\|_{L^\infty}\ dt &\le \int_0^T \|\tilde{\omega}\|_{L^\infty}\ dt + \int_0^T \left\|\omega^3\right\|_{L^\infty}\ dt \\ &\le \sqrt{T}A_T + \left[\left\|\omega_0^3\right\|_{L^\infty} + CA_T^2\right] T \exp\left(C\sqrt{T}A_T\right)\end{aligned}$$

where $A_T \equiv \left(\int_0^T \|\tilde{\omega}\|^2_{\dot{B}^2_{\infty,1}}\ dt\right)^{1/2}$. Thus ends the proof for the necessity part. The sufficient part is trivial from the embedding $H^m \hookrightarrow \dot{B}^0_{\infty,1}$ for $m > 5/2$.

This result is sharper than the BKM criterion, but its disadvantage is that it is not as applicable to numerical simulations as the BKM one. For example, it is not always as easy to measure the Besov norm as the L^∞ norm accurately in numerical computations.

5 Recent Global Existence Results

In this chapter we review some recent results which are in the same line with the BKM criterion. Due to the limited scope of this lecture note, we will not be able to cover all relevant results in this area, even for those results that are related to the Beale-Kato-Majda criterion.

5.1 Sufficient Conditions by Constantin-Fefferman-Majda

In 1996, Constantin-Fefferman-Majda [14] proposed an non-blow-up condition based on the BKM criterion. To understand the main idea, we recall the BKM criterion: If $\int_0^T \|\omega(\cdot,t)\|_{L^\infty}\ dt < \infty$, then no blow-up can happen in $[0, T]$. This implies that one should investigate the vorticity magnitude $|\omega(x,t)|$.

The first step would naturally be deriving the evolution equation for this quantity. This equation is derived in Constantin [13]. It is

$$\frac{D}{Dt}|\omega| = \alpha(x,t)\,|\omega|\,. \tag{5.1}$$

where

$$\begin{aligned}\alpha(x,t) &\equiv \xi(x,t)\cdot\nabla u(x,t)\cdot\xi(x,t) \\ &= \xi(x,t)\cdot S(x,t)\cdot\xi(x,t)\end{aligned}$$

where $S(x,t)$ is the symmetric part of ∇u and $\xi(x,t) = \frac{\omega(x,t)}{|\omega(x,t)|}$ is the direction of $\omega(x,t)$.

Remark 5.1. Note that ξ is well defined only for those points where $\omega(x,t) \neq 0$. For those points where $\omega(x,t) = 0$, $\omega(x,t)$ will always be 0 as long as the flow is not singular, along the trajectory path of the same point, forward and backward in time. This can be seen from the formula

$$\omega(X(\alpha,t),t) = \nabla_\alpha X \cdot \omega(\alpha,0).$$

and the fact that $\nabla_\alpha X$ is non-singular as long as the flow is not singular. So at those points where vorticity vanishes, one can reasonably define $\alpha(x,t) = 0$.

(5.1) can be derived by applying the inner product of the vorticity equation (2.8) with ξ, and using the fact that $\partial_{x_j}\xi \cdot \xi = 0$ since $\xi \cdot \xi = 1$. The proof is left as an exercise.

Next we recall that

$$\nabla u = pv \int_{\mathbb{R}^3} \nabla K(x-y)\omega(y)\ dy + C\omega(x).$$

where C is a third order tensor $C = [C_1, C_2, \ldots, C_d]$ where $C_j = \int_{|z|=1} K(z) z_j\ dz$ as defined in the proof to Lemma 4.2. Note that, since $C_j\omega = c_j \times \omega$ for some $c_j \equiv \int_{|z|=1} \frac{z}{|z|^3} z_j\ dz$,

$$\xi \cdot (C\omega) \cdot \xi = 0.$$

Now it is easy to get

$$\alpha(x,t) = \frac{3}{4\pi} pv \int_{\mathbb{R}^3} (\hat{y} \cdot \xi(x)) \det(\hat{y}, \xi(x+y), \xi(x)) \left|\omega(x+y)\right| \frac{dy}{|y|^3}. \quad (5.2)$$

where $\hat{y} = y/|y|$ is the direction of y, and $\det(a,b,c)$ is the determinant of the matrix with columns a, b, c in that order. The constant $\frac{3}{4\pi}$ will have no effect in the following argument, and will thus be neglected from now on.

The main idea of Constantin-Fefferman-Majda's argument comes from the following observation. Consider the 2D Euler equations. We know that no blow-up can ever occur. Put into the framework of (5.1) and (5.2), we see that the reason can be interpreted as the fact that for 2D flows, $\xi(x+y) = \xi(x) = e_3$ for all x and y, which means $\alpha(x,t) \equiv 0$. This implies that, if the orientation of the vorticity vectors varies only mildly, there would be no blow-up. Thus comes the following theorem. First we give some definitions.

Definition 5.2. (Smoothly directed). We say a set W_0 is *smoothly directed* if there exists $\rho > 0$ and r, $0 < r \leq \frac{\rho}{2}$ such that the following three conditions are satisfied.

First, for every $q \in W_0^* \equiv \{q \in W_0; |\omega_0(q)| \neq 0\}$ and all time $t \in [0,T)$, the function $\xi(\cdot,t)$ has a Lipschitz extension (denoted by the same letter) to the Euclidean ball of radius 4ρ centered at $X(q,t)$, denoted as $B_{4\rho}(X(q,t))$, and

$$M = \lim_{t\to T} \sup_{q\in W_0^*} \int_0^t \|\nabla\xi(\cdot,t)\|^2_{L^\infty(B_{4\rho}(X(q,t)))}\ dt < \infty.$$

Secondly,

$$\sup_{B_{3r}(W_t)} |\omega(x,t)| \leq m \sup_{B_r(W_t)} |\omega(x,t)|$$

holds for all $t \in [0,T)$ with $m \geq 0$ constant. Here

$$W_t \equiv X(W_0,t).$$

Thirdly, for all $t \in [0,T)$,

$$\sup_{B_{4\rho}(W_t)} |u(x,t)| \leq U.$$

Theorem 5.3. *(Constantin-Fefferman-Majda 1996). Assume W_0 is smoothly directed. Then there exists $\tau > 0$ and Γ such that*

$$\sup_{B_r(W_t)} |\omega(x,t)| \leq \Gamma \sup_{B_\rho(W_{t_0})} |\omega(x,t_0)|$$

holds for any $0 \leq t_0 < T$ and $0 \leq t - t_0 \leq \tau$.

Noticing that, in (5.2), $\alpha(x,t)$ would also be zero when $\xi(x+y) = -\xi(x)$. This inspires the following pair of definition and theorem.

Definition 5.4. W_0 is said to be regularly directed, if there exists $\rho > 0$ such that

$$\sup_{q\in W_0^*} \int_0^T K_\rho(X(q,t))\ dt < \infty$$

where

$$K_\rho(x) = \int_{|y|\leq\rho} (\hat{y}\cdot\xi(x))\det(\hat{y},\xi(x+y),\xi(x))\,|\omega(x+y)|\,\frac{dy}{|y|^3}.$$

Theorem 5.5. *(Constantin-Fefferman-Majda 1996) Assume W_0 regularly directed. Then there exists a constant Γ such that*

$$\sup_{q\in W_0} |\omega(X(q,t),t)| \leq \Gamma \sup_{q\in W_0} |\omega_0(q)|$$

holds for all $t \in [0,T]$.

Remark 5.6. An easy corollary to either theorem is that, there will be no blow-up up to time T.

The remaining of this subsection is devoted to the proof of Theorem 5.3. As will be seen during the proof, proving Theorem 5.5 is quite easy and will thus be omitted.

We decompose

$$\alpha(x) = \alpha_{in}(x) + \alpha_{out}(x)$$

where

$$\alpha_{in}(x) = pv \int \chi\left(\frac{|y|}{\rho}\right)(\hat{y}\cdot\xi(x))\det(\hat{y},\xi(x+y),\xi(x))\,|\omega(x+y)|\,\frac{dy}{|y|^3}$$

and

$$\alpha_{out}(x) = \int \left(1-\chi\left(\frac{|y|}{\rho}\right)\right)(\hat{y}\cdot\xi(x))\det(\hat{y},\xi(x+y),\xi(x))\,|\omega(x+y)|\,\frac{dy}{|y|^3}$$

with $\chi(r)$ being a smooth non-negative function satisfying $\chi(r) = 1$ for $r \le 1/2$ and 0 for $r \ge 1$. Then, recalling $\omega(x) = \nabla\times u(x)$ and $\xi(x+y)\,|\omega(x+y)| = \omega(x+y)$, we can do integration by parts in α_{out} and get

$$|\alpha_{out}(x)| \lesssim \rho^{-1}\int_{|y|\ge\rho/2}|u(x+y)|\,\frac{dy}{|y|^3}.$$

Then by Cauchy-Schwarz and the conservation of $\int |u|^2\ dx$, we easily reach

$$|\alpha_{out}(x)| \lesssim C\rho^{-5/2}\,\|u_0\|_{L^2}$$

which remains bounded.

To estimate α_{in}, denote

$$G_\rho(x) = \sup_{|y|\le\rho}|\nabla\xi(x+y)|\,.$$

Observe that $\det(\hat{y},\xi(x+y),\xi(x)) = \hat{y}\cdot(\xi(x+y)\times\xi(x)) = \hat{y}\cdot((\xi(x+y)-\xi(x))\times\xi(x))$ which is bounded by $G_\rho(x)\,|y|$. Thus we have

$$|\alpha_{in}(x)| \le G_\rho(x)I(x)$$

with

$$I(x) \equiv \int \chi\left(\frac{|y|}{\rho}\right)|\omega(x+y)|\,\frac{dy}{|y|^2}.$$

Next we split $I = I_1 + I_2$, where

$$I_1(x) = \int \chi\left(\frac{|y|}{\delta}\right)\chi\left(\frac{|y|}{\rho}\right)|\omega(x+y)|\,\frac{dy}{|y|^2}$$

and

$$I_2(x) = \int \left[1 - \chi\left(\frac{|y|}{\delta}\right)\right] \chi\left(\frac{|y|}{\rho}\right) |\omega(x+y)| \frac{dy}{|y|^2}$$

with $\delta \leq \rho/2$. Clearly we get

$$|I_1(x)| \leq C\delta\Omega_\delta$$

where

$$\Omega_\delta(x) = \sup_{|y|\leq\delta} |\omega(x+y)|$$

by evaluating the integration through polar coordinates. To estimate I_2, we replace $|\omega(x+y)|$ by $\xi(x+y)\cdot\omega(x+y) = \xi(x+y)\cdot(\nabla\times u(x+y))$ and invoke integration by parts, which gives

$$I_2(x) = \int u(x+y)\cdot\left\{\nabla\times\left[\xi(x+y)\frac{1}{|y|^2}\chi\left(\frac{|y|}{\rho}\right)\left(1-\chi\left(\frac{|y|}{\delta}\right)\right)\right]\right\} dy.$$

By putting $\nabla\times$ on each of the four terms, we decompose I_2 into four terms as follows:

$$I_2(x) = A + B + D + E.$$

It is easy to see that

$$|A| \leq CG_\rho(x)\int_{|y|\leq\rho} |u(x+y)| \frac{dy}{|y|^2},$$

$$|B| \leq C\int |u(x+y)| \left[1-\chi\left(\frac{|y|}{\delta}\right)\right]\chi\left(\frac{|y|}{\rho}\right) \frac{dy}{|y|^3},$$

$$|D| \leq \frac{C}{\rho}\int_{|y|\leq\rho} |u(x+y)| \frac{dy}{|y|^2}$$

and

$$|E| \leq \frac{C}{\delta}\int_{\frac{\delta}{2}\leq|y|\leq\delta} |u(x+y)| \frac{dy}{|y|^2}.$$

If we denote

$$U_\rho(x) = \sup_{|y|\leq\rho} |u(x+y)|,$$

then we can easily estimate

$$|A| \leq C\rho U_\rho(x) G_\rho(x)$$
$$|D|, |E| \leq CU_\rho(x)$$

and

$$|B| \leq CU_\rho(x)\log\left(\frac{\rho}{\delta}\right).$$

Putting them together, we have

$$|\alpha(x)| \leq A_\rho(x)\left[1+\log\left(\frac{\rho}{\delta}\right)\right] + G_\rho(x)\delta\Omega_\delta(x).$$

where

$$A_\rho(x) = C\rho^{-5/2}\left\|u_0\right\|_{L^2} + CG_\rho(x)U_\rho(x)(1+\rho G_\rho(x)).$$

Studying what we have for a while, we see that if we can replace $\Omega_\delta(x)$ by $|\omega(x)|$, then by taking $\delta = |\omega(x)|^{-1}$, we will have

$$\int_0^T |\alpha| \ dt \leq \int_0^T G_\rho(x)^2 \ dt < \infty$$

by the smoothly directness of our set W_0, since we have U_ρ to be bounded all the time. And this will effectively end the proof. So the final step should be to relate $\Omega_\delta(x)$ with $|\omega(x)|$, although the final proof doesn't go along the idea described above for technical reasons.

Consider a bunch of trajectories $X(q,t)$ and a neighborhood

$$\mathcal{B}_{4\rho} \equiv \left\{(x,t) : 0 \leq t < T, \exists q \in W_0, |X(q,t)-x| \leq 4\rho\right\}.$$

By the smoothly directness,

$$\sup_{(x,t)\in\mathcal{B}_{4\rho}} |u(x,t)| \leq U < \infty$$

and

$$M = \lim_{t\to T} \sup_{q\in W_0^*} \int_0^t G_{4\rho}^2\left(X(q,s)\right) \ ds < \infty.$$

Now define

$$B_r(W_t) = \{x; \exists q \in W_0, |x - X(q,t)| \leq r\}$$

with $2r \leq \rho$.

Let

$$\tau = \frac{r}{4U}$$

be a (possibly very short) time interval. Denote

$$w_r(t) = \sup_{B_r(W_t)} |\omega(x,t)|.$$

By assumption

$$w_{3r}(t) \leq m w_r(t).$$

Now consider $x \in B_r(W_t)$ for some $t < T$. The Lagrangian trajectory passing through x at time t is denoted $X(q',t)$. Note that q' may not be in W_0. Nevertheless, if $r \le \frac{\rho}{2}$ and $0 \le t-s \le \tau$ then $X(q', s) \in B_{2r}(W_s)$, i.e.,

$$|X(q,s) - X(q',s)| \le 2r \le \rho$$

for some $q \in W_0$. Then it follows that

$$G_\rho(X(q',s)) \le G_{4\rho}(X(q,s))$$

and

$$|\alpha(X(q',s))| \le A_{4\rho}(X(q,s)) \left[1 + \log \frac{\rho}{\delta}\right] + G_{4\rho}(X(q,s))\delta\Omega_\delta(X(q',s)).$$

Denoting

$$\mathcal{A}(s) = \sup_{q\in W_0^*} A_{4\rho}(X(q,s))$$
$$\mathcal{G}(s) = \sup_{q\in W_0^*} G_{4\rho}(X(q,s)).$$

Then integrating (5.1) would give us

$$|\omega(X(q',t))| \le K e^{\int_{t_0}^t \left\{\mathcal{A}(s)[1+\log(\rho/\delta)]+\mathcal{G}(s)\delta\Omega_\delta(X(q',s))\right\}\, ds}.$$

where

$$K = w_\rho(t_0).$$

Now we choose $\delta \le r$, then $X(q', s) \in B_{2r}(W_s)$ and by assumption

$$\Omega_\delta(X(q',s)) \le m w_r(s),$$

which implies

$$w_r(t) \le K e^{\int_{t_0}^t \{\mathcal{A}(s)[1+\log(\rho/\delta)]+m\delta\mathcal{G}(s)w_r(s)\}\, ds}$$

for any $0 < \delta \le r$ and $0 \le t - t_0 \le \tau$.

To simplify, define

$$A = A(t, t_0) = \int_{t_0}^t \mathcal{A}(s)\, ds$$

and

$$Q = K\rho \int_0^T \mathcal{G}(s)\, ds.$$

Let

$$y(t) = \max_{t_0 \le s \le t} \left(\frac{w_r(s)}{K}\right),$$

and

$$\frac{\rho}{\delta} = \max\left\{my(t)Q, \frac{\rho}{r}\right\}.$$

Then we obtain

$$y(t) \le \left(\frac{\rho}{\delta}\right)^A e^{1+A}.$$

Finally, we can choose τ such that

$$A(t, t_0) \le \frac{1}{2}.$$

This can be done since by assumption $\mathcal{A}$ is integrable. Now fix this τ, we have

$$y(t) \le \max\left\{me^3 Q; \frac{\rho}{mrQ}\right\} \equiv \Gamma$$

and thus ends the proof.

5.2 Sufficient Conditions by Deng-Hou-Yu

The result by Constantin, Fefferman and Majda reveals the subtlety between the smoothness of the vorticity direction field and the accumulation rate of vorticity. But on the other hand, their theorems are not quite applicable to various numerical simulations studying the blow-up issue of the 3D Euler equations in recent years. The most interesting ones among them are Kerr [26, 27, 28, 29] and Pelz [39, 40]. From their observations the following seem to hold for flows that may be singular, i.e., flows that seems to have the critical singular vorticity growth rate $(T-t)^{-1}$ for some $T > 0$ (Note: unforced flows that have higher vorticity growth rate have never been observed):

1. Large vorticity, or more specifically, those $|\omega| \ge c \|\omega\|_{L^\infty}$, are concentrated in small regions of length $O\left((T-t)^{1/2}\right)$ in the vorticity direction and with cross-section area $O\left((T-t)^2\right)$. These regions look like two vortex sheets with thickness $O(T-t)$ meeting at an angle.
2. The vorticity direction field $\xi(x, t)$ looks more regular inside this region than outside, where $\xi(x, t)$ is wildly helical.

Checking these observations against Definition 5.2 and Theorem 5.3 (Note that Definition 5.4 is obviously unverifiable with numerical quantities, so we won't consider Theorem 5.5.), we see that the conditions there are not satisfied. The main reason is that, according to numerical simulations, the "smoothly directed" region can never have fixed size, instead is always rapidly shrinking in all three directions. Thus there is a gap between theoretical theorems and numerical observations and leaving Theorem 5.3 unable to explain the numerical results.

In 2005, Deng, Hou and Yu [19] made a first step in filling this gap. The key is to focus on one vortex line and study its local stretching behaviors. Before introducing the main result, we introduce some notations.

Denote by $\Omega(t)$ the maximum vorticity magnitude at time t. Let L_t be a family of vortex line segments and $L(t)$ be the length of L_t. Denote $U_\xi(t) \equiv \max_{x,y\in L_t} |(\mathbf{u}\cdot\xi)(x,t) - (\mathbf{u}\cdot\xi)(y,t)|$, $U_n(t) \equiv \max_{L_t} |\mathbf{u}\cdot\mathbf{n}|$ where $\mathbf{n}$ is the normal of the curve L_t, i.e., $\frac{\partial}{\partial s}\xi = (\xi\cdot\nabla)\xi \equiv \kappa\mathbf{n}$ where κ is the curvature, and $M(t) \equiv \max\left(\|\nabla\cdot\xi\|_{L^\infty(L_t)}, \|\kappa\|_{L^\infty(L_t)}\right)$. We also define $X(a,t_1,t_2)$ as follows:

$$\frac{dX(\alpha,t_1,t)}{dt} = \mathbf{u}(X(\alpha,t_1,t),t); \quad X(\alpha,t_1,t_1) = \alpha.$$

It is related to the usual flow map $X(q,t)$ as follows:

$$X(q,t_2) = X(X(q,t_1),t_1,t_2)$$

for any q, t_1, t_2.

Now the main theorem reads

Theorem 5.7. *(Deng-Hou-Yu, 2005) Assume there is a family of vortex line segments L_t and $T_0 \in [0,T)$, such that $X(L_{t_1},t_1,t_2) \supseteq L_{t_2}$ for all $T_0 < t_1 < t_2 < T$. We also assume that $\Omega(t)$ is monotonically increasing and $\|\omega(t)\|_{L^\infty(L_t)} \geq c_0\Omega(t)$ for some $c_0 > 0$ when t is sufficiently close to T. Furthermore, we assume that*

1. $[U_\xi(t) + U_n(t)M(t)L(t)] \lesssim (T-t)^{-\alpha}$ *for some* $\alpha \in (0,1)$,
2. $M(t)L(t) \leq C_0$, *and*
3. $L(t) \gtrsim (T-t)^\beta$ *for some* $\beta < 1-\alpha$.

Then there will be no blow-up in the 3D incompressible Euler flow up to time T.

Remark 5.8. Note that the conditions 1–3 are inspired by the numerical observations. In Kerr's computations, the velocity blows up like $O\left((T-t)^{-1/2}\right)$, which gives $alpha = 1/2$. On the other hand, $M(t) = (T-t)^{-1/2}$. If we take $L(t) = (T-t)^{1/2}$, then the second condition is satisfied, but it would just violate the third condition. Thus Kerr's computations fall into the critical case of our theorem.

Remark 5.9. In a follow-up paper [21], Deng, Hou and Yu improved the above result and obtained non-blowup conditions for the critical case $\beta = 1-\alpha$. The new conditions depend on some fine relations among the asymptotic behaviors of the rescaled quantities $(T-t)^\alpha\left[U_\xi(t) + U_n(t)M(t)L(t)\right]$, $(T-t)^{\alpha-1}L(t)$ and the bound C_0. In [25], Hou and Li repeated Kerr's computations using a pseudo-spectral method with resolution up to

$1536 \times 1024 \times 3072$ up to $T = 19$, beyond the singularity time $T_c = 18.7$ predicted by Kerr. They found that there is a tremendous dynamic depletion of the vortex stretching term. The velocity field is found to be bounded, and the maximum vorticity does not grow faster than doubly exponential in time. The fact that velocity is bounded allows us to apply the non-blowup conditions of [22], which provides further theoretical evidence of the non-blowup of the Euler equations with Kerr's initial data.

We give a simple proof of the non-blowup result of Deng-Hou-Yu.

First we investigate the incompressibility condition of vorticity. $\nabla \cdot \omega = 0$. It is easy to see that

$$\frac{\partial |\omega|}{\partial s}(x,t) = -\left(\nabla \cdot \xi(x,t)\right) |\omega| (x,t).$$

where s is the arc length of the vortex line containing (x,t), so that $\frac{\partial}{\partial s} = \xi \cdot \nabla$. This implies that for any two points $x, y \in L_t$, as long as $|\int_x^y \nabla \cdot \xi ds| \leq M(t)L(t) \leq C$, we have

$$e^{-M(t)L(t)} \leq \frac{|\omega(y,t)|}{|\omega(x,t)|} \leq e^{M(t)L(t)}. \tag{5.3}$$

Next we study the relation between vorticity magnitude and vortex line stretching. Recall that

$$\omega(X(\alpha,t),t) = \nabla_\alpha X(\alpha,t) \cdot \omega_0(\alpha).$$

Multiplying both side by $\xi(X(\alpha,t),t)$ we have

$$|\omega(X(\alpha,t),t)| = \xi(X(\alpha,t),t) \cdot \nabla_\alpha X(\alpha,t) \cdot \xi(\alpha) |\omega_0(\alpha)| .$$

Noticing

$$\xi(X(\alpha,t),t) = \frac{\partial X}{\partial s}$$

along the vortex line at time t, and similarly

$$\xi(\alpha) = \frac{\partial \alpha}{\partial \beta}$$

where β is the arc length parameter at time 0. Substituting these relations in, we have

$$\begin{aligned}
|\omega(X(\alpha,t),t)| &= \frac{\partial X(\alpha,t)}{\partial s} \cdot \nabla_\alpha X(\alpha,t) \cdot \frac{\partial \alpha}{\partial \beta} |\omega_0(\alpha)| \\
&= \frac{\partial X}{\partial s} \cdot \frac{\partial X}{\partial \beta} |\omega_0(\alpha)| \\
&= \left(\frac{\partial X}{\partial s} \cdot \frac{\partial X}{\partial s}\right) \frac{\partial s}{\partial \beta} |\omega_0(\alpha)| \\
&= \frac{\partial s}{\partial \beta} |\omega_0(\alpha)|
\end{aligned}$$

since $\frac{\partial X}{\partial s} = \xi$ is a unit vector. It is easy to generalize the above result to prove that

$$\frac{\partial s}{\partial \beta}(X(\alpha, t_1, t), t) = \frac{|\omega(X(\alpha, t_1, t), t)|}{|\omega(\alpha, t_1)|}.$$

Now we have the relations between any two points on L_t, and between vortex line stretching and growth of vorticity magnitude. A third ingredient is the evolution equation of s_β. It is easy to see that s_β is governed by the same equation as $|\omega|$ in (5.1).

$$\begin{aligned}\frac{D}{Dt}s_\beta &= \xi \cdot \nabla \mathbf{u} \cdot \xi \; s_\beta \\ &= [(\xi \cdot \nabla)(\mathbf{u} \cdot \xi) - u \cdot (\xi \cdot \nabla)\xi]\, s_\beta \\ &= (\mathbf{u} \cdot \xi)_\beta - \kappa\,(\mathbf{u} \cdot \mathbf{n})\, s_\beta,\end{aligned}$$

where we have used $\xi \cdot \nabla \xi = \partial_s \xi = \kappa \mathbf{n}$ by the Frènet relationship. Integrating it along L_t and in time, we easily get the estimate

$$l(t_2) \leq l(t_1) + \int_{t_1}^{t_2} U_\xi \; d\tau + \int_{t_1}^{t_2} M(\tau) U_n(\tau) l(\tau) \; d\tau$$

where l_t is a segment of L_t such that $l_{t_2} = X(l_{t_1}, t_1, t_2)$, and $l(t)$ is the arclength of l_t.

Next we will show how $l(t_2)/l(t_1)$ is related to the vorticity growth.

$$e^{-(M(t)l(t)+M(t_1)l(t_1))} \frac{|\omega(X(\alpha', t_1, t), t)|}{|\omega(\alpha', t_1)|} \leq \frac{l(t)}{l(t_1)} \leq e^{(M(t)l(t)+M(t_1)l(t_1))} \frac{|\omega(X(\alpha', t_1, t), t)|}{|\omega(\alpha', t_1)|}. \tag{5.4}$$

The proof of (5.4) is not difficult. Let β denote the arc length parameter at time t_1. Denote by l_t the vortex line segment from 0 to β, and use s as the arc length parameter at time t. Now by the mean value theorem, we have (β is the arclength variable at t_1)

$$\frac{l(t)}{l(t_1)} = \frac{\int_0^\beta s_\beta(\eta) \; d\eta}{\beta} = s_\beta(\eta') = \frac{|\omega(X(\alpha'', t_1, t), t)|}{|\omega(\alpha'', t_1)|},$$

for some α'' on the same vortex line. Now the inequality (5.4) follows from (5.3).

Now putting the three ingredients together, we get an estimate for the vorticity magnitude.

$$\Omega_l(t_2) \leq e^{C_0} \Omega_l(t_1) \left[1 + \frac{1}{l(t_1)} \int_{t_1}^{t_2} (U_\xi(\tau) + M(\tau) U_n(\tau) l(\tau)) \; d\tau\right]. \tag{5.5}$$

where $\Omega_l(t)$ denotes the maximum vorticity magnitude along l_t.

Now we start the proof of Theorem 5.7 itself. The idea is the following. Note that the above inequality actually controls the growth rate of vorticity. So we can expect to prove non-blow-up if $l(t_1)$ does not shrink to zero too fast. If we assume, in the same spirit as those by Constantin-Fefferman-Majda, that $l(t) > c > 0$ for some fixed c, then effectively we have

$$\Omega(t_2) \leq e^{C_0}\Omega(t_1)$$

and obviously no blow-up can happen. Now we illustrate the proof along this simple idea.

We prove by contradiction. First, by translating the initial time we can assume that the assumptions hold in $[0, T)$. Define

$$r \equiv (R/c_0) + 1$$

where $R \equiv e^{2C_0}$. Recall that C_0 is the bound of $M(t)L(t)$, and c_0 is the lower bound of $\Omega_L(t)/\Omega(t)$, where $\Omega_L(t) \equiv \|\omega(\cdot, t)\|_{L^\infty(L_t)}$.

If there is a finite time blow-up at time T, then we must have

$$\int_0^T \Omega(t)\ dt = \infty$$

and necessarily $\Omega(t) \nearrow \infty$ as $t \nearrow T$. Take $t_1, t_2, \ldots, t_n, \ldots$ such that

$$\Omega(t_{k+1}) = r\Omega(t_k).$$

Since $\Omega(t)$ is monotone by assumption, and T is the smallest time that $\int_0^T \Omega(t)\ dt = \infty$, we have $t_n \nearrow T$ as $n \to \infty$.

Now we choose $l_{t_2} = L_{t_2}$. By assumptions on L_t, we have $l_{t_1} \subset L_{t_1}$ such that $X(l_{t_1}, t_1, t_2) = l_{t_2}$. And furthermore, by using (5.4), we obtain

$$l(t_1) \geq l(t_2)\frac{1}{R}\frac{\Omega_L(t_1)}{\Omega_L(t_2)} \geq l(t_2)\frac{c_0}{R^2}\frac{1}{r} \gtrsim (T - t_2)^\beta,$$

where the hidden constant in $\gtrsim$ is independent of time. Now plugging this into (5.5) we have, after some algebra,

$$\Omega(t_2) \leq (r-1)\Omega(t_1) + \frac{C}{(1-\alpha)c_0}\frac{\Omega(t_1)}{(T-t_2)^\beta}(T-t_1)^{1-\alpha}.$$

Recalling $\Omega(t_2) = r\Omega(t_1)$, we have

$$r \leq (r-1) + C\frac{(T-t_1)^{1-\alpha}}{(T-t_2)^\beta}$$

which gives

$$(T - t_2) \leq C(T - t_1)^{1+2\delta}$$

with

$$\delta \equiv \frac{1-\alpha}{\beta} - 1$$

which is positive by assumption. By taking t_1 close enough to T, we can cancel C and have

$$(T - t_2) \leq (T - t_1)^{1+\delta}.$$

Next do the same thing for all pairs (t_n, t_{n+1}), (note that $(T-t_n)^\delta < (T-t_1)^\delta \leq C^{-1}$) we have

$$(T - t_{k+1}) \leq (T - t_k)^{1+\delta} \leq (T - t_1)^{(1+\delta)^k} \leq (T - t_1)(T - t_1)^{\delta k} \quad (5.6)$$

if we take $T - t_1 < 1$.

Now we study $\int_0^T \Omega(t)\, dt = \infty$. By assumption that $\Omega(t)$ is monotone, we have

$$\Omega(t_1)\sum_{k=1}^{\infty} r^k(t_{k+1} - t_k) = \sum_{k=1}^{\infty}\Omega(t_{k+1})(t_{k+1} - t_k) \geq \int_{t_1}^{T}\Omega(t)\; dt = \infty$$

which implies

$$\begin{aligned}
(r-1)\sum_{l=0}^{\infty} r^l(T - t_{l+1}) &= \sum_{l=0}^{\infty}(r^{l+1} - r^l)(T - t_{l+1}) \\
&= \sum_{l=0}^{\infty}\sum_{k=l+1}^{\infty}(r^{l+1} - r^l)(t_{k+1} - t_k) \\
&= \sum_{k=1}^{\infty}\sum_{l=0}^{k-1}(r^{l+1} - r^l)(t_{k+1} - t_k) \\
&= \sum_{k=1}^{\infty}(r^k - 1)(t_{k+1} - t_k) \\
&= \infty.
\end{aligned}$$

All the equalities are legitimate since all the terms in the summations are positive (Fubini's theorem).

On the other hand, from (5.6), we obtain

$$\infty = \sum_{k=0}^{\infty} r^k(T - t_{k+1}) \leq (T - t_1)\sum_{k=0}^{\infty}\left[r(T - t_1)^\delta\right]^k < \infty,$$

if we choose t_1 close to T so that $r(T - t_1)^\delta < 1$. Therefore, we reach a contradiction. Thus, we obtain

$$\int_{t_1}^{T}\Omega(t)dt < \infty.$$

By the BKM criterion, we conclude that there is no finite time blow-up up to T.

6 Lower Dimensional Models for the 3D Euler equations

6.1 1-D Model

In 1985, P. Constantin, P. Lax and A. Majda proposed the following 1-D model of the 3D Euler equations.

$$\omega_t = H\omega \cdot \omega$$

where H is the Hilbert transform:

$$Hf = pv \int_{\mathbb{R}} \frac{f(y)}{x-y}\, dy.$$

The relation to the 3D Euler equations is the following. In 3D Euler equation, the evolution of the vorticity magnitude is governed by the following equation:

$$\frac{D}{Dt}|\omega| = T(\omega)|\omega|.$$

where T is a Calderon-Zygmund operator with a convolution kernel that is homogeneous of degree $-d$ where d is the dimension. In 1-D, only one such singular integral kernel exists, i.e., the Hilbert transform.

This simplified model can be explicitly solved. To solve it, we first get familiar with some properties of the Hilbert transform.

Lemma 6.1. *The Hilbert transform has the following properties:*

1. *H is bounded from H^m to H^m for all $m \geq 0$.*
2. *$H(Hf) = -f$.*
3. *$H(fg) = f(Hg) + g(Hf) + H(Hf \cdot Hg)$.*

Proof. Properties (1) and (2) follow immediately from the fact that

$$\widehat{Hf}(\xi) = sgn(\xi)\hat{f}(\xi).$$

For property (3), we check

$$\begin{aligned}
\widehat{H(fg)} - H(\widehat{Hf \cdot Hg}) &= \int_{-\infty}^{\infty} sgn(\xi)\hat{f}(\eta)\hat{g}(\xi-\eta)\, d\eta \\
&\quad - \int_{-\infty}^{\infty} sgn(\xi)sgn(\eta)sgn(\xi-\eta)\hat{f}(\eta)\hat{g}(\xi-\eta)\, d\eta \\
&= \int_{-\infty}^{\infty} sgn(\xi)\left(1 - sgn(\eta)sgn(\xi-\eta)\right)\hat{f}(\eta)\hat{g}(\xi-\eta)\, d\eta \\
&= \int_{-\infty}^{\infty} \left(sgn(\xi-\eta) + sgn(\eta)\right)\hat{f}(\eta)\hat{g}(\xi-\eta)\, d\eta \\
&= \widehat{f(Hg)} + \widehat{g(Hf)},
\end{aligned}$$

and thus ends the proof. □

Now we set out to find the explicit solutions. We define

$$z(x,t) = H\omega(x,t) + i\omega(x,t).$$

By Lemma 6.1, the equation for z is

$$\frac{dz}{dt} = \frac{1}{2}z^2$$

whose explicit solution is

$$z(t) = \frac{2z_0}{2 - z_0 t}$$

which implies

$$\omega(x,t) = \frac{4\omega_0(x)}{(2 - tH\omega_0)^2 + t^2\omega_0^2(x)}.$$

It is obvious that $\omega(x,t)$ will blow-up at points with $\omega_0(x) = 0$ but $H\omega_0 > 0$.

6.2 The 2-D QG Equation

The 2D QG equation (see Pedlosky [41]) is given by

$$\frac{D\theta}{Dt} \equiv \theta_t + u \cdot \nabla\theta = 0, \tag{6.1}$$

where $\theta(x,t)$ is a scalar, and u is defined by

$$\begin{aligned} (-\triangle)^{1/2}\,\psi &= -\theta \\ u &= \nabla^{\perp}\psi \end{aligned}$$

Here $(-\triangle)^{1/2}$ is defined by

$$(-\triangle)^{1/2}\,\psi = \int e^{2\pi i x\cdot\xi} 2\pi\,|\xi|\,\hat{\psi}(\xi)\ d\xi$$

if

$$\psi = \int e^{2\pi i x\cdot\xi}\hat{\psi}(\xi)\ d\xi.$$

The 2D QG equation (aka surface-quasi-geostrophic equations, SQG) describes the variation of the density variation θ at the surface of the earth. The name θ, usually represents temperature, is chosen because in the case the ideal gas, the density variation is proportional to the temperature.

To get an explicit form of the formula for ψ in the space variable x instead of the Fourier modes ξ, we use the following lemma:

Lemma 6.2. *Denote*

$$h_a(x) = \frac{\Gamma(a/2)}{\pi(a/2)} |x|^{-a},$$

then we have

$$\hat{h}_a = h_{N-a}$$

for $0 < \Re(a) < N$, *where* N *is the dimension of the space.* Γ *is the Gamma function, defined as*

$$\Gamma(s) = \int_0^\infty e^{-t} t^{s-1} \; dt.$$

Proof. See e.g. Thomas Wolff [46]. □

By the above lemma we easily derive

$$\psi(x) = - \int_{\mathbb{R}^2} \frac{\theta(x+y)}{|y|} \; dy.$$

Thus we get

$$u(x) = \int_{\mathbb{R}^2} \frac{y^\perp}{|y|^2} \theta(x+y) \; dy.$$

If we define "vorticity"

$$\omega(x) = \nabla^\perp \theta$$

we obtain by differentiating (6.1) that

$$\frac{D\omega}{Dt} = \nabla u \cdot \omega,$$

from which we can derive

$$\begin{aligned}
\frac{D|\omega|}{Dt} &= \frac{1}{2} \xi \left(\nabla u + \nabla u^T \right) \xi \, |\omega| \\
&\equiv S(x,t) \, |\omega| \\
&= \int_{\mathbb{R}^2} \frac{\left(\hat{y} \cdot \xi^\perp(x)\right) \left(\xi(x+y) \cdot \xi^\perp(x)\right)}{|y|^2} |\omega(x+y)| \; dy \;\; |\omega| \\
&= \int_{\mathbb{R}^2} \frac{\left(\hat{y} \cdot \xi(x)\right) \det\left(\xi(x+y), \xi(x)\right)}{|y|^2} |\omega(x+y)| \; dy \;\; |\omega|
\end{aligned}$$

where

$$\xi(x,t) \equiv \frac{\omega(x,t)}{|\omega(x,t)|}$$

as long as it is well-defined, and $\hat{y} = y/|y|$. Note that those points with $\omega(x,t) = 0$ is transported by the flow, since $\omega = 0$ implies $\nabla\theta = 0$ and

$$\begin{aligned}\nabla\theta(X(q,t)) &= \nabla_x\theta_0(q) \\ &= (\nabla_q X)^{-1} \cdot \nabla_q\theta_0(q).\end{aligned}$$

which means $\nabla_q\theta_0(q) = 0 \Leftrightarrow \nabla_x\theta(X(q,t)) = 0$. So those points where ξ is not well-defined are not important to the stretching.

Recall that for the evolution of the vorticity magnitude in 3D Euler, we have

$$\frac{D|\omega|}{Dt} = \alpha(x,t)\,|\omega|$$

where

$$\alpha(x,t) = \frac{3}{4\pi}\int_{\mathbb{R}^3} \frac{(\hat{y}\cdot\xi(x))\det(\hat{y},\xi(x+y),\xi(x))}{|y|^3}\,|\omega(x+y)|\;dy.$$

We see that $S(x,t)$ and $\alpha(x,t)$ indeed share very similar cancellation properties. Thus the 2D QG equation can be viewed as a 2D model of the 3D Euler equation, especially in the vorticity form.

There are several other similarities between 2D QG and 3D Euler. For example, the levelsets of $\theta(x,t)$, which are lines that are always tangent to $\omega(x,t)$ so can be defined as "vortex lines", are carried by the flow, similar to the vortex lines in the 3D Euler dynamics. For more comparison between 2D QG and 3D Euler equations, as well as other properties of the 2D QG equations, see Constantin-Majda-Tabak [15], or the book by Majda-Bertozzi [35].

Remark 6.3. Note that in the 2D QG equation, we no longer have the property

$$\frac{1}{2}\left(\nabla u - \nabla u^T\right)\omega = 0$$

as in the 3D Euler case. This implies that, the "vorticity" here doesn't satisfy

$$\frac{D\omega}{Dt} = \frac{1}{2}\left(\nabla u + \nabla u^T\right)\omega$$

as in the Euler case. Only the evolution of the vorticity magnitude $|\omega|$ satisfies the same equation as in the 3D Euler equation.

6.2.1 Existence and blow-up Criteria

By the same technique as in Chapter 2, we can prove the local in time existence and blow-up criterion.

Theorem 6.4. *(Constantin-Majda-Tabak [15]). If the initial value $\theta_0(x)$ belongs to the Sobolev space $H^k(\mathbb{R}^2)$ for some integer $k \geq 3$, then there is a smooth solution $\theta(x,t) \in H^k(\mathbb{R}^2)$ for the 2D QG equation for each time t, in a sufficiently small time interval $[0, T^*)$, where T^* is characterized by*

$$\|\theta(\cdot, t)\|_k \nearrow \infty \text{ as } t \nearrow T^*$$

and can be estimated from below by

$$T^* \gtrsim \frac{1}{1 - \|\theta_0\|_k}.$$

We can also apply the technique for the BKM criterion in Chapter 4 to obtain similar blow-up criteria:

Theorem 6.5. *(Constantin-Majda-Tabak [15]). Consider the unique smooth solution of the 2D QG equations with initial data $\theta_0(x) \in H^k(\mathbb{R}^2)$ for some $k \geq 3$. Then the following are equivalent:*

1. *The time interval $[0, T^*)$ for some $T^* < \infty$ is maximal for the solution to be in $H^k(\mathbb{R}^2)$.*
2. *The vorticity magnitude accumulates so rapidly that*

$$\int_0^T \|\omega(\cdot, t)\|_{L^\infty} \, dt \nearrow \infty \text{ as } T \nearrow \infty$$

3. *Let $S^*(t) \equiv \max_{x \in \mathbb{R}^2} S(x,t)$, then*

$$\int_0^{T^*} S^*(t) \, dt = \infty.$$

There are, though, properties that seems to hold only in the 2D QG case. For example, when we assume that there is a smooth curve $x(t)$, such that each point $(x(t), t)$ is an isolated maximum of $|\omega(x,t)|$, we can have the following result:

$$\frac{d}{dt} \|\omega(\cdot, t)\|_{L^\infty} = S(x(t), t) \|\omega(\cdot, t)\|_{L^\infty}.$$

To prove it, let $q(t)$ be the Lagrange marker of the points $(x(t), t)$, i.e.,

$$X(q(t), t) = x(t)$$

then we have

$$\begin{aligned}
\frac{d}{dt}\|\omega(\cdot,t)\|_{L^\infty} &= \frac{d}{dt}|\omega(x(t),t)| \\
&= \frac{d}{dt}|\omega\left(X(q(t),t),t\right)| \\
&= \frac{D}{Dt}|\omega|\,(x(t),t) + \nabla_x|\omega|\cdot\nabla_q X\cdot\dot{q} \\
&= S(x(t),t)\,|\omega(x(t),t)| \\
&= S(x(t),t)\,\|\omega(\cdot,t)\|_{L^\infty}
\end{aligned}$$

Note that $\nabla_x|\omega| = 0$ by our assumption that $x(t)$ is an isolated maximum.

The above result implies that, under the assumption on $x(t)$, we can just consider $S(x,t)$ for the particular point $(x(t),t)$ instead of the maximum of $S(x,t)$ over the whole space. The assumption on $x(t)$ is very likely to hold in practical cases according to various numerical results, see e.g. Constantin-Majda-Tabak [15].

Remark 6.6. It is claimed in Constantin-Majda-Tabak [15] that the assumption on $x(t)$ can be dropped with a more lengthy proof, while that proof is omitted.

6.2.2 Global existence result by Constantin-Majda-Tabak

In their 1994 paper [15], Constantin, Majda and Tabak studied the evolution of the vorticity magnitude both numerically and theoretically, concluded that when the vorticity direction $\xi(x,t)$ varies not too fast in space, there can be no finite time blow-up, i.e., the classical solution exists globally in time.

To understand the basic idea, we recall the evolution equation for $|\omega|$:

$$\frac{D|\omega|}{Dt} = S(x,t)\,|\omega|$$

where

$$S(x,t) = \int_{\mathbb{R}^2} \frac{\left(\hat{y}\cdot\xi^\perp(x)\right)\left(\xi(x+y)\cdot\xi^\perp(x)\right)}{|y|^2}\,|\omega(x+y)|\ dy.$$

In general, since $S(x,t) = T\omega$ with T being a singular integral operator, $\|S(\cdot,t)\|_{L^\infty}$ can not be bounded by $\|\omega(\cdot,t)\|_{L^\infty}$. Even if it can, the right hand side would be quadratic and give us a finite time blow-up. But if we make assumptions on $\xi(x+y)$, the situation would be different. We illustrate this through several examples.

Example 6.7. (Constantin-Majda-Tabak [15]). We consider the classical frontogenesis with trivial topology. Let

$$x_2 = f(x_1)$$

be a smooth curve in the plane, we study the possibility that the solution $\theta(x,t)$ developing a sharp front along this curve, through the simplified ansatz

$$\theta(x,t) = F\left(\frac{x_2 - f(x_1)}{\delta(t)}\right),$$

where $F(s)$ is a smooth function on $\mathbb{R}$, with the properties that $F(s) = 1$ for $s \geq 3$, $F(s) = 0$ for $s \leq 1$ and $F'(s) \geq 0$ for all s. Assume that

$$\delta(t) \to 0, \quad as \quad t \to T^*$$

for some $T^* < \infty$.

We can plug the formula for θ into the 2D QG equation and get

$$F'\left[\frac{d}{dt}\left(\frac{1}{\delta(t)}\right) + \mathbf{u}\cdot\begin{pmatrix} f'(x_1) \\ 1 \end{pmatrix}\left(\frac{1}{\delta(t)}\right)\right] = 0.$$

Since obviously $\|\omega\|_{L^\infty}(t) \sim 1/\delta(t)$, we have the estimate

$$\frac{d}{dt}\left(\log \|\omega\|_{L^\infty}(t)\right) \lesssim \|u\|_{L^\infty}(t).$$

It can be shown that for 2D QG equation

$$\|u\|_{L^\infty}(t) \lesssim \log \|\omega\|_{L^\infty}. \tag{6.2}$$

We see that the growth rate of the maximum vorticity is at most double exponential, and there will be no finite time blow-up.

The last thing is to prove the estimate (6.2), which first appears in Cordoba [17].

Recall that, for teh 2D QG equation, we have

$$u = (-\triangle)^{-1/2}\omega = \int \frac{1}{|y|}\omega(x+y)\, dy.$$

Now let $r > 0$ fixed, large enough, $\rho \in (0, r)$ to be specified later, and χ be the standard cut-off function, we decompose u into 3 terms as follows

$$|u(x)| = U_{in}(x) + U_{med}(x) + U_{out}(x)$$

where

$$\begin{aligned} U_{in}(x) &= \int \chi\left(\frac{|x|}{\rho}\right)\frac{1}{|y|}\omega(x+y)\, dy \\ &\leq \|\omega\|_{L^\infty}\rho \end{aligned}$$

by simply using polar coordinates. For U_{med}, we have

$$\begin{aligned} U_{med}(x) &= \int \chi\left(\frac{|x|}{r}\right)\left(1-\chi\left(\frac{|x|}{\rho}\right)\right)\frac{1}{|y|}\omega(x+y)\ dy \\ &= \int \chi\left(\frac{|x|}{r}\right)\left(1-\chi\left(\frac{|x|}{\rho}\right)\right)\frac{1}{|y|}\nabla^{\perp}\theta(x+y)\ dy \\ &\lesssim \int_{2r\geq|y|\geq\rho/2}\frac{1}{|y|^2}\theta(x+y)\ dy + \frac{1}{\rho}\int_{2\rho\geq|y|\geq\rho/2}\frac{\theta(x+y)}{|y|}\ dy \\ &\quad + \frac{1}{r}\int_{2r\geq|y|\geq r/2}\frac{1}{|y|}\theta(x+y)\ dy \\ &\lesssim -\left\|\theta\right\|_{L^\infty}(1+|\log\rho|) = -\left\|\theta_0\right\|_{L^\infty}(1+|\log\rho|), \end{aligned}$$

as long as $\rho < c < 1$ for some fixed constant c. Here we have used the fact that $\nabla\chi\left(\frac{|x|}{\rho}\right) = 0$ for all $|x| \leq \rho/2$ or $|x| \geq 2\rho$ and the maximum of $|\theta|$ is bounded by the initial data.

Now we estimate U_{out},

$$\begin{aligned} U_{out}(x) &= \int\left(1-\chi\left(\frac{|x|}{r}\right)\right)\frac{1}{|y|}\nabla^{\perp}\theta(x+y)\ dy \\ &\lesssim \frac{1}{r}\int_{2r\geq|y|\geq r/2}\frac{1}{|y|}\theta(x+y)\ dy + \int_{|y|\geq r/2}\theta(x+y)\ \frac{dy}{|y|^2} \\ &\equiv I + II. \end{aligned}$$

I is obviously bounded by some constant since $\|\theta\|_\infty \leq \|\theta_0\|_\infty$. For II, we use he Cauchy-Schwarz inequality and the fact that the L^2 norm of θ is conserved. We get

$$II \lesssim r^{-1}\left\|\theta_0\right\|_{L^2}$$

which is also bounded by a constant.

Finally, if $\|\omega\|_{L^\infty} \leq e$, (6.2) trivially holds. If not, taking $\rho = \|\omega\|_{L^\infty}^{-1}$ immediately gives the desired estimate.

We look at another example, the singular thermal ridge.

Example 6.8. (Constantin-Majda-Tabak [15]). The assumptions are similar to the previous example, the only difference is that $F(s) = 0$ for both $s \geq 3$ and $s \leq 1$, with $F'(s) > 0$ for $1 < s < 2$, $F'(s) < 0$ for $2 < s < 3$. There can be no finite time blow-up for these ridges either. The proof is similar to that in the last example and is omitted.

The above two examples implies that, for θ whose levelsets form simple geometries, there may be no finite time blow-up. To quantify what we mean by "simple geometry", we use the direction of the "vorticity vectors" $\xi = \omega/|\omega|$. The precise statement of the theorem is the following (Constantin-Majda-Tabak [15]):

Definition 6.9. A set Ω_0 is *smoothly directed* if there exists $\rho > 0$ such that

$$\sup_{q\in\Omega_0} \int_0^T |u(X(q,t),t)|^2 \, dt < \infty$$

and

$$\sup_{q\in\Omega_0^*} \int_0^T \|\nabla\xi(\cdot,t)\|_{L^\infty(B_\rho(X(q,t),t)))} \, dt < \infty$$

where $B_\rho(x)$ is the ball of radius ρ centered at x and

$$\Omega_0^* = \{q \in \Omega_0 \mid |\omega_0(q)| \neq 0\}.$$

We use the following notation:

$$\Omega_t = X(\Omega_0, t)$$

$$O_T(\Omega_0) = \{(x,t) \mid x \in \Omega_t, 0 \le t \le T\}$$

Theorem 6.10. *Assume Ω_0 is smoothly directly, then*

$$\sup_{O_T(\Omega_0)} |\nabla\theta(x,t)| < \infty$$

i.e., there can be no blow-up in $O_T(\Omega_0)$.

Definition 6.11. We say that the set Ω_0 is *regularly directed* if there exists $\rho > 0$ such that

$$\sup_{q\in\Omega_0^*} \int_0^T K_\rho(X(q,t)) \, dt < \infty$$

where

$$K_\rho(x) = \int_{|y|\le\rho} \left|\hat{y}\cdot\xi^\perp(x)\right| \left|\xi(x+y)\cdot\xi^\perp(x)\right| |\omega(x+y)| \, \frac{dy}{|y|^2}$$

Theorem 6.12. *Assume that Ω_0 is regularly directed, then*

$$\sup_{O_T(\Omega_0)} |\omega(x,t)| < \infty$$

The proofs to these theorems are similar to the ones in the global existence results by Constantin-Fefferman-Majda for the 3D Euler equations, only less technical. The main difference is that here we have a conserved quantity θ, whose L^p norm is conserved for all $1 \le p \le \infty$. This simplifies the proof a lot. First, $S(x,t)$ is bounded by

$$|S(x,t)| \le C\left[G(t)\,|u(x,t)| + (\rho G(t)+1)\left(G(t)\,\|\theta\|_{L^\infty} + \rho^{-2}\,\|\theta\|_{L^2}\right)\right]$$

where $G(t) \equiv \sup_{|y|\le\rho} |\nabla\xi(x+y)|$ for some fixed $\rho > 0$, via similar estimates as in Chapter 2. Next we integrate the above in time and use the Cauchy-Schwarz inequality. For details see Constantin-Majda-Tabak [15].

Remark 6.13. The reader may notice that our condition on the maximum velocity, i.e., L^2-integrable in time, is much weaker than the one in the 3D Euler case, i.e., L^∞ bounded. This is because, in 2D QG, we have $\omega = (\partial_2, -\partial_1)\theta$ with θ being bounded. For 3D Euler, we have $\omega = \nabla \times u$ and we do not have *a priori* bound on u. Thus in the case of the 3D Euler equation, we have a term

$$G(t)^2 U(t)$$

which won't be integrable if $U(t) \equiv \|u\|_{L^\infty}(t)$ is not bounded in addition.

6.2.3 Global existence result by Cordoba and Fefferman

The results by Constantin-Majda-Tabak claims that, as long as the direction field of the levelsets are smooth enough locally around the maximum stretching point, there can be no finite time blow-up in the 2D QG equations. This leaves one candidate for finite-time blow-up in their numerical simulations, i.e., the "hyperbolic saddle" situation. In fact, they performed detailed numerical experiments and found that the maximum vorticity can be fitted by $1/(8.25 - t)^{1.7}$, which suggests a finite time blow-up. In 1997, Ohkitani and Yamada re-did the simulations and pushed further to higher resolutions ([38]), and found that the same result can be fitted as well by double exponential growth, indicating that no finite time blow-up can occur, at least up to the time of their computations. Subsequently, Constantin-Nie-Schörghofer [16]) found that the double exponential is in several aspects a better fit, suggesting that no finite-time blow-up can occur. Around the same time, D. Cordoba [17] proved that under some mild assumptions, the hyperbolic saddles will not cause a finite time blow-up, instead the growth of $|\omega|$ is bounded by quadruple exponential. The proof is technical and we will not reproduce it here.

In 2002, D. Cordoba and C. Fefferman [18] considered a case that covers most of the scenarios considered by Constantin-Majda-Tabak and the hyperbolic saddle case by Cordoba, which they called "semi-uniform collapse", and obtained the numerically observed double exponential growth by clever estimates. We will recap their work here.

Assume that there is an interval $[a, b]$ such that

$$\theta(x_1, \phi_\rho(x_1, t), t) = G(\rho)$$

for $x_1 \in [a, b]$, where $x_2 = \phi_\rho(x_1, t)$ is a level curve of θ, $\phi_\rho \in C^1([a, b] \times [0, T))$ for some alleged blow-up time T. By a "semi-uniform" collapse we mean that the level sets are almost parallel to each other (Note that the sharpening front and ridge in Examples 6.7 and 6.8 satisfy that the level curves are exactly parallel to each other). More specifically, if we denote

$$\delta(x_1, t) \equiv |\phi_\rho(x_1, t) - \phi_{\rho'}(x_1, t)|,$$

then δ satisfies

$$\min_{[a,b]} \delta(x_1, t) \geq c \max_{[a,b]} \delta(x_1, t).$$

By this assumption, we always have

$$|\omega(x_1, \phi_\rho(x_1, t), t)| \sim \frac{1}{\delta(x_1', t)}$$

for any $x_1, x_1' \in [a, b]$.

From this observation, it is enough to consider

$$I = \frac{d}{dt}\left(\int_a^b \left[\phi_{\rho_2}(x_1, t) - \phi_{\rho_1}(x_1, t)\right]\ dx_1\right)$$

since the quantity being differentiated is comparable to $|\omega|^{-1}$(Note that, since different level curves will never cross, the sign of the difference is fixed.).

We compute

$$\frac{d}{dt}\phi_\rho(x_1, t)$$

for some fixed ρ. First note that, the curve $(x_1, \phi_\rho(x_1, t))$ is transported by the flow, since it always parametrized the level curve $\theta = G(\rho)$. So we have

$$\frac{d}{dt}\phi_\rho(x_1, t) = u_2 - u_1 \frac{\partial \phi_\rho}{\partial x_1} = \frac{d}{dx_1}\psi(x_1, \phi_\rho(x_1, t), t)$$

where $\psi = (-\triangle)^{-1/2}\,\theta$ so that $u = \nabla^\perp \psi$. The first equality can be seen by drawing a picture and studying the difference between ϕ_ρ at t and $t + \delta t$, or go through the argument using the QG equation as in Cordoba-Fefferman [18].

Now it is immediate that

$$\begin{aligned} I = {} & \psi(b, \phi_{\rho_2}(b, t), t) - \psi(a, \phi_{\rho_2}(a, t), t) \\ & + \psi(a, \phi_{\rho_1}(a, t), t) - \psi(b, \phi_{\rho_2}(b, t), t). \end{aligned}$$

Let

$$A(t) \equiv \frac{1}{b-a}\int_a^b \left[\phi_{\rho_2}(x_1, t) - \phi_{\rho_1}(x_1, t)\right]\ dx_1,$$

we have

$$\left|\frac{d}{dt}A(t)\right| \lesssim \sup_{[a,b]} \left|\psi(x_1, \phi_{\rho_2}(x_1, t), t) - \psi(x_1, \phi_{\rho_1}(x_1, t), t)\right|.$$

Finally we prove a general estimate

$$|\psi(z_1, t) - \psi(z_2, t)| \lesssim \left||z_1 - z_2| \log |z_1 - z_2|\right|.$$

Obviously, that will end the proof, and bound the maximum growth by some double exponential.

Recall that

$$\psi(x,t) = (-\triangle)^{-1/2}\,\theta = -\int \frac{\theta(x+y)}{|y|}\,dy.$$

Taking $\tau = |z_1 - z_2|$ we have

$$\begin{aligned}\psi(z_1) - \psi(z_2) &= \int \theta(y)\left(\frac{1}{|y-z_1|} - \frac{1}{|y-z_2|}\right) dy \\ &= \int_{|y-z_1|\le 2\tau} + \int_{2\tau<|y-z_1|\le k} + \int_{k<|y-z_1|} \\ &= I_1 + I_2 + I_3\end{aligned}$$

where $k > 2\tau$ is some constant.

Now trivially,

$$|I_1| \le C\tau.$$

For I_2, by the mean value theorem

$$\left|\frac{1}{|y-z_1|} - \frac{1}{|y-z_2|}\right| = \tau\left|\nabla\frac{1}{|y-z'|}\right|$$

for some z' lying on the line segment connecting z_1 and z_2. Thus we can further bound it by

$$\tau \max_s \frac{1}{|y-s|^2}$$

where the maximum is taken over the line connecting z_1 and z_2. Now it is clear that

$$|II| \le C\tau\,|\log\tau|\,.$$

III is also trivially bounded by $C\tau$ using the conservation of the L^2 norm of θ, and the mean value theorem.

Thus ends the proof.

6.2.4 Final Remarks about the QG equation

The global existence/blow-up issue for the 2D quasi-geostrophic equation is still open today, and solving it would for sure shed light on and help solving the same problem for the 3D Euler equations. A recent progress is Deng-Hou-Li-Yu [22], where the authors applied the method developed in their papers dealing with the 3D Euler equations [19, 21], and obtained triple exponential growth bound for $\|\nabla\theta\|_\infty$ under very mild conditions. Furthermore, under slightly stronger conditions the authors show that the growth rate of $\|\nabla\theta\|_\infty$ can be bounded by double exponential, which is the real growth rate observed in numerical computations. High resolution numerical computations carried out by the authors suggest that these conditions are indeed satisfied in the 2D QG flow. This observation suggests that these conditions may have touched the essence of the QG dynamics. The authors are currently making an effort to further investigate this problem.

7 Vortex Patch

A vortex patch is a bounded, simply connected, open material domain $\mathcal{D}_t$ such that the vorticity is constant inside it and 0 elsewhere. It is a special case of the $L^1 \cap L^\infty$ weak solutions. Here we will describe the problem without using the general weak solution formalism.

7.1 The contour dynamics equation (CDE)

By definition and our expectation that the vorticity will be conserved along particle trajectories (should check that they really exist), it is (hopefully) enough to derive an equation that governs the evolution of the boundary.

Assume that the solution do behave this way, i.e., the vorticity at any time t is ω_0 in some smooth region $\mathcal{D}(t)$ and 0 outside, where $\mathcal{D}(t)$ is smoothly parametrized by t. Then the velocity is

$$u(x,t) = \frac{\omega_0}{2\pi} \int_{\mathcal{D}(t)} \frac{(x-y)^\perp}{|x-y|^2} \, dy.$$

By the Divergence Theorem we can rewrite it as a contour integral

$$u(x,t) = \frac{\omega_0}{2\pi} \int_{\partial\mathcal{D}(t)} \log|x-y| \; n^\perp(y) dS(y),$$

where $n(y)$ is the unit outer normal vector. Note that in our setting, $\mathcal{D}(t)$ and then $\omega(x,t)$ is determined by the evolution of the boundary $\partial\mathcal{D}(t)$. If we parametrize it by $x = x(s,t)$, we have

$$\frac{\partial x(s,t)}{\partial t} = -\frac{\omega_0}{2\pi} \int_{\partial\mathcal{D}(t)} \log|x(s,t) - x(s',t)| \frac{\partial x}{\partial s'}(s',t) \, ds'$$

This is called the CDE (contour dynamics equation). It can be checked that as long as the boundary remains smooth enough, $\omega(x,t)$ defined by the CDE is a weak solution.

In [34], A. Majda observed that, $Y = \frac{\partial x}{\partial s}$ satisfies an evolution equation very similar to the 1-D model:

$$\frac{DY}{Dt} = (M(Y))\, Y,$$

where $M(Y)$ is a matrix whose entries are Cauchy integrals on a curve, i.e., a generalization of the 1D Hilbert transform. He further conjectured that a finite time singularity would form from smooth initial data.

In 1991, J.-Y. Chemin [10] proved that in fact the above resemblance is just superficial. The evolution of the vortex patch boundary behaves much better than the 3D Euler equations. Namely, the boundary will remain in $C^{1,\mu}$ if it is started in this function class. In [4], A. Bertozzi and P. Constantin give an alternative proof that is easier to understand. We will present this proof in the next subsection.

7.2 Levelset formulation and global existence

Let $0 < \mu < 1$ and $\mathcal{D}$ be a simply connected, bounded and open subset of the plane whose boundary is $C^{1,\mu}$ smooth, i.e., for any $x^0 \in \partial\mathcal{D}$ there exists a ball $B(x^0; r_0)$ and a $C^{1,\mu}$ function $\varphi : \mathbb{R} \mapsto \mathbb{R}$ such that, after a rotation,

$$\partial\mathcal{D} \cap B(x^0, r_0) = \left\{x \in B(x^0, r_0) \mid x_2 = \varphi(x_1)\right\}.$$

Now we introduce the levelset formulation. Let $\varphi \in C^{1,\mu}(\mathbb{R}^2)$ be such that

$$\mathcal{D} = \{x \mid \varphi(x) > 0\}$$

and $|\nabla\varphi| \geq c > 0$ on the boundary. By the implicit function theorem we see that $\partial\mathcal{D}$ defined by $\varphi = 0$ is indeed $C^{1,\mu}$. Thus to establish the long time existence, we only need to show the existence of $C^{1,\mu}$ function $\varphi(x,t)$ such that $\mathcal{D}(t) = \{x \mid \varphi(x,t) > 0\}$ and $\nabla\varphi(x,t)$ is bounded below by $c > 0$ uniformly in t.

It is easy to see that the evolution of $\varphi(x,t)$ should be governed by

$$\varphi_t + u \cdot \nabla\varphi = 0 \tag{7.1}$$

and thus

$$\frac{D}{Dt}\nabla^\perp\varphi \equiv \nabla u \cdot \nabla^\perp\varphi$$

which looks similar to the 3D Euler equation.

We need to show two things, first $\left\|\nabla^\perp\varphi\right\|_{C^{0,\mu}}$ is bounded above, second $\left|\nabla^\perp\varphi\right| = |\nabla\varphi|$ is bounded below at $\varphi = 0$.

Proposition 7.1. *Let u be the velocity field associated to a vortex patch. Denote*

$$\sigma(z) = \begin{pmatrix} \frac{2z_1z_2}{|z|^2} & \frac{z_2^2 - z_1^2}{|z|^2} \\ \frac{z_2^2 - z_1^2}{|z|^2} & -\frac{2z_1z_2}{|z|^2} \end{pmatrix}.$$

Then

$$\nabla u(x) = \frac{\omega_0}{2\pi} pv \int_{\mathcal{D}} \frac{\sigma(x-y)}{|x-y|^2}\, dy + \frac{\omega_0}{2}\begin{pmatrix} 0 & -1 \\ 1 & 0 \end{pmatrix}\chi_{\mathcal{D}}(x).$$

Proof. The proof is straightforward, similar to those in Chapter 4. □

First we need to notice some properties of $\sigma(x-y)$.

1. It is smooth outside of the origin and homogeneous of degree 0.
2. It is symmetric with respect to reflection about the origin, i.e., $\sigma(z) = \sigma(-z)$.
3. It has mean 0 on the unit circle.
4. By (2) and (3), it has mean 0 on any half circle centered at 0.

By (1) the kernel in the integral is a singular integral kernel. But one important difference with the 3D Euler or other model equations (1D Constantin-Lax-Majda Model, 2D QG) is that, this singular integral kernel is acting on a characteristic function instead of $\nabla^{\perp}\varphi$, thus it can be expected to behave much better than the 3D Euler equation.

To see this point, we consider a naïve approach. Instead of the technical $C^{1,\gamma}$, suppose we would like to prove that the level set equation (7.1) is well-posed in C^1. For this purpose, it is enough to prove that $\|\nabla u\|_{L^\infty}$ is bounded. We have

$$\nabla u(x) = \frac{\omega_0}{2\pi} pv \int_{\mathcal{D}} \frac{\sigma(x-y)}{|x-y|^2}\, dy + \frac{\omega_0}{2}\begin{pmatrix} 0 & -1 \\ 1 & 0 \end{pmatrix} \chi_{\mathcal{D}}(x).$$

So it is enough to prove that

$$pv \int_{\mathcal{D}} \frac{\sigma(x-y)}{|x-y|^2}\, dy$$

remains bounded for all x. Suppose that we only need to worry about the integral

$$I(x) \equiv pv \int_{\mathcal{D}\cap B(x,\delta)} \frac{\sigma(x-y)}{|x-y|^2}\, dy$$

for some $\delta > 0$. Obviously when $d(x) \equiv dist(x, \partial\mathcal{D}) \geq \delta$, $I(x) = 0$. On the other hand, when $d(x) < \delta$, we need subtle cancellations. To get some insight, assume that locally $\partial\mathcal{D}$ is $x_2 = 0$, and $x = (0, x_2) \in \mathcal{D}$ with $\delta > x_2 > 0$. By the properties of σ, we see that σ has mean 0 on semi-circles. This implies that,

$$I(x) = \int_{\mathcal{D}_{\text{eff}}} \frac{\sigma(x-y)}{|x-y|^2}\, dy,$$

where $\mathcal{D}_{\text{eff}} \equiv \mathcal{D} \cap (B(x,\delta) \setminus B(x, d(x)) \cap \{0 < y_2 < d(x)\}$ is illustrated in the following figure by the shaded area:

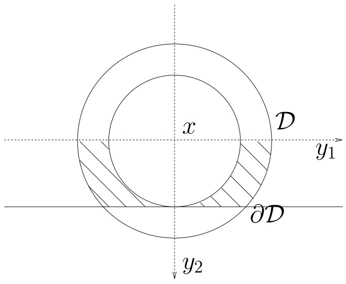

Using Polar coordinates, we have

$$|I(x)| \leq 2 \int_{d(x)}^{\delta} \frac{1}{\rho^2} \theta(\rho) \rho d\rho,$$

where $\theta(\rho)$ is the size of the angle interval corresponding to the curve

$$\{y = (y_1, y_2) \mid |y - x| = \rho, \ 0 < y_1, 0 < y_2 < d(x)\}.$$

See the following figure.

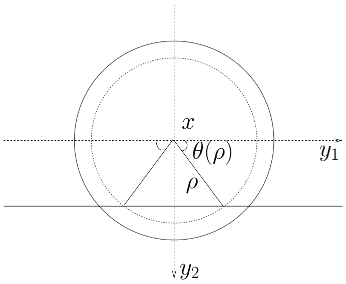

By the inequality

$$\arcsin t \leq \frac{\pi}{2} t$$

for $t \in [0, 1]$, we have

$$t \leq \sin \frac{\pi}{2} t \leq \frac{\pi}{2} \sin t$$

which implies

$$\theta(\rho) \leq \frac{\pi}{2} \frac{d(x)}{\rho}.$$

Now it is easy to see that

$$|I(x)| \leq C \int_{d(x)}^{\delta} \frac{d(x)}{\rho^2} \, d\rho \leq C \left(1 - \frac{d(x)}{\delta}\right) \leq C$$

is bounded. Thus $\|\nabla u\|_{L^\infty}$ is bounded and φ stays in C^1.

The above "proof" is easy, but there are several un-bridgeable gaps in the argument. The major one is the following. Recall that we assumed $\partial\mathcal{D}$ to be straight when estimating the integral. In fact it can be at most as smooth as φ, i.e., C^1, and our argument breaks down when the boundary is only C^1. It turns out that, to get a good estimate on ∇u, we need the boundary to be at least $C^{1,\mu}$ with some $\mu > 0$. But then we need to prove that φ stays in $C^{1,\mu}$ instead of C^1, which means that it is not enough to estimate $\|\nabla u\|_{L^\infty}$. Thus the real proof is much more complicated although the main idea is the same as the one presented above. Now we turn to the real proof.

The next Proposition is very important.

Proposition 7.2. *We have*

$$\nabla u(x)\nabla^\perp\varphi(x) = \frac{\omega_0}{2\pi} pv \int_{\mathcal{D}} \frac{\sigma(x-y)}{|x-y|^2}\left(\nabla^\perp\varphi(x) - \nabla^\perp\varphi(y)\right)\, dy.$$

Proof. First we observe that

$$\frac{\sigma(z)}{|z|^2} = \nabla\left(\nabla^\perp \log|z|\right).$$

Thus

$$\left(\frac{\sigma(x-y)}{|x-y|^2}\cdot\nabla^\perp\varphi(y)\right)_i = \nabla\cdot\left(\left(\nabla^\perp\log|z|\right)_i\cdot\nabla^\perp\varphi(y)\right).$$

Now if we consider the i-th component of the integral and omit the subscript i,

$$\begin{aligned} pv\int_{\mathcal{D}}\frac{\sigma(x-y)}{|x-y|^2}\nabla^\perp\varphi(y)\, dy &= \lim_{\delta\to 0}\int_{\mathcal{D}\cap\{|x-y|\geq\delta\}} \nabla\nabla^\perp\log|x-y|\cdot\nabla^\perp\varphi(y)\, dy \\ &= \lim_{\delta\to 0}\int_{\mathcal{D}\cap\{|x-y|\geq\delta\}} \nabla\cdot\left(\nabla^\perp\log|x-y|\cdot\nabla^\perp\varphi(y)\right)\, dy \\ &= -\lim_{\delta\to 0}\int_{\mathcal{D}\cap\{|x-y|=\delta\}} \frac{(x-y)^\perp}{|x-y|^2}\left(\nabla^\perp\varphi(y)\cdot\frac{x-y}{\delta}\right)\, dS(y) \\ &= -\pi\begin{pmatrix}0 & -1\\ 1 & 0\end{pmatrix}\chi_{\mathcal{D}}(x)\nabla^\perp\varphi(x). \end{aligned}$$

And then the proposition is straightforward. □

We denote

$$|f|_\mu = \sup_{x\neq y}\frac{|f(x)-f(y)|}{|x-y|^\mu}$$

to be the $C^{0,\mu}$ semi-norm.

Proposition 7.3. *There exists a constant $C = C(\mu)$ such that*

$$\left|\nabla u(\cdot)\nabla^{\perp}\varphi(\cdot)\right|_{\mu} \leq C\left(1 + \|\nabla u\|_{L^\infty}\right)|\nabla\varphi|_{\mu}.$$

Proof. Let $x, h \in \mathbb{R}^2$. We estimate

$$\begin{aligned}
&\frac{2\pi}{\omega_0}\left|\left(\nabla u \cdot \nabla^{\perp}\varphi\right)(x+h) - \left(\nabla u \cdot \nabla^{\perp}\varphi\right)(x)\right| \\
&\leq \left|pv\int_{\mathcal{D}} \frac{\sigma(x+h-y)}{|x+h-y|^2}\left(\nabla^{\perp}\varphi(x+h) - \nabla^{\perp}\varphi(y)\right)\, dy\right| \\
&\quad + \left|pv\int_{\mathcal{D}} \frac{\sigma(x-y)}{|x-y|^2}\left(\nabla^{\perp}\varphi(x) - \nabla^{\perp}\varphi(y)\right)\, dy\right| \\
&\leq \left|pv\int_{\mathcal{D}\cap\{|x-y|\leq 2|h|\}} \frac{\sigma(x+h-y)}{|x+h-y|^2}\left(\nabla^{\perp}\varphi(x+h) - \nabla^{\perp}\varphi(y)\right)\, dy\right| \\
&\quad + \left|\int_{\mathcal{D}\cap\{|x-y|>2|h|\}} \frac{\sigma(x+h-y)}{|x+h-y|^2}\left(\nabla^{\perp}\varphi(x+y) - \nabla^{\perp}\varphi(y)\right)\, dy\right| \\
&\quad + \left|pv\int_{\mathcal{D}\cap\{|x-y|\leq 2|h|\}} \frac{\sigma(x-y)}{|x-y|^2}\left(\nabla^{\perp}\varphi(x) - \nabla^{\perp}\varphi(y)\right)\, dy\right| \\
&\quad + \left|\int_{\mathcal{D}\cap\{|x-y|>2|h|\}} \left(\frac{\sigma(x-y)}{|x-y|^2} - \frac{\sigma(x+h-y)}{|x+h-y|^2}\right)\left(\nabla^{\perp}\varphi(x+h) - \nabla^{\perp}\varphi(y)\right)\, dy\right| \\
&\equiv I_1 + I_2 + I_3 + I_4.
\end{aligned}$$

We estimate them one by one.

For I_1, we use the fact that $\varphi \in C^{1,\mu}$ and get

$$I_1 \leq C|h|^{\mu}|\nabla\varphi|_{\mu}.$$

For I_2, by Cotlar's lemma, we have

$$I_2 \leq C\left(\|\nabla u\|_{\infty} + 1\right)$$

For I_3, Similar to I_1, we have

$$I_3 \leq C|h|^{\mu}|\nabla\varphi|_{\mu}.$$

Lastly, for I_4, by the mean value theorem, we have

$$I_4 \leq \int_{\mathcal{D}\cap\{|x-y|\geq 2|h|\}} |h|\frac{C}{|x-y|^3}|x-y|^{\mu}|\nabla\varphi|_{\mu} \leq C|h|^{\mu}|\nabla\varphi|_{\mu}.$$

□

Remark 7.4. Cotlar's lemma is the following result:

For any singular integral kernel $K(x)$, define

$$K^{\varepsilon}(x) \equiv \begin{cases} 0 & |x| \leq \varepsilon \\ K(x) & |x| > \varepsilon \end{cases}.$$

Then there is a constant $C > 0$, such that for any $\varepsilon > 0$,

$$|K^{\varepsilon} * f|(x) \leq C\left(M(K * f)(x) + M(f)(x)\right).$$

where $M(f)$ denotes the maximal function of f.

$$M(f) \equiv \sup_{r>0} \frac{1}{|B(x,r)|} \int_{B(x,r)} f(y)\, dy.$$

Thus in particular, if both $K * f$ and f are in L^{∞}, then we can replace $M(K * f)(x)$ by $\|K * f\|_{L^{\infty}}$ and $M(f)$ by $\|f\|_{L^{\infty}}$. For more about Cotlar's lemma, see e.g. Section 1.7 of Stein [45] or Chapter 7 of Meyer-Coifman [37].

Our next task is to give a upper bound for $\|\nabla u\|_{L^{\infty}}$. Denote the infimum norm of a function f on $\partial\mathcal{D}$ by

$$|f|_{inf} = \inf_{x \in \partial\mathcal{D}} |\nabla\varphi(x)|.$$

Proposition 7.5. *Let u be the velocity and φ be a solution to (7.1). Then there is a constant $C = C(\mu) > 0$ such that*

$$\|\nabla u\|_{L^{\infty}} \leq C\,|\omega_0|\left(1 + \log\left(\frac{|\nabla\varphi|_{\mu}}{|\nabla\varphi|_{inf}}\right)\right).$$

Proof. First note that we only need to estimate the principal integral

$$pv \int_{\mathcal{D}} \frac{\sigma(x-y)}{|x-y|^2}\, dy.$$

Denote

$$\delta = \frac{|\nabla\varphi|_{inf}}{|\nabla\varphi|_{\mu}}.$$

and $d(x) = dist(x, \partial\mathcal{D})$ for any $x \in \mathbb{R}^2$. Intuitively, the main difficulty would come from near the boundary.

First we assume $d(x) \geq \delta$. Take η small enough, we have

$$\begin{aligned} \left| \int_{\mathcal{D}\cap\{|x-y|\geq\eta\}} \frac{\sigma(x-y)}{|x-y|^2}\, dy \right| &\leq \left| \int_{\mathcal{D}\cap\{\eta\leq|x-y|\leq d(x)\}} \frac{\sigma(x-y)}{|x-y|^2}\, dy \right| \\ &\quad + \left| \int_{\mathcal{D}\cap\{|x-y|>d(x)\}} \frac{\sigma(x-y)}{|x-y|^2}\, dy \right| \\ &= \left| \int_{\mathcal{D}\cap\{|x-y|>d(x)\}} \frac{\sigma(x-y)}{|x-y|^2}\, dy \right| \\ &\leq \left| \int_{\mathcal{D}\cap\{|x-y|>d(x)\}} \frac{1}{|x-y|^2}\, dy \right| \\ &\leq \left| \int_{d(x)<|x-y|\leq R} \frac{1}{|x-y|^2}\, dy \right| \end{aligned}$$

where πR^2 is the area of $\mathcal{D}$, which is conserved by the imcompressibility of the flow. The last inequality can be readily checked by using Polar coordinates and the fact that $\frac{1}{r^2}$ is monotonically decreasing in r. The proof is left as an exercise. Now it is easy to see that the integral is bounded by what we want.

Now for the case $d(x) < \delta$. Again taking η small enough, we have

$$\begin{aligned} \left| \int_{\mathcal{D}\cap\{|x-y|\geq\eta\}} \frac{\sigma(x-y)}{|x-y|^2}\, dy \right| &\leq \left| \int_{\mathcal{D}\cap\{\eta\leq|x-y|\leq d(x)\}} \frac{\sigma(x-y)}{|x-y|^2}\, dy \right| \\ &\quad + \left| \int_{\mathcal{D}\cap\{d(x)\leq|x-y|<\delta\}} \frac{\sigma(x-y)}{|x-y|^2}\, dy \right| \\ &\quad + \left| \int_{\mathcal{D}\cap\{|x-y|\geq\delta\}} \frac{\sigma(x-y)}{|x-y|^2}\, dy \right|. \end{aligned}$$

We know that the first integral vanishes due to symmetry, and the third term can be estimated as in the $d(x) \leq \delta$ case.

For the second one, we denote

$$S = \{d(x) \leq |x-y| \leq \delta\}$$

and study its special geometrical properties. The heuristic is the following. Assume that the boundary is a straight line, then we try to bound the integral by estimating the area of the integration in which the integral doesn't vanish. This is where the regularity of the boundary comes in to play. To make the above idea rigorous, we denote by $\tilde{x}$ the point on $\partial\mathcal{D}$ such that $d(x, \tilde{x}) = d(x)$. Let $\mathcal{L}$ be the line through x in the direction that is tangent to $\partial\mathcal{D}$ at $\tilde{x}$. Then the annulus $\{d(x) \leq |x-y| \leq \delta\}$

is divided into two half annuli. Denote the one containing $\tilde{x}$ by A_s and the other by A_l. First note that the integration on A_l vanishes. So

$$\left|\int_{S\cap\mathcal{D}} \frac{\sigma(x-y)}{|x-y|^2}\,dy\right| = \left|\int_{(A_s\cap\mathcal{D})\cup(A_l\cap\mathcal{D}^c)} \frac{\sigma(x-y)}{|x-y|^2}\,dy\right| \le \int_{(A_s\cap\mathcal{D})\cup(A_l\cap\mathcal{D}^c)} \frac{C}{|x-y|^2}\,dy.$$

Note that S should more and more resembles a half-annulus as $d(x)\to 0$. So our integral should vanish. We estimate the area of $S_e \equiv (A_s\cap\mathcal{D})\cup(A_l\cap\mathcal{D}^c)$. Write it in polar coordinates and denote by $H(E_\rho)$ the 1-D Hausdorff measure of

$$\{\theta\in(0,2\pi]\mid(\rho,\theta)\in S_e\}\,.$$

for $d(x)\le\rho\le\delta$. By the Geometric lemma that will be proved later,

$$H(E_\rho)\le C\left(\frac{d(x)}{\rho}+\left(\frac{\rho}{\delta}\right)^{\mu}\right)$$

and then the result is straightforward. □

Now we prove the Geometric Lemma.

Lemma 7.6. *(Geometric Lemma). We have*

$$H(E_\rho)\le 2\pi\left[(1+2^\mu)\frac{d(x_0)}{\rho}+2^\mu\left(\frac{\rho}{\delta}\right)^{\mu}\right]$$

for all $\rho\ge d(x_0)$, $1>\mu>0$ *and* x_0 *so that* $d(x_0)<\delta=\left(|\nabla\phi|_{inf}\,/\,|\nabla\varphi|_\mu\right)^{1/\mu}$.

Proof. Let

$$S_\rho(x_0)=\{z\mid |z|=1, x=x_0+\rho z\in\mathcal{D}\}\,,$$
$$\Sigma(x_0)=\{z\mid |z|=1, \nabla_x\varphi(\tilde{x})\cdot z\ge 0\}$$

where $\tilde{x}\in\partial\mathcal{D}$ such that $|x_0-\tilde{x}|=d(x_0)$. This point exists since the boundary is $C^{1,\mu}$. Then we have

$$E_\rho=[S_\rho\backslash\Sigma_\rho]\cup[\Sigma_\rho\backslash S_\rho]\,.$$

The readers should draw a picture to see what E_ρ looks like (there are two cases, $x_0\in\mathcal{D}$ and $x_0\notin\mathcal{D}$). Note that since $\varphi(x)>0$ for $x\in\mathcal{D}$, the direction of $\nabla\varphi$ at $\tilde{x}$ should be pointing inward instead of outward.

We use polar coordinates and denote the angle for a point z in E_ρ by $\theta(z)$, with $\theta(z)$ defined by

$$\sin\theta(z)=\frac{\nabla\varphi(\tilde{x})\cdot z}{|\nabla\varphi(\tilde{x})|\cdot|z|}.$$

See the following illustration.

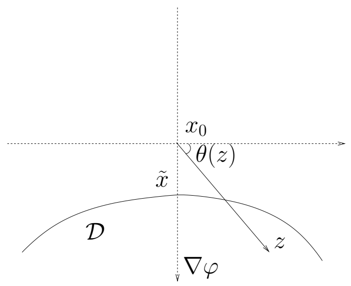

Thus we have

$$\sin\theta(z) = \frac{\nabla\varphi(\tilde{x})\cdot(\tilde{x}-x_0)}{|\nabla\varphi(\tilde{x})|\,\rho} + \frac{\nabla\varphi(\tilde{x})\cdot(x_0+\rho z-\tilde{x})}{|\nabla\varphi(\tilde{x})|\,\rho}.$$

Now in the RHS z is in the unit circle.

For any $z \in E_\rho(x_0)$, we can see that either $\sin\theta(z) > 0$ and $\varphi(x_0 + \rho z) < 0$ or $\sin\theta(z) < 0$ and $\varphi(x_0+\rho z) > 0$. In either case, noting that $\varphi(\tilde{x}) = 0$ and $\nabla\varphi(\tilde{x}) \parallel (x_0 - \tilde{x})$, we have

$$|\sin\theta(z)| \le \frac{d(x_0)}{\rho} + \left| \frac{\nabla\varphi(\tilde{x})\cdot(x_0+\rho z-\tilde{x})}{|\nabla\varphi(\tilde{x})|\,\rho} - \frac{\varphi(x_0+\rho z)-\varphi(\tilde{x})}{|\nabla\varphi(\tilde{x})|\,\rho} \right|.$$

Since $-\frac{\varphi(x_0+\rho z)}{|\nabla\varphi(\tilde{x})|\rho}$ is always of the same sign as $\sin\theta(z)$, so adding it will only increase the absolute value. Now by the mean value theorem we have

$$|\varphi(x) - \varphi(y) - \nabla\varphi(y)\cdot(x-y)| \le |\nabla\varphi|_\mu\, |x-y|^{1+\mu}$$

which gives

$$\begin{aligned}
|\sin\theta(z)| &\le \frac{d(x_0)}{\rho} + \frac{|\nabla\varphi|_\mu\, |x_0+\rho z-\tilde{x}|^{1+\mu}}{\rho\, |\nabla\varphi|_{inf}} \\
&\le \frac{d(x_0)}{\rho} + \frac{|\nabla\varphi|_\mu}{\rho\, |\nabla\varphi|_{inf}} \left[d(x_0)+\rho\right]^{1+\mu} \\
&\le \frac{d(x_0)}{\rho} + 2^\gamma \frac{|\nabla\varphi|_\mu}{\rho\, |\nabla\varphi|_{inf}} \left[d(x_0)^{1+\mu}+\rho^{1+\mu}\right]
\end{aligned}$$

where the last inequality comes from the Jensen's inequality applying to the convex function $x^{1+\mu}$ for positive x.

Now the estimate is easy to see by the fact that $\arcsin t \le \frac{\pi}{2} t$ for $t \in [0,1]$. Since we are estimating the absolute value of $\sin\theta$ over $[0, 2\pi]$, the factor should be $\frac{\pi}{2}\cdot 4 = 2\pi$. This completes the proof. □

Finally we take the dynamics into account.

Proposition 7.7. *If the initial data $\varphi_0 \in C^{1,\mu}(\mathbb{R}^2)$, such that $\mathcal{D}_0 = \{\varphi_0(x) > 0\}$ is simply connected and bounded. And $|\nabla\varphi_0| \geq C > 0$ on the boundary $\partial\mathcal{D}_0$, then the following a priori estimates holds:*

1. $\|\nabla\varphi(\cdot,t)\|_{L^\infty} \leq \|\nabla\varphi_0\|_{L^\infty} \exp\left(\int_0^t \|\nabla u(\cdot,s)\|_{L^\infty}\ ds\right)$;
2. $|\nabla\varphi(\cdot,t)|_{inf} \geq |\nabla\varphi_0|_{inf} \exp\left(-\int_0^t \|\nabla u(\cdot,s)\|_{L^\infty}\ ds\right)$;
3. $|\nabla\varphi(\cdot,t)|_\mu \leq |\nabla\varphi_0|_\mu \exp\left((C_0+\mu)\int_0^t \|\nabla u(\cdot,s)\|_{L^\infty}\ ds\right)$.

Proof. Let $X = X(\alpha,t)$ denote a particle trajectory and

$$Y(\alpha,t) = \nabla^\perp\varphi(X(\alpha,t),t).$$

Then we have

$$\frac{d}{dt}Y(\alpha,t) = \nabla u(X(\alpha,t),t)Y(\alpha,t).$$

and therefore

$$\left|\frac{d}{dt}\log|Y(\alpha,t)|\right| \leq \|Du(\cdot,t)\|_{L^\infty}.$$

Now by Gronwall's lemma we have

$$e^{-\int_0^t \|\nabla u\|_{L^\infty}\ ds} \leq \frac{|Y(\alpha,t)|}{|\nabla^\perp\varphi_0(\alpha)|} \leq e^{\int_0^t \|\nabla u\|_{L^\infty}\ ds},$$

which proves both (1). and (2).

For (3), we write the integral formulation of the equation for $\nabla^\perp\varphi$,

$$\nabla^\perp\varphi(x,t) = \nabla^\perp\varphi_0(X(x,-t)) + \int_0^t \left(\nabla u\nabla^\perp\varphi\right)(X(x,s-t),s)\ ds.$$

And we estimate

$$\begin{aligned}
&\left|\nabla^\perp\varphi(x+h,t) - \nabla^\perp\varphi(x,t)\right| \leq \left|\nabla^\perp\varphi_0\left(X(x+h,-t)\right) - \nabla^\perp\varphi_0\left(X(x,-t)\right)\right| \\
&+\left|\int_0^t \left(\left(\nabla u\nabla^\perp\varphi\right)(X(x+h,s-t),s) - \left(\nabla u\nabla^\perp\varphi\right)(X(x,s-t),s)\right)\ ds\right| \\
&\leq \left|\nabla^\perp\varphi_0\right|_\mu \|\nabla X(\cdot,-t)\|_{L^\infty}^\mu |h|^\mu \\
&+\int_0^t \left|\nabla u\nabla^\perp\varphi(\cdot,s)\right|_\mu \|\nabla X(\cdot,s-t)\|_{L^\infty}^\mu |h|^\mu\ ds.
\end{aligned}$$

For the evolution of ∇X, we have

$$\frac{d}{dt}\nabla X(z,-t) = -\nabla u\left(X(z,-t),-t\right)\nabla X(z,-t).$$

Now by the Gronwall's lemma we have

$$\|\nabla X(\cdot, s-t)\|_{L^\infty} \leq \exp\left(\int_s^t \|\nabla u(\cdot, s')\|_{L^\infty}\ ds'\right).$$

Plug it into the inequality above, we get the estimate in (3). □

Finally we put everything together, and obtain the following theorem:

Theorem 7.8. *Given $\omega_0 \neq 0$, $\mathcal{D}_0$ a simply connected, bounded, $C^{1,\mu}$ smooth domain with $0 < \mu < 1$, and a function $\varphi_0 \in C^{1,\mu}(\mathbb{R}^2)$ such that $\mathcal{D}_0 = \{\varphi_0 > 0\}$, $|\nabla\varphi_0|_{inf} \geq C > 0$, then the solution φ belongs to $C^{1,\mu}$ for all time. Furthermore, there exists a constant $C > 0$, which depends only on the initial data such that*

1. $\|\nabla u(\cdot, t)\|_{L^\infty} \leq \|\nabla u_0\|_{L^\infty} e^{Ct}$,
2. $|\nabla\varphi(\cdot, t)|_\mu \leq |\nabla\varphi_0|_\mu \exp\left((C_0 + \mu)\, e^{Ct}\right)$,
3. $\|\nabla\varphi(\cdot, t)\|_{L^\infty} \leq \|\nabla\varphi_0\|_{L^\infty} \exp\left(e^{Ct}\right)$,
4. $|\nabla\varphi(\cdot, t)|_{inf} \geq |\nabla\varphi_0|_{inf} \exp\left(-e^{Ct}\right)$.

Proof. We have

$$\log|\nabla\varphi|_{inf} \geq \log|\nabla\varphi_0|_{inf} - C\int_0^t \left(1 + \log\frac{|\nabla\varphi|_\mu}{|\nabla\varphi|_{inf}}\right)\ ds$$

after taking logarithm on both sides of estimate (2) in Proposition 5.2.7. Similarly we obtain

$$\log|\nabla\varphi|_\mu \leq \log|\nabla\varphi_0|_\mu + (C_0 + \mu)\int_0^t \left(1 + \log\frac{|\nabla\varphi|_\mu}{|\nabla\varphi|_{inf}}\right)\ ds.$$

Combining these two, we have

$$\log\frac{|\nabla\varphi|_\mu}{|\nabla\varphi|_{inf}} \leq \log\frac{|\nabla\varphi_0|_\mu}{|\nabla\varphi_0|_{inf}} + (C_0 + \mu + 1)\int_0^t \left(1 + \log\frac{|\nabla\varphi|_\mu}{|\nabla\varphi|_{inf}}\right)\ ds.$$

By Gronwall's lemma, we easily get

$$\log\frac{|\nabla\varphi|_\mu}{|\nabla\varphi|_{inf}} \leq Ce^{Ct}.$$

This also provides a bound for ∇u in (1) from Proposition 5.2.5. The others are straightfoward by using the estimate on ∇u given by Property (1). □

Remark 7.9. The problem of global existence of vortex patch with boundary only C^1 or worse is still open. In [6], J. Carrillo and J. Soler showed numerically that, for initial boundary that is only Lipschitz continuous, the evolution develops cusps from corners.

References

[1] Adams, R. A., Sobolev Spaces, Academic Press, New York 1975.

[2] Arnold V. I., Khesin, B., Topological Methods in Hydrodynamics, Applied Mathematical Sciences 125, Springer, 1998.

[3] Bergh J., Löfström, J., Interpolation Spaces: An Introduction, Springer-Verlag, 1976.

[4] Bertozzi, A., Constantin, P., Global regularity for vortex patches, Comm. Math. Phys., 152 (1993), 19–26.

[5] Caflisch, R. E., Orellana, O. F., Long Time Existence for a Slightly Perturbed Vortex Sheet, Comm. Pure Appl. Math., 39 (1986), 807–838.

[6] Carrillo, J. A., Soler, J., On the Evolution of an Angle in a Vortex Patch, Journal of Nonlinear Science, 10 (2000), no. 1, 23–47.

[7] Chae, D., On the well-posedness of the Euler equations in the Triebel-Lizorkin spaces, Comm. Pure Appl. Math., 55 (2002), 654-678.

[8] Chae, D., On the Euler equations in the critical Triebel-Lizorkin spaces, Arch. Ration. Mech. Anal., 170 (2003), 185-210.

[9] Chae, D., Remarks on the blow-up criterion of the three-dimensional Euler equations, Nonlinearity, 18 (2005), 1021-1029.

[10] Chemin, J. Y., Sur le mouvement des particules d'un fluide parfait incompressible bidimensionnels, Invent. Math., 103 (1991), 599–629.

[11] Chorin, A., Vorticity and Turbulence, Applied Mathematical Sciences 103, Springer-Verlag, 1994.

[12] Chorin, A. J., Marsden, J. E., A Mathematical Introduction to Fluid Mechanics, 2nd ed., Texts in Applied Mathematics 4, Springer-Verlag, 1990.

[13] Constantin, P., Geometric statistics in turbulence, SIAM Review, 36 (1994), 73–98.

[14] Constantin, P., Fefferman, C., and Majda, A., Geometric constraints on potentially singular solutions for the 3-D Euler equations, Comm. PDE, 21 (1996), no. 3&4, 559–571.

[15] Constantin, P., Majda, A. J., Tabak, E., Formation of strong fronts in the 2-D quasigeostrophic thermal active scalar, Nonlinearity 7(1994), 1495–1533.

[16] Constantin, P., Nie, Q., Schörghofer, N., Nonsingular Surface-Quasi-Geostrophic Flow, Phys. Lett. A, 241(1998), 168–172.

[17] Cordoba, D., Nonexistence of simple hyperbolic blow-up for the quasi-geostrophic equation, Annals of Mathematics, 148 (1998), 1135–1152.

[18] Cordoba, D., Fefferman, C., Growth of solutions for QG and 2D Euler equations, J. AMS, 15 (2002), no. 3, 665–670.

[19] Deng, J., Hou, T. Y., and Yu, X., Geometric Properties and Non-blowup of 3-D Incompressible Euler Flow, Comm. PDE., 30 (2005), no. 1, 225-243.

[20] Deng, J., Hou, T. Y., and Yu, X., A Level Formulation for the 3D Incompressible Euler Equations, Methods and Applications of Analysis, 12 (2005), no. 4, 427-440.

[21] Deng, J., Hou, T. Y., and Yu, X., Improved Geometric Conditions for Non-blowup of the 3D Incompressible Euler Equation, Comm. PDE., 31 (2006), no. 2, 293-306.

[22] Deng, J., Hou, T. Y., Li, R. and Yu, X., Level Set Dynamics and Non-blowup of the 2D Quasi-geostrophic Equation, accepted by Methods and Applications of Analysis, 2008.

[23] Ebin, D.G., Fischer, A. E., and Marsden, J. E., Diffeomorphism groups, hydrodynamics and relativity. In Vanstone, J., editor, Prod. of the 13th Biennial Seminar of Canadian Mathematical Congress, 135 – 279, Montreal.

[24] Goodman, J., Hou, T.Y., Lowengrub, J., The Convergence of the Point Vortex Method for the 2-D Euler Equations, Comm. Pure Appl. Math., 43 (1990), 415-430.

[25] Hou, T. Y., Li, R., Dynamic Depletion of Vortex Stretcing and Non-Blowup of the 3-D Incompressible Euler Equations, J. Nonlinear Science, 16 (2006), no. 6, 639-664.

[26] Kerr, R. M., Evidence for a singularity of the three-dimensional incompressible Euler equations, Phys. Fluids A, 5 (1993), 1725–1746.

[27] Kerr, R. M., The role of singularities in Euler, in Small-scale structure in hydro and magnetohydrodynamic turbulence, eds. Pouquet, A., Sulem, P. L., Lecture Notes, Springer-Verlag, 1995.

[28] Kerr, R. M., Euler Singularities and Turbulence, in 19th ICTAM Kyoto' 96, Eds. Tatsumi, T., Watanabe, E., Kambe, T., Elsevier Science, 1997.

[29] Kerr, R. M., The Outer Regions in Singular Euler, in Fundamental Problematic Issues in Turbulence, eds. Tsinober and Gyr, Birkhäuser, 1998.

[30] Kozono, H., Taniuchi, Y., Bilinear estimates in BMO and to the Navier-Stokes equations, Math. Z., 235 (2000), 173–194.

[31] Lamb, H., Hydrodynamics, 6th ed., Dover, 1945.

[32] Lions, P. L., Mathematical Topics in Fluid Mechanics, Vol. 1. Incompressible Models, Oxford Lecture Series in Mathematics and its Applications 3, Oxford Science Publications, 1996.

[33] Lopes Filho, M.C., Nussenzveig Lopes, H.J. and Zheng, Y., Weak solutions to the equations of incompressible, ideal flow. Text of minicourse for the 22nd Brazilian Colloquium of Mathematics, 1999. Full text at http://www.ime.unicamp.br/˜mlopes/publications.html.

[34] Majda, A., Vorticity and the mathematical theory of Incompressible fluid flow, Comm. Pure. Appl. Math., 39 (1986), 187–220.

[35] Majda, A. J., Bertozzi, A. L., Vorticity and Incompressible Flow, Cambridge Texts in Applied Mathematics, Cambridge University Press, 2002.

[36] Marchioro, C., Pulvirenti, M., Mathematical Theory of Incompressible Nonviscous Fluids, Chapter 6. Applied Mathematical Sciences 96. Springer-Verlag, 1994.

[37] Meyer, Y., Coifman, R., Wavelets: Calderón-Zygmund operators and multilinear operators, Cambridge University Press, 1997.

[38] Ohkitani, K., Yamada, M., Inviscid and inviscid-limit behavior of a surface quasigeostrophic flow, Phys. Fluids 9 (1997), no. 4, 876–882.

[39] Pelz, R. B., Locally self-similar, finite-time collapse in a high-symmetry vortex filament model, Physical Review E, 55 (1997), no. 2, 1617–1620.

[40] Pelz, R. B., Symmetry and the hydrodynamic blow-up problem, J. Fluid Mech., 444 (2001), 299–320.

[41] Pedlosky, J., Geophysical Fluid Dynamics, 345 – 368, 653–670, Springer, 1987.

[42] Planchon, F., An extension of the Beale-Kato-Majda criterion for the Euler equations, Comm. Math. Phys., 232 (2003), 319-326.

[43] Ponce, G., Remarks on a paper by J. T. Beale, T. Kato, and A. Majda, Comm. Math. Phys., 98 (1985), 349–353.

[44] Stein, E., Singular Integrals and Differentiability Properties of Functions, Princeton University Press, 1970.

[45] Stein, E., Harmonic Analysis, Princeton University Press, 1993.

[46] Wolff, T., Lecture Notes on Harmonic Analysis, University Lecture Series, 29, AMS, 2003.

Acta Numerica (2009), pp. 1–70
doi: 10.1017/S0962492906420018

Blow-up or no blow-up? A unified computational and analytic approach to 3D incompressible Euler and Navier–Stokes equations

Thomas Y. Hou
Applied and Computational Mathematics, 217-50,
Caltech, Pasadena, CA 91125, USA
E-mail: hou@acm.caltech.edu

Whether the 3D incompressible Euler and Navier–Stokes equations can develop a finite-time singularity from smooth initial data with finite energy has been one of the most long-standing open questions. We review some recent theoretical and computational studies which show that there is a subtle dynamic depletion of nonlinear vortex stretching due to local geometric regularity of vortex filaments. We also investigate the dynamic stability of the 3D Navier–Stokes equations and the stabilizing effect of convection. A unique feature of our approach is the interplay between computation and analysis. Guided by our local non-blow-up theory, we have performed large-scale computations of the 3D Euler equations using a novel pseudo-spectral method on some of the most promising blow-up candidates. Our results show that there is tremendous dynamic depletion of vortex stretching. Moreover, we observe that the support of maximum vorticity becomes severely flattened as the maximum vorticity increases and the direction of the vortex filaments near the support of maximum vorticity is very regular. Our numerical observations in turn provide valuable insight, which leads to further theoretical breakthrough. Finally, we present a new class of solutions for the 3D Euler and Navier–Stokes equations, which exhibit very interesting dynamic growth properties. By exploiting the special nonlinear structure of the equations, we prove nonlinear stability and the global regularity of this class of solutions.

CONTENTS

1. Introduction

The question of whether the 3D incompressible Navier–Stokes equations can develop a finite-time singularity from smooth initial data is one of the most long-standing open problems in fluid dynamics and mathematics. This is also one of the seven Millennium Open Problems posted by the Clay Mathematical Institute (see www.claymath.org). The understanding of this problem could improve our understanding on the onset of turbulence and the intermittency properties of turbulent flows.

The 3D incompressible Navier–Stokes equations are given by

$$\mathbf{u}_t + (\mathbf{u}\cdot\nabla)\mathbf{u} = -\nabla p + \nu\Delta\mathbf{u}, \tag{1.1}$$

$$\nabla\cdot\mathbf{u} = 0, \tag{1.2}$$

with initial condition $\mathbf{u}(\mathbf{x},0) = \mathbf{u}_0(\mathbf{x})$. Here $\mathbf{u}$ is velocity, p is pressure, and ν is viscosity. We consider only the initial value problem and assume that the solution decays rapidly at infinity. Defining vorticity by $\boldsymbol{\omega} = \nabla\times\mathbf{u}$, then $\boldsymbol{\omega}$ is governed by

$$\boldsymbol{\omega}_t + (\mathbf{u}\cdot\nabla)\boldsymbol{\omega} = \nabla\mathbf{u}\cdot\boldsymbol{\omega} + \nu\Delta\boldsymbol{\omega}. \tag{1.3}$$

The first term on the right-hand side of (1.3) is called the vortex stretching term, which is absent in the two-dimensional problem. Note that $\nabla\mathbf{u}$ is formally of the same order as $\boldsymbol{\omega}$. Thus the vortex stretching term has a formal quadratic scaling with respect to vorticity. This formal quadratic nonlinearity in the vortex stretching term is the main difficulty in studying the dynamic stability and global regularity of the 3D Navier–Stokes equations. Under suitable smallness assumptions on the initial condition, global existence and regularity results have been obtained for some time (Ladyzhenskaya 1970, Constantin and Foias 1988, Temam 2001, Majda and Bertozzi 2002). But these methods based on energy estimates do not generalize to the 3D Navier–Stokes with large data. Energy estimates seem to be too crude to give a definite answer to whether diffusion is strong enough to control the nonlinear growth due to vortex stretching. A more refined analysis seems to be needed, which takes into account the special nature of the nonlinearities and their local interactions.

We believe that the global regularity of the 3D Navier–Stokes equations is closely related to that of the 3D Euler equations. Since the nonlinearity of the 3D Navier–Stokes equations is supercritical, the balance among different nonlinear terms in the Euler equations may play an even more important role than the diffusion term. Thus, it makes sense to investigate the mechanism which may lead to finite-time blow-up or dynamic depletion of the nonlinear vortex stretching in the 3D Euler equations.

There has been some interesting development in the theoretical understanding of the 3D incompressible Euler equations. In particular, Constantin, Fefferman and Majda have shown that the local geometric regularity of vortex lines can play an important role in depleting nonlinear vortex stretching (Constantin 1994, Constantin, Fefferman and Majda 1996). Inspired by their work, Deng, Hou and Yu (2005, 2006*a*) recently showed that geometric regularity of vortex lines, even in an extremely localized region containing the maximum vorticity, can lead to depletion of nonlinear vortex stretching, thus avoiding finite-time singularity formation of the 3D Euler equations. To obtain these results, Deng, Hou and Yu used a Lagrangian approach and explored the connection between the stretching of local vortex lines and the growth of vorticity. In particular, they showed that if the vortex lines near the region of maximum vorticity satisfy some local geometric regularity conditions and the maximum velocity field is integrable in time, then no finite-time blow-up is possible. These localized non-blow-up criteria provide stronger constraints on the local geometry of a potential finite-time singularity.

There have been many computational attempts to find finite-time singularities of the 3D Euler and Navier–Stokes equations: see, *e.g.*, Chorin (1982), Pumir and Siggia (1990), Kerr and Hussain (1989), Grauer and Sideris (1991), Shelley, Meiron and Orszag (1993), Kerr (1993), Caflisch (1993), Boratav and Pelz (1994), Fernandez, Zabusky and Gryanik (1995), Pelz (1997), Grauer, Marliani and Germaschewski (1998), Kerr (2005). One example that has been studied extensively is the interaction of two perturbed antiparallel vortex tubes. This example is interesting because of the vortex reconnection observed for the corresponding Navier–Stokes equations. It is natural to ask whether the 3D Euler equations would develop a finite-time singularity in the limit of vanishing viscosity. Kerr (1993, 2005) presented numerical evidence which suggested a finite-time singularity of the 3D Euler equations for two perturbed antiparallel vortex tubes. Kerr's blow-up scenario is consistent with the non-blow-up criterion of Beale, Kato and Majda (1984) and that of Constantin, Fefferman and Majda (1996). But it falls into the critical case of Deng, Hou and Yu's local non-blow-up criteria (Deng, Hou and Yu 2005, 2006*a*).

Guided by this local geometric non-blow-up analysis, Hou and Li (2006) performed *extremely large-scale computations* with resolution up to $1536 \times 1024 \times 3072$ to re-examine Kerr's blow-up scenario (Kerr 1993). They used a novel pseudo-spectral method with a 36th-order Fourier smoothing function which keeps a significant portion of the Fourier modes beyond the 2/3 cut-off point in the Fourier spectrum for the 2/3 de-aliasing rule. Their extensive numerical results demonstrated that the pseudo-spectral method with the high-order Fourier smoothing gives a much better performance than the pseudo-spectral method with the 2/3 de-aliasing rule. In particular, they showed that the Fourier smoothing method captures about $12 \sim 15\%$ more effective Fourier modes than the 2/3 de-aliasing method in each dimension. For 3D Euler equations, the total number of effective modes in the Fourier smoothing method is about 20% more than that in the 2/3 de-aliasing method. This is a very significant increase in the resolution for a large-scale computation.

There were several interesting findings in the large-scale computations of Hou and Li (2006) for the 3D Euler equations using the initial data for the antiparallel vortex tubes. First, they discovered a surprising dynamic cancellation in the vortex stretching term due to the local geometric regularity of the vortex filaments. Vortex stretching was found to deplete dynamically from a formally quadratic nonlinearity to a much weaker $O(\omega \log(\omega))$ type of nonlinearity, which leads to only double exponential growth in the maximum vorticity. Secondly, they showed that the velocity field is bounded up to $T = 19$, beyond the alleged singularity time $T = 18.7$ of Kerr (2005). With a bounded velocity field, the non-blow-up criterion of Deng, Hou and Yu (2005) applies, which provides theoretical support for their computational results. Thirdly, they found that the vorticity vector near the point of maximum vorticity aligns almost perfectly with the second eigenvector of the rate of strain tensor. The second eigenvalue of the rate of strain tensor is the smallest eigenvalue and does not seem to grow dynamically, while the first and third eigenvalues grow very rapidly in time. This is further strong evidence for the dynamic depletion of vortex stretching.

Inspired by the numerical findings of their paper of 2006, Hou and Li (2008*a*) investigated the dynamic stability of the 3D Navier–Stokes equations by introducing an exact 1D model of the axisymmetric Navier–Stokes equations along the symmetry axis. This 1D model is exact in the sense that one can construct a family of exact solutions for the 3D Navier–Stokes equations from this 1D model. Thus the 1D model preserves some essential features of the 3D Navier–Stokes equations. What is surprising is that they obtained a Lyapunov function which satisfies a new maximum principle. This provides a pointwise estimate on the dynamic stability of the Navier–Stokes equations. The traditional energy estimates are incapable of capturing such subtle cancellation effects. Based on the global regularity of the 1D model, they constructed a new class of solutions for the 3D Euler and Navier–Stokes equations, which exhibit very interesting dynamic growth properties, but remain smooth for all times.

Motivated by the work of Hou and Li (2008*a*), Hou and Lei (2009*b*) further proposed a new 3D model to study the stabilizing effect of convection. This model was derived by neglecting the convection term from a reformulated axisymmetric Navier–Stokes equations. It shares almost all the properties of the 3D Navier–Stokes equations. In particular, the strong solution of the model satisfies an energy identity similar to that of the full 3D Navier–Stokes equations. They proved a non-blow-up criterion of Beale–Kato–Majda type as well as a non-blow-up criterion of Prodi–Serrin type for the model. Moreover, they proved that, for any suitable weak solution of the 3D model in an open set in space-time, the one-dimensional Hausdorff measure of the associated singular set is zero (Hou and Lei 2009*a*). This partial regularity result is an analogue of the Caffarelli–Kohn–Nirenberg theory (Caffarelli, Kohn and Nirenberg 1982) for the 3D Navier–Stokes equations.

Despite the striking similarity at the theoretical level between the 3D model and the Navier–Stokes equations, the former has a completely different behaviour from the full Navier–Stokes equations. Hou and Lei's study showed that the 3D model seems to form a finite-time singularity, while the mechanism of generating such a finite-time singularity is removed when convection is added back to the 3D model. Convection seems to play a very important role in stabilizing the potential blow-up of the Navier–Stokes equations. This result may have an important impact on future global regularity analysis of 3D Navier–Stokes equations. Up to now, most analysis uses energy estimates in which convection plays no role at all. Such global methods of analysis are too crude. Their studies suggest that one needs to develop a new localized analysis which can in essence exploit the stabilizing effect of convection.

There has been some interesting development in the study of the 3D incompressible Navier–Stokes equations and related models. By exploiting the special structure of the governing equations, Cao and Titi (2007) proved the global well-posedness of the 3D viscous primitive equation for large-scale ocean and atmospheric dynamics. For the axisymmetric Navier–Stokes equations, Chen, Strain, Tsai and Yau (2008, 2009) and Koch, Nadirashvili, Seregin and Sverak (2009) recently proved that if $|\mathbf{u}(x,t)| \leq C_*|t|^{-1/2}$, where C_* is allowed to be large, then the velocity field $\mathbf{u}$ is regular at time zero. The 2D Boussinesq equations are closely related to the 3D axisymmetric Navier–Stokes equations with swirl (away from the symmetry axis). Recently, Hou and Li (2005) and Chae (2006) proved independently the global existence of the 2D Boussinesq equations with partial viscosity. By taking advantage of the limiting property of some rapidly oscillating operators and using nonlinear averaging, Babin, Mahalov and Nicolaenko (2001) proved global regularity of the 3D Navier–Stokes equations for some initial data characterized by uniformly large vorticity.

The rest of the paper is organized as follows. In Section 2, we study the dynamic depletion of vortex stretching for the 3D Euler equations. We also discuss at length how to design an effective high-resolution pseudo-spectral method to compute potentially singular solutions of the 3D Euler equations. Section 3 is devoted to studying the dynamic stability of the 3D Navier–Stokes equations. In Section 4, we investigate the stabilizing effect of convection for the 3D Navier–Stokes equations. Some concluding remarks are made in Section 5.

2. Dynamic depletion of vortex stretching in 3D Euler equations

Due to the supercritical nature of the nonlinearity of the 3D Navier–Stokes equations, the 3D Navier–Stokes equations with large initial data are convection-dominated, instead of diffusion-dominated. For this reason, we believe that the understanding of whether the corresponding 3D Euler equations would develop a finite-time blow-up could shed useful light on the global regularity of the Navier–Stokes equations.

Let us consider the 3D Euler equations in the vorticity form. One important observation is that when we consider the convection term together with the vortex stretching term, the two nonlinear terms can be actually represented as a commutator or a Lie derivative:

$$\boldsymbol{\omega}_t + (\mathbf{u}\cdot\nabla)\boldsymbol{\omega} - (\boldsymbol{\omega}\cdot\nabla)\mathbf{u} = 0. \tag{2.1}$$

It is reasonable to believe that the commutator would lead to some cancellation among the two nonlinear terms, thus weakening the nonlinearity dynamically. This points to the potential important role of convection in the 3D Euler equations. Another way to realize the importance of convection is to use the Lagrangian formulation of the vorticity equation. When we consider the two terms together, we preserve the Lagrangian structure of the solution (Chorin and Marsden 1993),

$$\boldsymbol{\omega}(X(\alpha,t),t) = X_\alpha(\alpha,t)\boldsymbol{\omega}_0(\alpha), \tag{2.2}$$

where $X_\alpha = \frac{\partial X}{\partial \alpha}$ and $X(\alpha,t)$ is the flow map,

$$\frac{\mathrm{d}X}{\mathrm{d}t}(\alpha,t) = \mathbf{u}(X(\alpha,t),t), \quad X(\alpha,0)=\alpha. \tag{2.3}$$

Therefore, vorticity increases in time only through the dynamic deformation of the Lagrangian flow map. On the other hand, due to the divergence-free property of the velocity field, the flow map is volume-preserving, that is,

$\det(X_\alpha(\alpha,t)) \equiv 1$. Thus, as vorticity increases dynamically, the parallelepiped spanned by the three vectors, $(X_{\alpha_1}, X_{\alpha_2}, X_{\alpha_3})$, will experience severe deformation and become flattened dynamically. A formal asymptotic analysis shows that the support of maximum vorticity also experiences a similar deformation and becomes severely flattened as vorticity increases. This is confirmed by our numerical experiments: see Section 2.5. Such deformation tends to weaken the nonlinearity of vortex stretching dynamically.

We remark that convection plays an essential role in deforming the support of maximum vorticity and induces an anisotropic scaling in the collapse of the support of maximum vorticity. By exploiting the anisotropic scaling of the support of maximum vorticity, Hou, Lei and Li (2008) recently proved the global regularity of the axisymmetric Navier–Stokes equations with a family of very large anisotropic initial data: see Section 2.8 for more discussions. On the other hand, if we ignore the convection term in the Euler equations, the vortex stretching term may indeed achieve the $O(|\omega|^2)$ scaling dynamically and develop an isotropic singularity in finite time: see Section 4 for more discussions.

2.1. A brief review

We begin with a brief review of the subject. Due to the formal quadratic nonlinearity in vortex stretching, only short time existence is known for the 3D Euler equations (Majda and Bertozzi 2002). One of the most well-known results on the 3D Euler equations is due to Beale, Kato and Majda (1984), who showed that the solution of the 3D Euler equations blows up at T if and only if $\int_0^T \|\boldsymbol{\omega}\|_\infty(t)\,\mathrm{d}t = \infty$, where $\boldsymbol{\omega}$ is vorticity.

There have been some interesting recent theoretical developments. In particular, Constantin, Fefferman and Majda (1996) showed that local geometric regularity of the unit vorticity vector can lead to depletion of the vortex stretching. Let $\boldsymbol{\xi} = \boldsymbol{\omega}/|\boldsymbol{\omega}|$ be the unit vorticity vector and let $\mathbf{u}$ be the velocity field. Roughly speaking, Constantin, Fefferman and Majda proved that if (1) $\|\mathbf{u}\|_\infty$ is bounded in a $O(1)$ region containing the maximum vorticity, (2) $\int_0^t \|\nabla\boldsymbol{\xi}\|_\infty^2\,\mathrm{d}\tau$ is uniformly bounded for $t < T$, then the solution of the 3D Euler equations remains regular up to $t = T$.

There has been some numerical evidence that suggests a finite-time blow-up of the 3D Euler equations. One of the most well-known examples is the finite-time collapse of two antiparallel vortex tubes by R. Kerr (1993, 2005). In his computations, Kerr used a pseudo-spectral discretization in the x- and y-directions, and a Chebyshev discretization in the z-direction with resolution of order $512 \times 256 \times 192$. His computations showed that the maximum vorticity blows up like $O((T-t)^{-1})$ with $T = 18.9$. In his subsequent paper, Kerr (2005) applied a high wavenumber filter to the data obtained in his original computations to ‘remove the noise that masked the structures in earlier graphics' presented in the 1993 paper. With this filtered solution, he presented some scaling analysis of the numerical solutions up to $t = 17.5$. Two new properties were presented in the 2005 paper. First, the velocity field was shown to blow up like $O(T-t)^{-1/2}$ with T being revised to $T = 18.7$. Secondly, he showed that the blow-up is characterized by two anisotropic length scales, $\rho \approx (T-t)$ and $R \approx (T-t)^{1/2}$. It is worth noting that there is still a considerable gap between the predicted singularity time $T = 18.7$ and the final time $t = 17$ of Kerr's original computations, which he used as the primary evidence for the finite-time singularity.

Kerr's blow-up scenario is consistent with the non-blow-up criterion of Beale, Kato and Majda (1984) and that of Constantin, Fefferman and Majda (1996). But it falls into the critical case of Deng, Hou and Yu's local non-blow-up criteria (Deng, Hou and Yu 2005, 2006*a*). Below we describe the local non-blow-up criteria of Deng, Hou and Yu.

2.2. The local non-blow-up criteria of Deng, Hou and Yu (2005, 2006a)

Motivated by the result of Constantin, Fefferman and Majda (1996), Deng, Hou and Yu (2005) have obtained a sharper non-blow-up condition which uses only very localized information of the vortex lines. Assume that at each time t there exists some vortex line segment L_t on which the local maximum vorticity is comparable to the global maximum vorticity. Further, we denote $L(t)$ as the arclength of L_t, $\mathbf{n}$ the unit normal vector of L_t, and κ the curvature of L_t.

Theorem 2.1. (Deng, Hou and Yu 2005) Assume that (1) $\max_{L_t}(|\mathbf{u}\cdot\boldsymbol{\xi}| + |\mathbf{u}\cdot\mathbf{n}|) \le C_U(T-t)^{-A}$ with $A < 1$, and (2) $C_L(T-t)^B \le L(t) \le C_0/\max_{L_t}(|\kappa|,\ |\nabla\cdot\boldsymbol{\xi}|)$ for $0 \le t < T$. Then the solution of the 3D Euler equations remains regular up to $t = T$ provided that $A + B < 1$.

In Kerr's computations, the first condition of Theorem 2.1 is satisfied with $A = 1/2$ if we use $\|\mathbf{u}\|_\infty \le C(T-t)^{-1/2}$ as alleged in Kerr (2005). Kerr's computations suggested that κ and $\nabla\cdot\boldsymbol{\xi}$ are bounded by $O((T-t)^{-1/2})$ in the inner region of size $(T-t)^{1/2}\times(T-t)^{1/2}\times(T-t)$ (Kerr 2005). Moreover, the length of the vortex tube in the inner region is of order $(T-t)^{1/2}$. If we choose a vortex line segment of length $(T-t)^{1/2}$ (*i.e.*, $B = 1/2$), then the second condition is satisfied. However, we violate the condition $A + B < 1$. Thus Kerr's computations fall into the critical case of Theorem 2.1. In a subsequent paper, Deng, Hou and Yu (2006*a*) improved the non-blow-up condition to include the critical case, $A + B = 1$.

Theorem 2.2. (Deng, Hou and Yu 2006*a*) Under the same assumptions as Theorem 2.1, in the case of $A + B = 1$, the solution of the 3D Euler equations remains regular up to $t = T$ if the scaling constants C_U, C_L and C_0 satisfy an algebraic inequality, $f(C_U, C_L, C_0) > 0$.

We remark that this algebraic inequality can be checked numerically if we obtain a good estimate of these scaling constants. For example, if $C_0 = 0.1$, which seems reasonable since the vortex lines are relatively straight in the inner region, Theorem 2.2 would imply no blow-up up to T if $2C_U < 0.43C_L$. Unfortunately, there was no estimate available for these scaling constants in Kerr (1993). One of our original motivations for repeating Kerr's computations using higher resolutions was to obtain a good estimate for these scaling constants.

2.3. Computing potentially singular solutions using pseudo-spectral methods

Computing Euler singularities numerically is an extremely challenging task. First of all, it requires huge computational resources. Tremendous resolutions are required to capture the nearly singular behaviour of the Euler equations. Secondly, one has to perform a careful convergence study. It is dangerous to interpret the blow-up of an under-resolved computation as evidence of finite-time singularities for the 3D Euler equations. Thirdly, if we believe that the numerical solution we compute leads to a finite-time blow-up, we need to demonstrate the validity of the asymptotic blow-up rate, *i.e.*, is the blow-up rate $\|\boldsymbol{\omega}\|_{L^\infty} \approx \frac{C}{(T-t)^\alpha}$ asymptotically valid as $t \to T$? If a numerical solution is well resolved only up to T_0 and there is still an order-one gap between T_0 and the predicted singularity time T, then one can not apply the Beale–Kato–Majda criterion (Beale, Kato and Majda 1984) to this fitted singularity, since the most significant contribution to $\int_0^T \|\boldsymbol{\omega}(t)\|_{L^\infty}\,\mathrm{d}t$ comes from the time interval $[T_0,\ T]$, but there is no accuracy in the extrapolated solution in this time interval if $(T - T_0) = O(1)$. Finally, one also needs to check if the blow-up rate of the numerical solution is consistent with other non-blow-up criteria (Constantin, Fefferman and Majda 1996, Deng, Hou and Yu 2005, Deng, Hou and Yu 2006*a*) which provide additional constraints on the blow-up rate of the velocity field and the local geometric regularity on the vortex filaments. The interplay between theory and numerics is clearly essential in our search for Euler singularities.

Hou and Li (2006, 2007) repeated Kerr's computations using two pseudo-spectral methods. The first pseudo-spectral method used the standard 2/3 de-aliasing rule to remove the aliasing error. For the second pseudo-spectral method, they used a novel 36th-order Fourier smoothing to remove the aliasing error. For the Fourier smoothing method, they used a Fourier smoother along the x_j-direction as follows: $\rho(2k_j/N_j) \equiv \exp(-36(2k_j/N_j)^{36})$, where k_j is the wavenumber ($|k_j| \le N_j/2$). The time integration was performed by using the classical fourth-order Runge–Kutta scheme. Adaptive time-stepping was used to satisfy the CFL stability condition with CFL number equal to $\pi/4$. In order to perform a careful resolution study, they used a sequence of resolutions: $768 \times 512 \times 1536$, $1024 \times 768 \times 2048$ and $1536 \times 1024 \times 3072$ in their computations. They computed the solution up to $t = 19$, beyond the alleged singularity time $T = 18.7$ by Kerr (2005). Their computations were carried out on the PC cluster LSSC-II in the Institute of Computational Mathematics and Scientific/Engineering Computing of Chinese Academy of Sciences and the Shenteng 6800 cluster in the Super Computing Center of the Chinese Academy of Sciences. The maximal memory consumption in their computations was about 120 Gbytes. The largest number of grid points is close to 5 billion.

2.4. Convergence study of spectral methods for the Burgers equation

As a first step, we demonstrate that the two pseudo-spectral methods can be used to compute a singular solution arbitrarily close to the singularity time. For this purpose, we perform a careful convergence study of the two pseudo-spectral methods in both physical and spectral spaces for the 1D inviscid Burgers equation. The advantage of using the inviscid 1D Burgers equation is that it shares some essential difficulties with the 3D Euler equations, yet we have a semi-analytic formulation for its solution. By using the Newton iterative method, we can obtain an approximate solution to the exact solution up to 13 digits of accuracy. Moreover, we know exactly when a shock singularity will form in time. This enables us to perform a careful convergence study in both physical space and spectral space very close to the singularity time. This provides a solid foundation to the convergence study of the two spectral methods.

We consider the inviscid 1D Burgers equation

$$u_t + \left(\frac{u^2}{2}\right)_x = 0, \quad -\pi \le x \le \pi, \tag{2.4}$$

with an initial condition given by

$$u|_{t=0} = u_0(x).$$

We impose a periodic boundary condition over $[-\pi, \pi]$. By the method of characteristics, it is easy to show that the solution of the 1D Burgers equation is given by

$$u(x,t) = u_0(x - tu(x,t)). \tag{2.5}$$

The above implicit formulation defines a unique solution for $u(x,t)$ up to the time when the first shock singularity develops. After the shock singularity develops, equation (2.5) gives a multi-valued solution. An entropy condition is required to select a unique physical solution beyond the shock singularity (LeVeque 1992).

We now use a standard pseudo-spectral method to approximate the solution. Let N be an integer, and let $h = \pi/N$. We denote by $x_j = jh$

($j = -N, \ldots, N$) the discrete grid points over the interval $[-\pi, \pi]$. To describe the pseudo-spectral methods, we recall that the discrete Fourier transform of a periodic function $u(x)$ with period 2π is defined by

$$\hat{u}_k = \frac{1}{2N} \sum_{j=-N+1}^{N} u(x_j) \mathrm{e}^{-\mathrm{i}kx_j}.$$

The inversion formula reads

$$u(x_j) = \sum_{k=-N+1}^{N} \hat{u}_k \mathrm{e}^{\mathrm{i}kx_j}.$$

We note that $\hat{u}_k$ is periodic in k with period $2N$. This is an artifact of the discrete Fourier transform, and the source of the aliasing error. To remove the aliasing error, one usually applies some kind of de-aliasing filtering when we compute the discrete derivative. Let $\rho(k/N)$ be a cut-off function in the spectrum space. A discrete derivative operator may be expressed in the Fourier transform as

$$\widehat{(D_h u)}_k = \mathrm{i}k\rho(k/N)\widehat{u}_k, \quad k = -N+1, \ldots, N. \tag{2.6}$$

Both the 2/3 de-aliasing rule and the Fourier smoothing method can be described by a specific choice of the high-frequency cut-off function, ρ (also known as Fourier filter). For the 2/3 de-aliasing rule, the cut-off function is chosen to be

$$\rho(k/N) = \begin{cases} 1, & \text{if } |k/N| \leq 2/3, \\ 0, & \text{if } |k/N| > 2/3. \end{cases} \tag{2.7}$$

In our computations, in order to obtain an alias-free computation on a grid of M points for a quadratic nonlinear equation, we apply the above filter to the high wavenumbers so as to retain only $(2/3)M$ unfiltered wavenumbers before making the coefficient-to-grid Fast Fourier Transform. This de-aliasing procedure is alternatively known as the 3/2 de-aliasing rule because to obtain M unfiltered wavenumbers one must compute nonlinear products in physical space on a grid of $(3/2)M$ points: see p. 229 of Boyd (2000) for more discussions.

For the Fourier smoothing method, we choose ρ as follows:

$$\rho(k/N) = \mathrm{e}^{-\alpha(|k|/N)^m}, \tag{2.8}$$

with $\alpha = 36$ and $m = 36$. In our implementation, both filters are applied to the numerical solution at every time step. Thus, for the 2/3 de-aliasing rule, the Fourier modes with wavenumbers $|k| \geq 2/3N$ are always set to zero. Thus there is no aliasing error being introduced in our approximation of the nonlinear convection term. For the Fourier smoothing method, the nonlinear term will have some non-zero modes beyond the 2/3 point cut-off

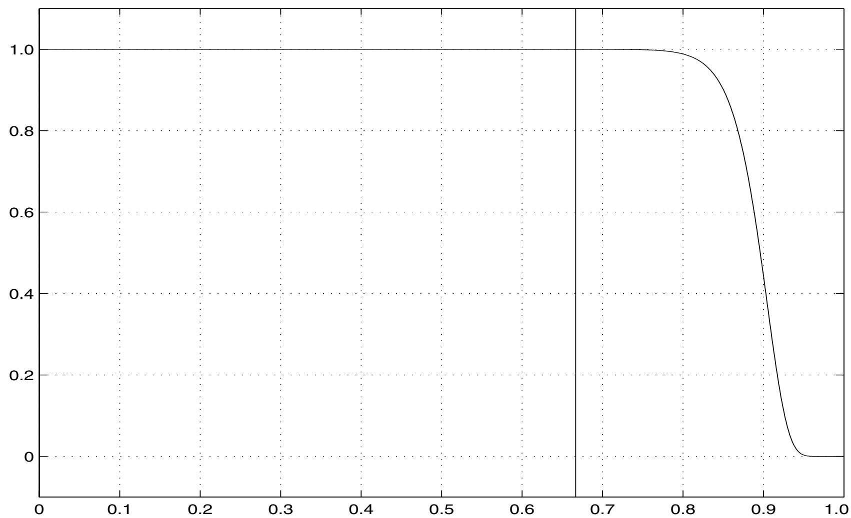

Figure 2.1. The profile of the Fourier smoothing, $\exp(-36(x)^{36})$, as a function of x. The vertical line corresponds to the cut-off point in the Fourier spectrum in the 2/3 de-aliasing rule. We can see that using this Fourier smoothing we keep about $12 \sim 15\%$ more modes than those using the 2/3 de-aliasing rule.

point in the Fourier space. However, these non-zero modes will accumulate in time to pollute the solution.

The Fourier smoothing method we choose is based on three considerations. The first one is that the aliasing instability is introduced by the highest-frequency Fourier modes. As demonstrated in Goodman, Hou and Tadmor (1994), as long as one can damp out a small portion of the highest-frequency Fourier modes, the mild instability caused by the aliasing error can be under control. The second observation is that the magnitude of the Fourier coefficient is decreasing with respect to the wavenumber $|k|$ for a function that has a certain degree of regularity. Typically, we have $|\widehat{u}_k| \leq C/(1+|k|^m)$ if the mth derivative of a function u is bounded in L^1. Thus the high-frequency Fourier modes have a relatively smaller contribution to the overall solution than the low- to intermediate-frequency modes. The third observation is that one should not cut off high-frequency Fourier modes abruptly to avoid the Gibbs phenomenon and the loss of the L^2-energy associated with the solution. This is especially important when we compute a nearly singular solution whose high-frequency Fourier coefficient has a very slow decay.

Based on the above considerations, we choose a smooth cut-off function which decays exponentially fast with respect to the high wavenumber. In our cut-off function, we choose the parameters $\alpha = 36$ and $m = 36$. These two parameters are chosen to achieve two objectives. (i) When $|k|$ is close to N, the cut-off function reaches machine precision, *i.e.*, 10^{-16}. (ii) The cut-off function remains very close to 1 for $|k| < 4N/5$, and decays rapidly and smoothly to zero beyond $|k| = 4N/5$. In Figure 2.1, we plot the cut-off function $\rho(x)$ as a function of x. The cut-off function used by the 2/3 de-aliasing rule is plotted on top of the cut-off function used by the Fourier smoothing method. We can see that the Fourier smoothing method keeps about $12 \sim 15\%$ more modes than the 2/3 de-aliasing method. In this paper, we will demonstrate by our numerical experiments that the extra modes we keep by the Fourier smoothing method give an accurate approximation of the correct high-frequency Fourier modes.

We have performed a sequence of resolution studies with the largest resolution being $N = 16384$ (Hou and Li 2007). Our extensive numerical results demonstrate that the pseudo-spectral method with the high-order Fourier smoothing (the Fourier smoothing method for short) gives a much more accurate approximation than the pseudo-spectral method with the 2/3 de-aliasing rule (the 2/3 de-aliasing method for short). One of the interesting observations is that the unfiltered high-frequency coefficients in the Fourier smoothing method approximate accurately the corresponding exact Fourier coefficients. Moreover, we observe that the Fourier smoothing method captures about $12 \sim 15\%$ more effective Fourier modes than the 2/3 de-aliasing method in each dimension: see Figure 2.2. The gain is even higher for the 3D Euler equations since the number of effective modes in the Fourier smoothing method is higher in three dimensions. Further, we find that the error produced by the Fourier smoothing method is highly localized near the region where the solution is most singular. In fact, the pointwise error decays exponentially fast away from the location of the shock singularities. On the other hand, the error produced by the 2/3 de-aliasing method spreads out to the entire domain as we approach the singularity time: see Figure 2.3.

2.5. The high-resolution 3D Euler computations of Hou and Li (2006, 2007)

Hou and Li (2006) performed high-resolution computations of the 3D Euler equations using the initial data for the two antiparallel vortex tubes. They used the same initial condition whose analytic formula was given by Kerr (see Section III of Kerr (1993), and also Hou and Li (2006) for corrections of some typos in the description of the initial condition in Kerr (1993)). However, there was some minor difference between their discretization and Kerr's discretization. Hou and Li used a pseudo-spectral discretization in all three directions, while Kerr used a pseudo-spectral discretization only in the x- and y-directions and used a Chebyshev discretization in the z-direction. Based on the results of early tests, positive vorticity in the symmetry plane was imposed in the initial condition of Kerr (1993). How this was imposed

(a)

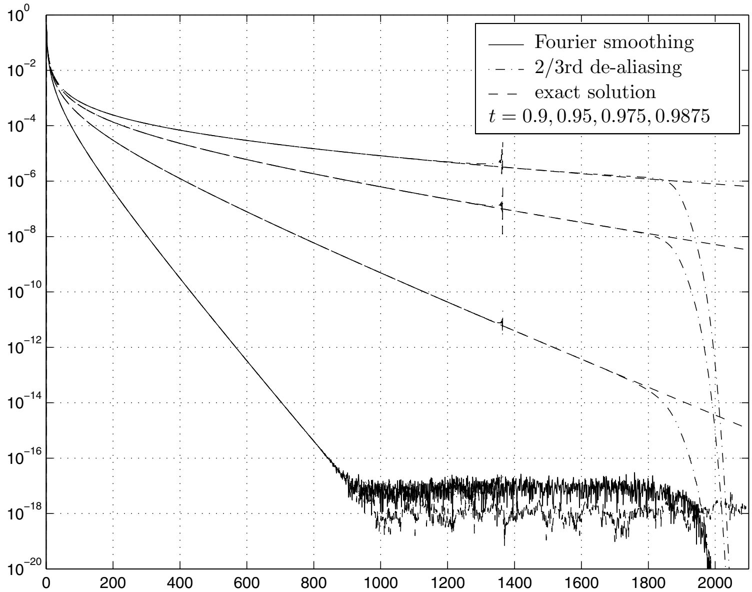

(b)

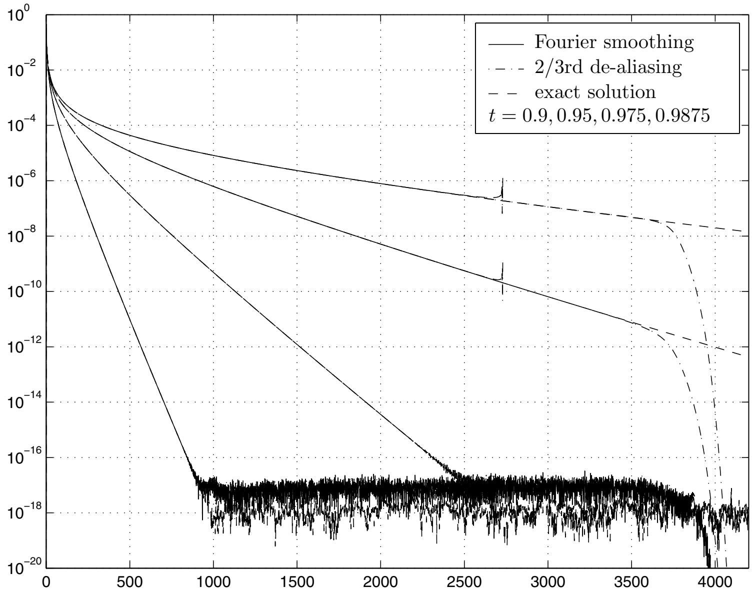

Figure 2.2. Comparison of Fourier spectra of the two methods on different resolutions at a sequence of times. (a) $N = 4096$, (b) $N = 8192$. Dashed lines, 'exact' spectra; solid lines, Fourier smoothing method; dash-dotted lines, 2/3 de-aliasing method. Times, $t = 0.9,\ 0.95,\ 0.975,\ 0.9875$ respectively (from bottom to top). Initial condition, $u_0(x) = \sin(x)$. Singularity time for this initial condition, $T = 1$.

(a)

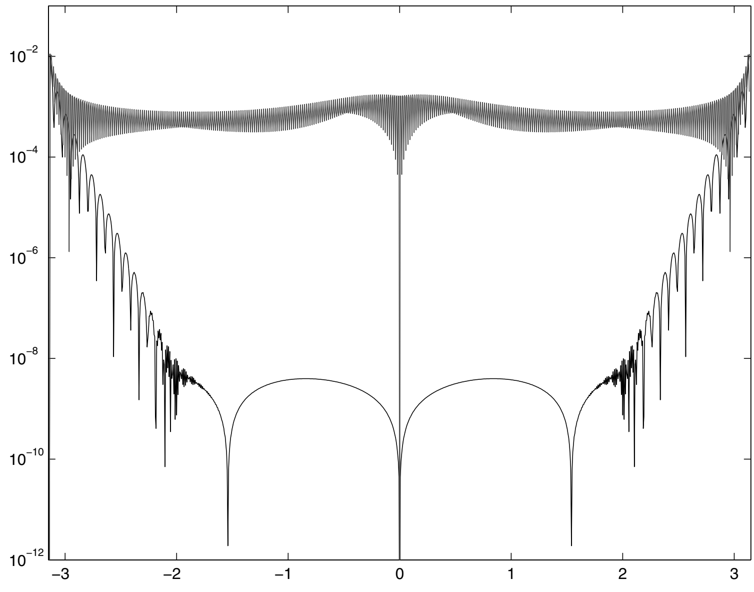

(b)

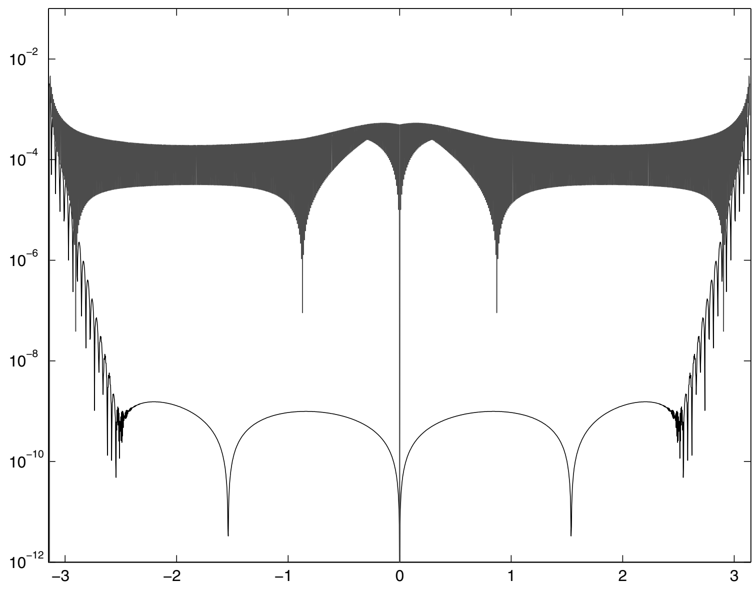

Figure 2.3. The pointwise errors of the two pseudo-spectral methods as a function of time using three different resolutions. The plot is in a log scale. (a) $N = 1024$, (b) $N = 2048$, both at $t = 0.9875$. Initial condition, $u_0(x) = \sin(x)$. The error of the 2/3 de-aliasing method (upper curve) is highly oscillatory and spreads out over the entire domain, while the error of the Fourier smoothing method (lower curve) is highly localized near the location of the shock singularity.

as the vorticity field was mapped onto the Chebyshev mesh was not documented by Kerr (1993). This has led to some ambiguity in reproducing that initial condition which is being resolved by Kerr's group (private communication).

We will summarize the main findings of Hou and Li (2006) in the rest of Section 2. We first illustrate the dynamic evolution of the vortex tubes. In Figure 2.4, we plot the isosurface of the 3D vortex tubes at $t = 0$ and $t = 6$ respectively. As we can see, the two initial vortex tubes are very smooth and relatively symmetric. Due to the mutual attraction of the two antiparallel vortex tubes, the two vortex tubes approach each other and become flattened dynamically. By time $t = 6$, there is already a significant flattening near the centre of the tubes. In Figure 2.5, we plot the local 3D vortex structure of the upper vortex tube at $t = 17$. By this time, the 3D vortex tube has essentially turned into a thin vortex sheet with rapidly decreasing thickness. The vortex lines become relatively straight. The vortex sheet rolls up near the left edge of the sheet.

In order to see better the dynamic development of the local vortex structure, we plot a sequence of vorticity contours on the symmetry plane at $t = 17.5, 18, 18.5$, and 19, respectively, in Figure 2.6. From these results, we can see that the vortex sheet is compressed in the z-direction. It is clear that a thin layer (or a vortex sheet) is formed dynamically. The head of the vortex sheet is a bit thicker than the tail at the beginning. The head of the vortex sheet begins to roll up around $t = 16$. By the time $t = 19$, the head of the vortex sheet has travelled backward for quite a distance, and the vortex sheet has been compressed quite strongly along the z-direction.

We would like to make a few important observations. First of all, the maximum vorticity at a later stage of the computation is actually located near the rolled-up region of the vortex sheet and moves away from the bottom of the vortex sheet. Thus the mechanism of strong compression between the two vortex tubes becomes weaker dynamically at the later time. Secondly, the location of maximum strain and that of maximum vorticity separate as time increases. Thirdly, the relatively 'strong' growth of the maximum velocity between $t = 15$ and $t = 17$ becomes saturated after $t = 17$ when the location of maximum vorticity moves to the rolled-up region: see Figure 2.14. All these factors contribute to the dynamic depletion of vortex stretching.

We now perform a convergence study for the two numerical methods using a sequence of resolutions. For the Fourier smoothing method, we use the resolutions $768 \times 512 \times 1536$, $1024 \times 768 \times 2048$, and $1536 \times 1024 \times 3072$ respectively. Except for the computation on the largest resolution, $1536 \times 1024 \times 3072$, all computations are carried out from $t = 0$ to $t = 19$. The computation on the final resolution, $1536 \times 1024 \times 3072$, is started from $t = 10$ with the initial condition given by the computation with the

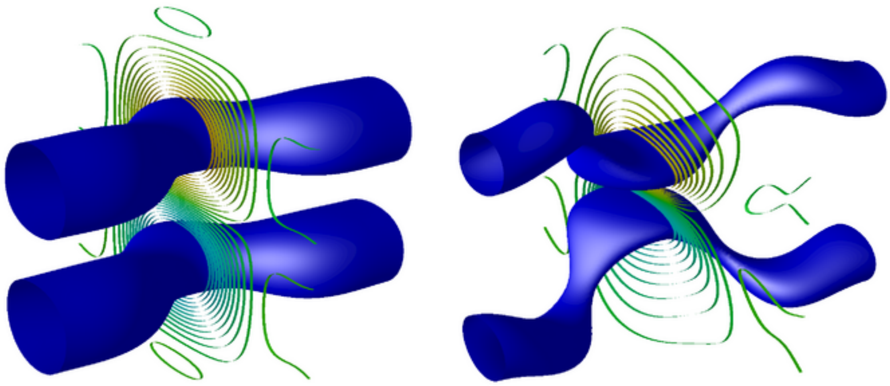

Figure 2.4. The 3D view of the vortex tube for $t = 0$ and $t = 6$. The tube is the isosurface at 60% of the maximum vorticity. The ribbons on the symmetry plane are the contours at other different values.

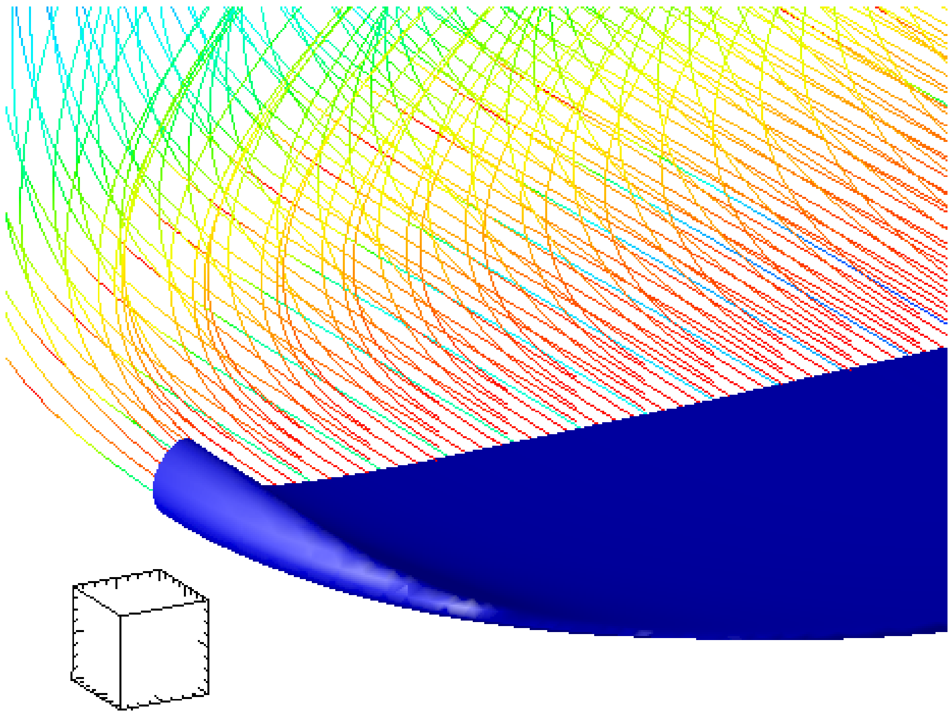

Figure 2.5. The local 3D vortex structures of the upper vortex tube and vortex lines around the maximum vorticity at $t = 17$.

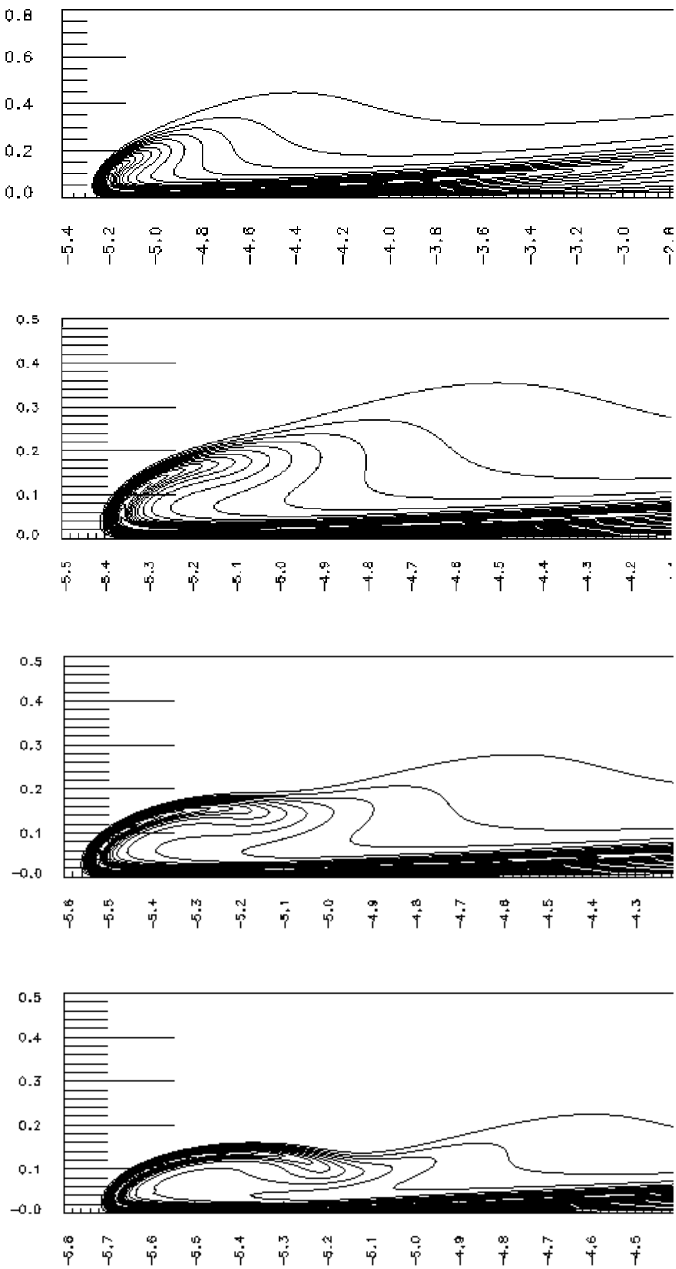

Figure 2.6. The contour of axial vorticity of the upper vortex tube around the maximum vorticity on the symmetry plane (the xz-plane) at $t = 17.5, 18, 18.5, 19$.

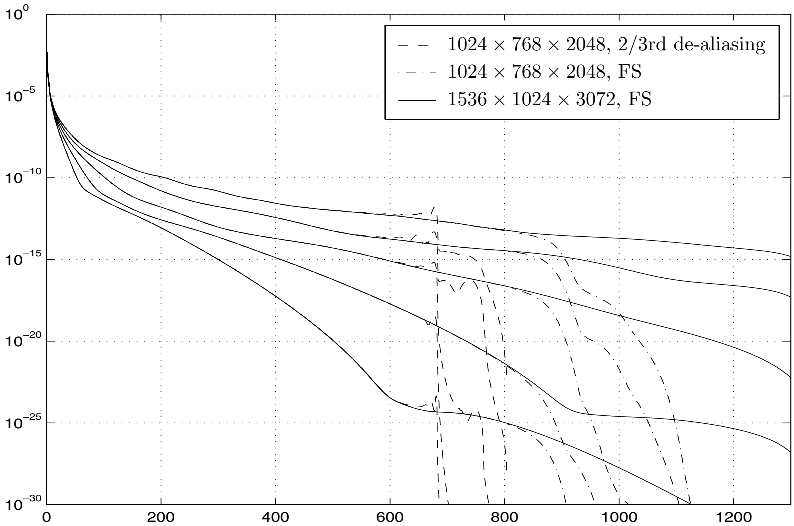

Figure 2.7. The energy spectra versus wavenumbers. The dashed lines and dash-dotted lines are the energy spectra, with resolution $1024 \times 768 \times 2048$, using the 2/3 de-aliasing rule and Fourier smoothing, respectively. The times for the spectra lines are $t = 15, 16, 17, 18, 19$ respectively.

resolution $1024 \times 768 \times 2048$. For the 2/3 de-aliasing method, we use the resolutions $512 \times 384 \times 1024$, $768 \times 512 \times 1536$ and $1024 \times 768 \times 2048$ respectively. The computations using these three resolutions are all carried out from $t = 0$ to $t = 19$. See Hou and Li (2006, 2007) for more details.

In Figure 2.7, we compare the Fourier spectra of the energy obtained by using the 2/3 de-aliasing method with those obtained by the Fourier smoothing method. For a fixed resolution, $1024 \times 768 \times 2048$, we can see that the Fourier spectra obtained by the Fourier smoothing method retain more effective Fourier modes than those obtained by the 2/3 de-aliasing method. This can be seen by comparing the results with the corresponding computations using a higher resolution, $1536 \times 1024 \times 3072$ (the solid lines). Moreover, the Fourier smoothing method does not give the spurious oscillations in the Fourier spectra. In comparison, the Fourier spectra obtained by the 2/3 de-aliasing method produce some spurious oscillations near the 2/3 cut-off point. We would like to emphasize that the Fourier smoothing method conserves the total energy extremely well. More studies including the convergence of the enstrophy spectra can be found in Hou and Li (2006, 2007).

It is worth emphasizing that a significant portion of those Fourier modes beyond the 2/3 cut-off position are still accurate for the Fourier smoothing method. This portion of the Fourier modes that go beyond the 2/3 cut-off point is about $12 \sim 15\%$ of total number of modes in each dimension. For 3D problems, the total number of effective modes in the Fourier smoothing method is about 20% more than that in the 2/3 de-aliasing method. For our largest resolution, we have about 4.8 billion unknowns. An increase of 20% in the effective Fourier modes represents a very significant increase in the resolution for a large-scale computation.

2.6. Comparison of the two spectral methods in physical space

Next, we compare the solutions obtained by the two methods in physical space for the velocity field and the vorticity. In Figure 2.8, we compare the maximum velocity as a function of time computed by the two methods using resolution $1024 \times 768 \times 2048$. The two solutions are almost indistinguishable. In Figure 2.9, we plot the maximum vorticity as a function of time. The two solutions also agree reasonably well. However, the comparison of the solutions obtained by the two methods at resolutions lower than $1024 \times 768 \times 2048$ shows more significant differences between the two methods: see Figure 2.10.

To understand better how the two methods differ in their performance, we examine the contour plots of the axial vorticity in Figures 2.11, 2.12 and 2.13. As we can see, the vorticity computed by the 2/3 de-aliasing method already develops small oscillations at $t = 17$. The oscillations grow bigger by $t = 18$ (see Figure 2.12), and bigger still at $t = 19$ (see Figure 2.13). We note that the oscillations in the axial vorticity contours concentrate near the region where the magnitude of vorticity is close to zero. Thus they have less of an effect on the maximum vorticity. On the other hand, the solution computed by the Fourier smoothing method is still relatively smooth.

2.7. Dynamic depletion of vortex stretching

In this section, we present some convincing numerical evidence which shows that there is a strong dynamic depletion of vortex stretching due to local geometric regularity of the vortex lines. We first present the result on the growth of the maximum velocity in time: see Figure 2.14. The growth rate of the maximum velocity plays a critical role in the non-blow-up criteria of Deng, Hou and Yu (2005, 2006*a*). As we can see from Figure 2.14, the maximum velocity remains bounded up to $t = 19$. This is in contrast to the claim in Kerr (2005) that the maximum velocity blows up like $O((T-t)^{-1/2})$ with $T = 18.7$. We note that the velocity field is smoother than the vorticity field. Thus it is easier to resolve the velocity field than the vorticity field. We observe an excellent agreement between the maximum velocity fields computed by the two largest resolutions. Since the velocity field is bounded, the first condition of Theorem 2.1 is satisfied by taking $A = 0$. Furthermore,

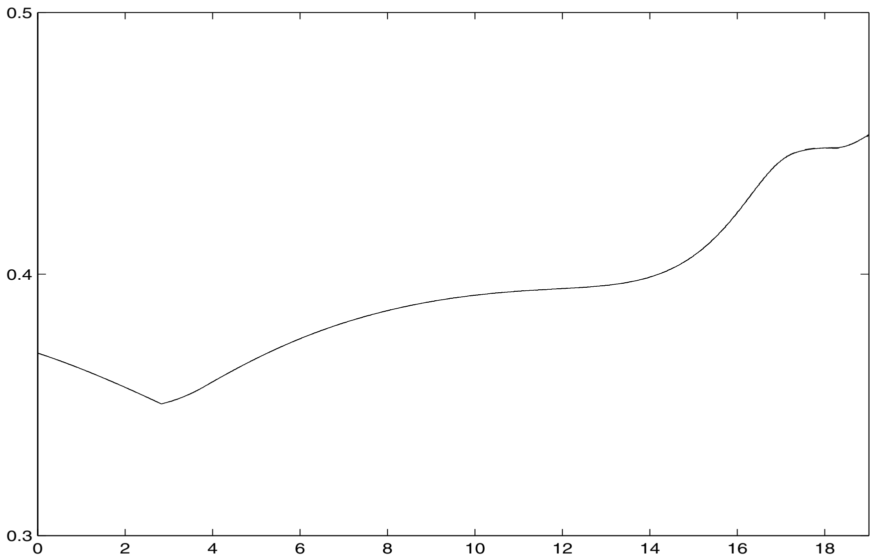

Figure 2.8. Comparison of maximum velocity as a function of time computed by two methods. Solid line, solution obtained by the Fourier smoothing method; dashed line, solution obtained by the 2/3 de-aliasing method. Resolution $1024 \times 768 \times 2048$ for both methods.

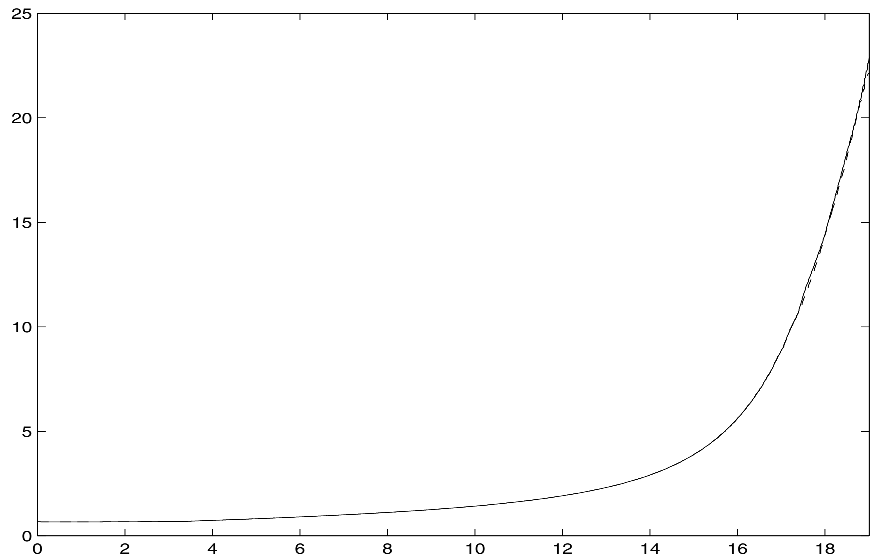

Figure 2.9. Comparison of maximum vorticity as a function of time computed by two methods. Solid line, solution obtained by the Fourier smoothing method; dashed line, solution obtained by the 2/3 de-aliasing method. Resolution $1024 \times 768 \times 2048$ for both methods.

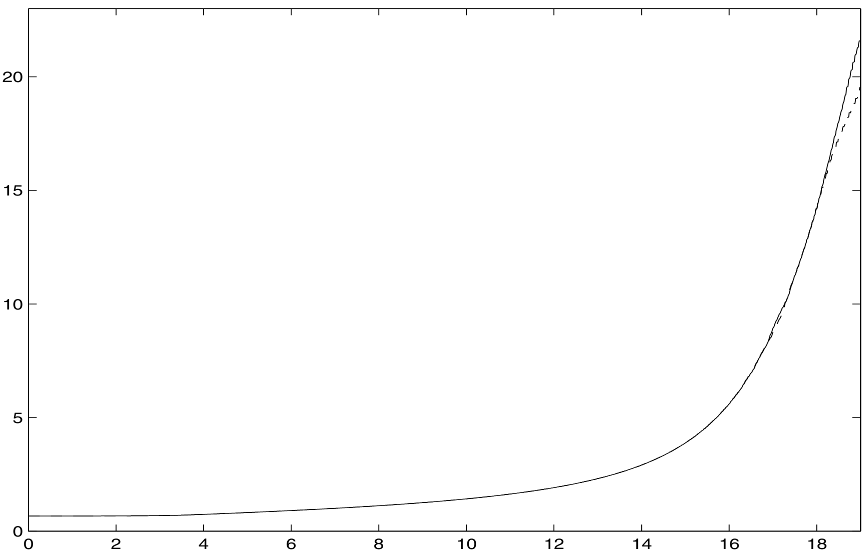

Figure 2.10. Comparison of maximum vorticity as a function of time computed by two methods. Solid line, solution obtained by the Fourier smoothing method; dashed line, solution obtained by the 2/3 de-aliasing method. Resolution $768 \times 512 \times 1024$ for both methods.

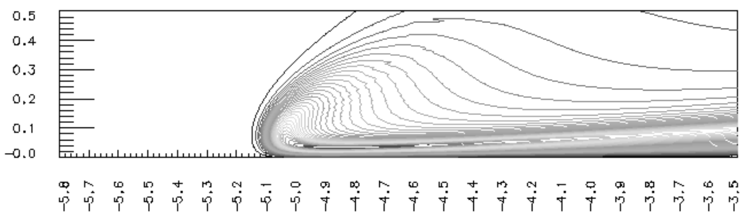

(a)

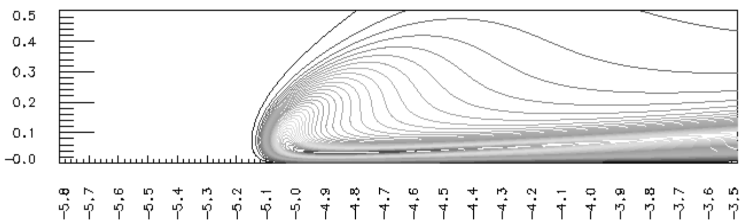

(b)

Figure 2.11. Comparison of axial vorticity contours at $t = 17$ computed by two methods. (a) Solution obtained by the 2/3 de-aliasing method, (b) solution obtained by the Fourier smoothing method. Resolution $1024 \times 768 \times 2048$ for both methods.

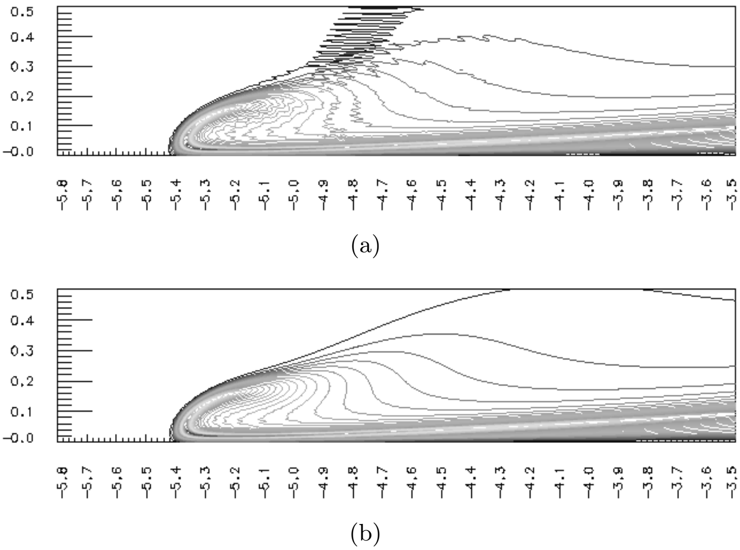

Figure 2.12. Comparison of axial vorticity contours at $t = 18$ computed by two methods. (a) Solution obtained by the 2/3 de-aliasing method, (b) solution obtained by the Fourier smoothing method. Resolution $1024 \times 768 \times 2048$ for both methods.

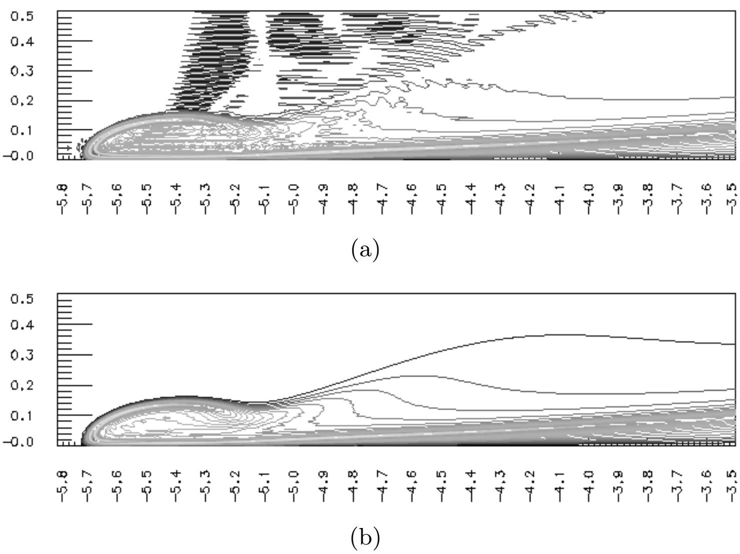

Figure 2.13. Comparison of axial vorticity contours at $t = 19$ computed by two methods. (a) Solution obtained by the 2/3 de-aliasing method, (b) solution obtained by the Fourier smoothing method. Resolution $1024 \times 768 \times 2048$ for both methods.

since both $\nabla \cdot \boldsymbol{\xi}$ and κ are bounded by $O((T-t)^{-1/2})$ in the inner region of size $(T-t)^{1/2} \times (T-t)^{1/2} \times (T-t)$ (Kerr 2005), the second condition of Theorem 2.1 is satisfied with $B = 1/2$ by taking a segment of the vortex line with length $(T-t)^{1/2}$ within this inner region. Thus Theorem 2.1 can be applied to our computation, which implies that the solution of the 3D Euler equations remains smooth at least up to $T = 19$.

We also study the maximum vorticity as a function of time. The maximum vorticity is found to increase rapidly from the initial value of 0.669 to 23.46 at the final time $t = 19$, a factor of 35 increase from its initial value. Our computations show no sign of finite-time blow-up of the 3D Euler equations up to $T = 19$, beyond the singularity time predicted by Kerr. The maximum vorticity computed by resolution $1024 \times 768 \times 2048$ agrees very well with that computed by resolution $1536 \times 1024 \times 3072$ up to $t = 17.5$. There is some mild disagreement towards the end of the computation. This indicates that a very high space resolution is needed to capture the rapid growth of maximum vorticity at the final stage of the computation.

In order to understand the nature of the dynamic growth in vorticity, we examine the degree of nonlinearity in the vortex stretching term. In Figure 2.15, we plot the quantity, $\|\xi \cdot \nabla \mathbf{u} \cdot \boldsymbol{\omega}\|_\infty$, as a function of time. If the maximum vorticity indeed blew up like $O((T-t)^{-1})$, as alleged in Kerr (1993), this quantity should have been quadratic as a function of maximum vorticity. We find that there is tremendous cancellation in this vortex stretching term. It actually grows more slowly than $C\|\vec{\omega}\|_\infty \log(\|\vec{\omega}\|_\infty)$: see Figure 2.15. It is easy to show that $\|\xi \cdot \nabla \mathbf{u} \cdot \boldsymbol{\omega}\|_\infty \leq C\|\vec{\omega}\|_\infty \log(\|\vec{\omega}\|_\infty)$ would imply at most doubly exponential growth in the maximum vorticity. Indeed, as demonstrated by Figure 2.16, the maximum vorticity does not grow more rapidly than doubly exponential in time. We have also generated a similar plot by extracting the data from Kerr (1993). We find that $\log(\log(\|\boldsymbol{\omega}\|_\infty))$ basically scales linearly with respect to t from $14 \leq t \leq 17.5$ when Kerr's computations are still reasonably resolved. This implies that the maximum vorticity up to $t = 17.5$ in his computations does not grow more rapidly than doubly exponential in time. This is consistent with our conclusion.

We study the decay rate in the energy spectrum in Figure 2.17 at $t = 16, 17, 18, 19$. A finite-time blow-up of enstrophy would imply that the energy spectrum decays no more rapidly than $|k|^{-3}$. Our computations show that the energy spectrum approaches $|k|^{-3}$ for $|k| \leq 100$ as time increases to $t = 19$. This is in qualitative agreement with Kerr's results. Note that there are fewer than 100 modes available along the $|k_x|$- or $|k_y|$-direction in Kerr's computations: see Figure 18(a),(b) of Kerr (1993). On the other hand, our computations show that the high-frequency Fourier spectrum for $100 \leq |k| \leq 1300$ decays much more rapidly than $|k|^{-3}$, as one can see from Figure 2.17. This indicates that there is no blow-up in enstrophy.

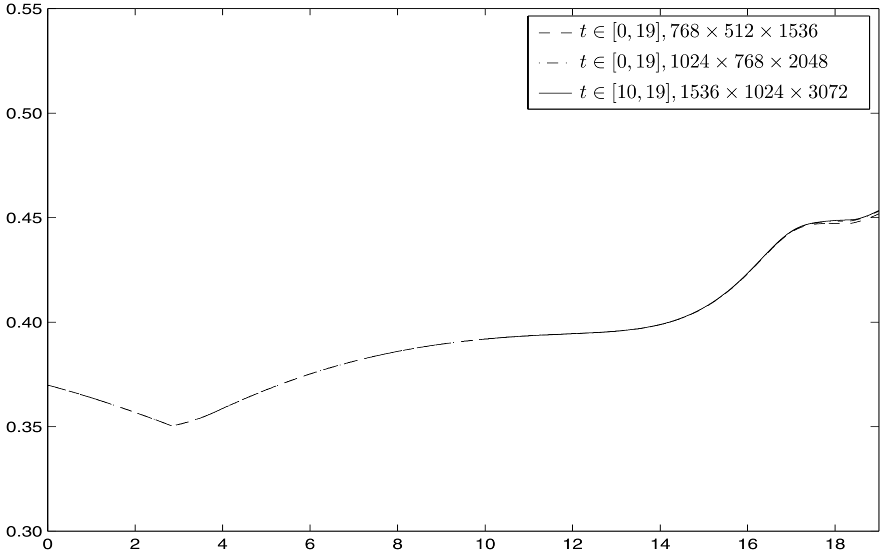

Figure 2.14. Maximum velocity $\|\mathbf{u}\|_\infty$ in time using three different resolutions.

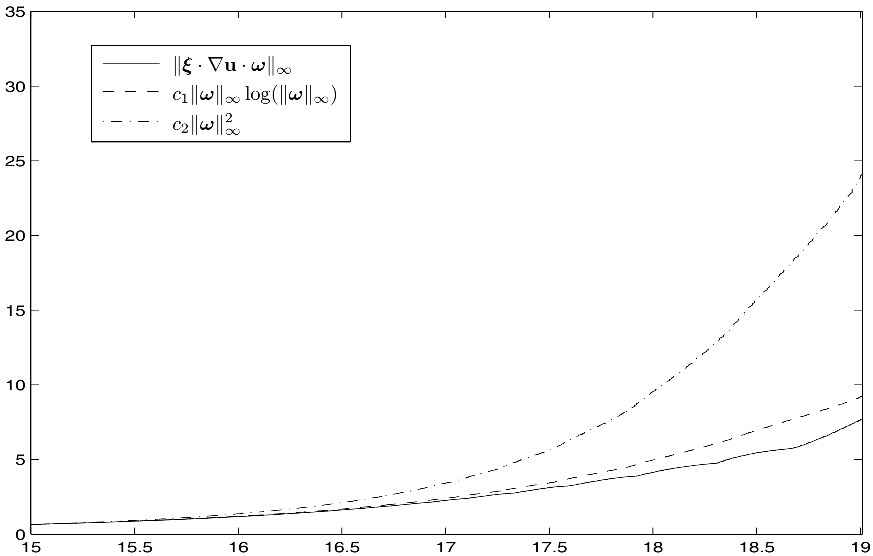

Figure 2.15. Study of the vortex stretching term in time, resolution $1536 \times 1024 \times 3072$. The inequality $|\boldsymbol{\xi} \cdot \nabla \mathbf{u} \cdot \boldsymbol{\omega}| \leq c_1 |\boldsymbol{\omega}| \log |\boldsymbol{\omega}|$ and $\frac{D}{Dt}|\boldsymbol{\omega}| = \boldsymbol{\xi} \cdot \nabla \mathbf{u} \cdot \boldsymbol{\omega}$ implies $|\boldsymbol{\omega}|$ bounded by a double exponential.

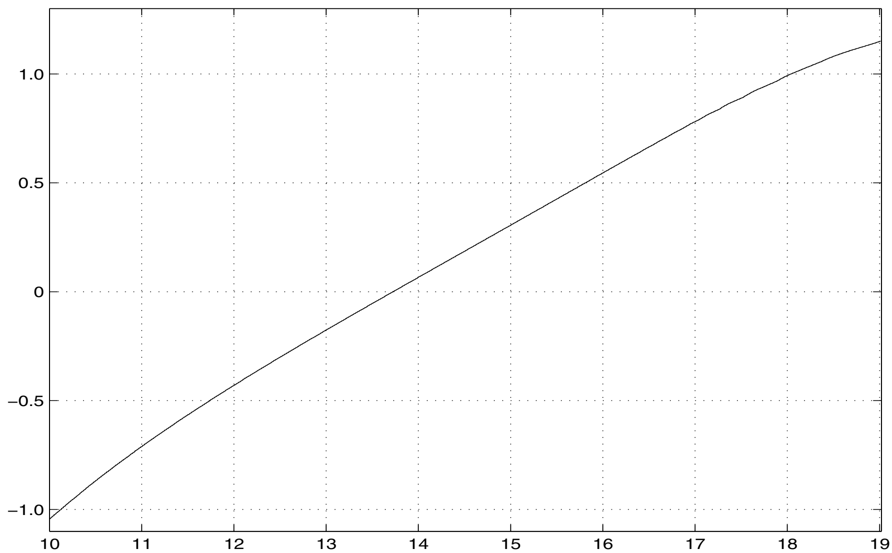

Figure 2.16. The plot of $\log\log\|\boldsymbol{\omega}\|_\infty$ versus time, resolution $1536 \times 1024 \times 3072$.

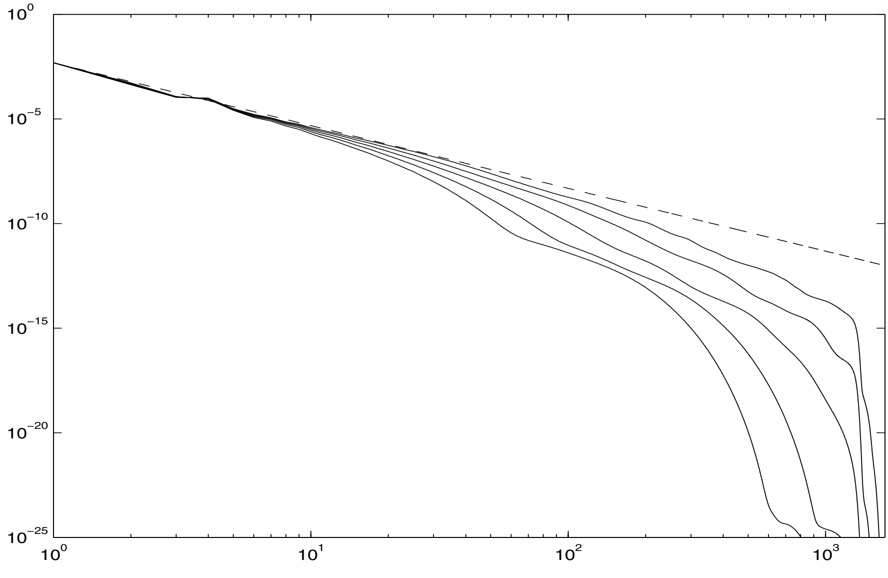

Figure 2.17. The energy spectra for velocity at $t = 15, 16, 17, 18, 19$ (from bottom to top) in log-log scale. Dashed line, k^{-3}.

Table 2.1. The alignment of the vorticity vector and the eigenvectors of S around the point of maximum vorticity with resolution $1536 \times 1024 \times 3072$. Here, θ_i is the angle between the ith eigenvector of S and the vorticity vector.

Time	$\lvert\boldsymbol{\omega}\rvert$	λ_1	θ_1	λ_2	θ_2	λ_3	θ_3
16.012	5.628	−1.508	89.992	0.206	0.007	1.302	89.998
16.515	7.016	−1.864	89.995	0.232	0.010	1.631	89.990
17.013	8.910	−2.322	89.998	0.254	0.006	2.066	89.993
17.515	11.430	−2.630	89.969	0.224	0.085	2.415	89.920
18.011	14.890	−3.625	89.969	0.257	0.036	3.378	89.979
18.516	19.130	−4.501	89.966	0.246	0.036	4.274	89.984
19.014	23.590	−5.477	89.966	0.247	0.034	5.258	89.994

It is interesting to ask how the vorticity vector aligns with the eigenvectors of the deformation tensor. Recall that the vorticity equations can be written as

$$\frac{\partial}{\partial t}\boldsymbol{\omega} + (\mathbf{u} \cdot \nabla)\boldsymbol{\omega} = S \cdot \boldsymbol{\omega}, \quad S = \frac{1}{2}(\nabla \mathbf{u} + \nabla^T \mathbf{u}) \tag{2.9}$$

(see Majda and Bertozzi (2002)). Let $\lambda_1 < \lambda_2 < \lambda_3$ be the three eigenvalues of S. The incompressibility condition implies that $\lambda_1 + \lambda_2 + \lambda_3 = 0$. If the vorticity vector aligns with the eigenvector corresponding to λ_3, which gives the maximum rate of stretching, then it is very likely that the 3D Euler equations would blow up in a finite time.

In Table 2.1, we document the alignment information of the vorticity vector around the point of maximum vorticity with resolution $1536 \times 1024 \times 3072$. In this table, θ_i is the angle between the ith eigenvector of S and the vorticity vector. One can see clearly that for $16 \leq t \leq 19$ the vorticity vector at the point of maximum vorticity is almost perfectly aligned with the second eigenvector of S. Note that the second eigenvalue, λ_2, is about 20 times smaller in magnitude than the largest eigenvalue λ_3, and does not grow much in time. The alignment of the vorticity vector with the second eigenvector of the deformation tensor is another indication that there is a strong dynamic depletion of vortex stretching.

2.8. Global regularity of large anisotropic initial data

The numerical studies of the 3D Euler equations by Hou and Li (2006) strongly suggest that the support of maximum vorticity becomes severely flattened and develops an anisotropic scaling as vorticity increases rapidly in time. This seems quite generic and is a consequence of the incompressibility and the Lagrangian structure of the vorticity equation. Convection plays an essential role in producing this anisotropic structure of the solution. Motivated by the desire to understand how the local anisotropic structure of the solution near the support of maximum vorticity may lead to the depletion of vortex stretching, Hou, Lei and Li (2008) recently studied the 3D axisymmetric Navier–Stokes equations with large anisotropic data. They proved the global regularity of the 3D Navier–Stokes equations for a family of large anisotropic initial data. Moreover, they obtained a global bound of the solution in terms of its initial data in some L^p-norm. Their results also revealed some interesting dynamic growth behaviour of the solution due to the interaction between the axial vorticity and the the derivative of vorticity.

Specifically, let u^θ and ω^θ be the angular velocity and vorticity components of the 3D axisymmetric Navier–Stokes equations. They considered initial data for u^θ and ω^θ that have the following scaling property:

$$u^\theta(r,z,0) = \frac{1}{\epsilon^{1-\delta}} U_0(\epsilon r, z), \quad \omega^\theta(r,z,0) = \frac{1}{\epsilon^{1-\delta}} W_0(\epsilon r, z), \tag{2.10}$$

where $r = \sqrt{x^2+y^2}$, δ and ϵ are some small positive parameters, and the rescaled profiles U_0/r and W_0/r are bounded in L^{2p} and L^{2q}, respectively, for some p and q with $p = 2q$; note that u^θ and ω^θ must satisfy a compatibility condition: $u^\theta|_{r=0} = 0 = \omega^\theta|_{r=0}$ (Liu and Wang 2006). We remark that these initial data are not small. In fact, we have

$$\|\mathbf{u}_0\|_{L^2(\mathbb{R}^2\times[0,1])} \|\nabla \mathbf{u}_0\|_{L^2(\mathbb{R}^2\times[0,1])} = \frac{C_0}{\epsilon^{4-2\delta}} \gg 1,$$

for ϵ small, where $\mathbf{u}_0$ is the initial velocity vector. Thus the classical regularity analysis for small initial data does not apply to these sets of anisotropic initial data.

Hou, Lei and Li (2008) proved the global regularity of the 3D axisymmetric Navier–Stokes equations for initial data (2.10) by exploring the anisotropic structure of the solution for ϵ small. They also obtained a global bound on $\|u^\theta/r\|_{L^{2p}}$ and $\|\omega^\theta/r\|_{L^{2q}}$ in terms of their initial data. Note that by using the scaling invariance property of the Navier–Stokes equations, their global regularity result also applies to the following rescaled initial data:

$$u^\theta(r,z,0) = \frac{1}{\epsilon^{2-\delta}} U_0\left(r, \frac{z}{\epsilon}\right), \quad \omega^\theta(r,z,0) = \frac{1}{\epsilon^{3-\delta}} W_0\left(r, \frac{z}{\epsilon}\right), \tag{2.11}$$

and

$$u^\theta(r,z,0) = \frac{1}{\epsilon} U_0\left(\frac{r}{\epsilon^{1-\delta}}, \frac{z}{\epsilon}\right), \quad \omega^\theta(r,z,0) = \frac{1}{\epsilon^2} W_0\left(\frac{r}{\epsilon^{1-\delta}}, \frac{z}{\epsilon}\right). \tag{2.12}$$

Note that the parameters ϵ in the initial data (2.10)–(2.11) and δ in (2.12) measure the degree of anisotropy of the initial data. If $\delta = 0$, then the initial data (2.12) become isotropic, *i.e.*,

$$\mathbf{u}_0(x,y,z) = \frac{1}{\epsilon}\mathbf{U}_0\left(\frac{x}{\epsilon},\frac{y}{\epsilon},\frac{z}{\epsilon}\right).$$

Their analysis would break down when there is no anisotropic scaling in the initial data, *i.e.*, $\delta = 0$. Clearly, if the analysis could be extended to the case of $\delta = 0$, one would prove the global regularity of the 3D axisymmetric Navier–Stokes equations for general initial data by using the scaling invariance property of the Navier–Stokes equations. It is interesting to note that by using an anisotropic scaling of the initial data, we turn the global regularity of the 3D Navier–Stokes equations into a critical case of $\delta = 0$.

We remark that the global regularity results of Hou, Lei and Li (2008) were obtained on a regular size domain, $\mathbb{R}^2 \times [0,1]$, for initial data (2.10). In this sense, their results are different from those global regularity results obtained for a thin domain, $\Omega_\epsilon = Q_1 \times [0,\epsilon]$ with Q_1 being a bounded domain in $\mathbb{R}^2$. The global regularity of the 3D Navier–Stokes equations in a thin domain of the form Ω_ϵ has been studied by Raugel and Sell in a series of papers (Raugel and Sell 1993*a*, 1994, 1993*b*). They proved the global regularity of the 3D Navier–Stokes equations under the assumption that $\|\nabla \mathbf{u}_0\|^2_{L^2(\Omega_\epsilon)} \le C_0 \ln \frac{1}{\epsilon}$. This is an improvement over the classical global regularity result for small data, which requires $\|\nabla \mathbf{u}_0\|^2_{L^2(\Omega_\epsilon)} \le C^*\epsilon$ (Raugel and Sell 1993*a*). One may interpret the global regularity result of Hou, Lei and Li with initial data (2.11) as a result on a generalized thin domain. Note that the initial data given by (2.11) satisfy the following bound: $\|\nabla \mathbf{u}_0\|^2_{L^2(\Omega_\epsilon)} = C_0\epsilon^{-5+2\delta}$ (here $\delta > 0$ can be made arbitrarily small), which is much larger than the corresponding bound $C_0 \ln \frac{1}{\epsilon}$ required by the global regularity analysis of Raugel and Sell (1993*a*, 1994, 1993*b*).

3. Dynamic stability of 3D Navier–Stokes equations

The axisymmetric 3D Navier–Stokes equation with swirl is perhaps the simplest form of the 3D Navier–Stokes equations, yet still retains the most essential difficulties of the 3D Navier–Stokes equations. It has attracted a lot of attention in recent years. Although some partial progress has been made in studying the global regularity of the axisymmetric Navier–Stokes equations with swirl using energy estimates (see, *e.g.*, Chae and Lee (2002) and references cited there), the question of global regularity for general initial data is still an open question.

Hou and Li (2008*a*) studied the dynamic stability of the axisymmetric Navier–Stokes equations with swirl via a new 1D model. This model is derived from the axisymmetric Navier–Stokes equations along the symmetry axis. Surprisingly, this model is an exact reduction of the 3D axisymmetric

Navier–Stokes equations along the symmetry axis. It captures the essential nonlinear features of the 3D Navier–Stokes equations. One of the important findings by Hou and Li (2008*a*) was that the convection term plays an essential role in cancelling some of the vortex stretching terms. Specifically, they found a positive Lyapunov function which satisfies a new conservation law and a maximum principle. This holds for both the viscous and inviscid cases. This *a priori* pointwise estimate plays a critical role in obtaining nonlinear stability and global regularity of the 1D model. Using this *a priori* estimate, they proved global regularity of the 3D Navier–Stokes equations for a family of large data, which can experience large transient dynamic growth but remain smooth for all times.

It is worth emphasizing that such subtle dynamic stability properties of the 3D Navier–Stokes equations would have been completely missed by using the traditional energy estimates. Traditional energy estimates are too crude to capture some of the most essential properties of the 3D incompressible Navier–Stokes equations. To illustrate its limitations, we briefly review how the energy estimates are used in proving global regularity of the 3D Navier–Stokes equations.

For incompressible Navier–Stokes equations, one of the most important *a priori* estimates is the energy identity. More precisely, for any strong solution $\mathbf{u}$, we have

$$\frac{1}{2}\frac{\mathrm{d}}{\mathrm{d}t}\int |\mathbf{u}|^2\,\mathrm{d}\mathbf{x} + \nu \int |\nabla \mathbf{u}|^2\,\mathrm{d}\mathbf{x} = 0, \tag{3.1}$$

by observing $\int \mathbf{u}\cdot(\mathbf{u}\cdot\nabla\mathbf{u})\,\mathrm{d}\mathbf{x} = -\frac{1}{2}\int(\nabla\cdot\mathbf{u})|\mathbf{u}|^2\,\mathrm{d}\mathbf{x} = 0$, since $\mathbf{u}$ is divergence-free. Unfortunately, this energy identity is not strong enough to rule out finite-time singularities. To prove global regularity, we need to obtain control in a stronger norm, either in $\|\mathbf{u}\|_{L^p}$ with $p \geq 3$ or in $\|\boldsymbol{\omega}\|_{L^2}$. To illustrate the main difficulty of the traditional energy estimates, let us perform energy estimates for the vorticity equation:

$$\frac{1}{2}\frac{\mathrm{d}}{\mathrm{d}t}\int |\boldsymbol{\omega}|^2\,\mathrm{d}\mathbf{x} + \nu \int |\nabla \boldsymbol{\omega}|^2\,\mathrm{d}\mathbf{x} = \int \boldsymbol{\omega}\cdot\nabla\mathbf{u}\cdot\boldsymbol{\omega}\,\mathrm{d}\mathbf{x}. \tag{3.2}$$

Again, the convection term does not contribute to the L^2-norm of vorticity (or any L^p-norm with $p > 1$). The main difficulty is to control the vortex stretching term. Using the Sobolev embedding theory, one can show that

$$\int \boldsymbol{\omega}\cdot\nabla\mathbf{u}\cdot\boldsymbol{\omega}\,\mathrm{d}\mathbf{x} \leq C_\nu\left(\int |\boldsymbol{\omega}|^2\,\mathrm{d}\mathbf{x}\right)^3 + \frac{\nu}{2}\int |\nabla\boldsymbol{\omega}|^2\,\mathrm{d}\mathbf{x}, \tag{3.3}$$

which can not be improved. This implies that

$$\frac{1}{2}\frac{\mathrm{d}}{\mathrm{d}t}\int |\boldsymbol{\omega}|^2\,\mathrm{d}\mathbf{x} + \frac{\nu}{2}\int |\nabla\boldsymbol{\omega}|^2\,\mathrm{d}\mathbf{x} \leq C_\nu\left(\int |\boldsymbol{\omega}|^2\,\mathrm{d}\mathbf{x}\right)^3. \tag{3.4}$$

Unfortunately, the above estimate does not imply global regularity for large data even if we use the energy identity (3.1). However, the estimate (3.4) can be used to obtain global regularity for small initial data. To see this, we substitute the following interpolation inequality,

$$\left(\int |\boldsymbol{\omega}|^2 \,\mathrm{d}\mathbf{x}\right)^2 = \|\boldsymbol{\omega}\|_{L^2}^4 \le C_0 \|\mathbf{u}\|_{L^2}^2 \|\nabla \boldsymbol{\omega}\|_{L^2}^2, \tag{3.5}$$

into (3.4) to obtain

$$\frac{1}{2}\frac{\mathrm{d}}{\mathrm{d}t}\|\boldsymbol{\omega}\|_{L^2}^2 \le \left(C_\nu C_0 \|\mathbf{u}\|_{L^2}^2 \|\boldsymbol{\omega}\|_{L^2}^2 - \frac{\nu}{2}\right)\|\nabla \boldsymbol{\omega}\|_{L^2}^2 \le 0, \tag{3.6}$$

provided that

$$C_\nu C_0 \|\mathbf{u}_0\|_{L^2}^2 \|\boldsymbol{\omega}_0\|_{L^2}^2 \le \frac{\nu}{2}. \tag{3.7}$$

Since $\|\mathbf{u}(t)\|_{L^2}^2 \le \|\mathbf{u}_0\|_{L^2}^2$ for all t, condition (3.7) and inequality (3.6) imply that $\|\boldsymbol{\omega}(t)\|_{L^2}^2 \le \|\boldsymbol{\omega}_0\|_{L^2}^2$ for all times. Note that $\|\boldsymbol{\omega}_0\|_{L^2}^2 = \|\nabla \mathbf{u}_0\|_{L^2}^2$. Thus we can also replace (3.7) by

$$C_\nu C_0 \|\mathbf{u}_0\|_{L^2}^2 \|\nabla \mathbf{u}_0\|_{L^2}^2 \le \frac{\nu}{2}. \tag{3.8}$$

Due to the incompressibility condition, convection plays no role in the energy estimate. The same estimate can be also applied to the following nonlinear diffusion equation:

$$w_t = w^2 + \nu \Delta w. \tag{3.9}$$

An energy estimate gives

$$\frac{1}{2}\frac{\mathrm{d}}{\mathrm{d}t}\int |w|^2 \,\mathrm{d}\mathbf{x} + \nu \int |\nabla w|^2 \,\mathrm{d}\mathbf{x} = \int w^3 \,\mathrm{d}\mathbf{x}. \tag{3.10}$$

Using an embedding inequality similar to (3.3), we get

$$\frac{1}{2}\frac{\mathrm{d}}{\mathrm{d}t}\int |w|^2 \,\mathrm{d}\mathbf{x} + \frac{\nu}{2}\int |\nabla w|^2 \,\mathrm{d}\mathbf{x} \le C_\nu \left(\int |w|^2 \,\mathrm{d}\mathbf{x}\right)^3, \tag{3.11}$$

which is identical to (3.4).

However, it is well known that (3.9) can develop a finite-time isotropic self-similar blow-up solution, which does not violate the energy identity (3.1), in the sense that $\int_0^T \|w(t)\|_{L^2}^2 \,\mathrm{d}t < \infty$. The above analysis shows that energy estimates can not distinguish a nonlinear diffusion equation, which has a finite-time blow-up solution, from the 3D Navier–Stokes equations, which have completely different physical properties and may not necessarily blow up in finite time.

3.1. Reformulation of 3D axisymmetric Navier–Stokes equations

Consider the 3D axisymmetric incompressible Navier–Stokes equations

$$u_t^\theta + u^r u_r^\theta + u^z u_z^\theta = \nu\left(\nabla^2 - \frac{1}{r^2}\right)u^\theta - \frac{1}{r}u^r u^\theta, \tag{3.12}$$

$$\omega_t^\theta + u^r \omega_r^\theta + u^z \omega_z^\theta = \nu\left(\nabla^2 - \frac{1}{r^2}\right)\omega^\theta + \frac{1}{r}\left((u^\theta)^2\right)_z + \frac{1}{r}u^r \omega^\theta, \tag{3.13}$$

$$-\left(\nabla^2 - \frac{1}{r^2}\right)\psi^\theta = \omega^\theta, \tag{3.14}$$

where $r = \sqrt{x^2+y^2}$, u^θ, ω^θ and ψ^θ are the angular components of the velocity, vorticity and stream function respectively, and

$$u^r = -(\psi^\theta)_z \quad u^z = \frac{1}{r}(r\psi^\theta)_r.$$

Note that equations (3.12)–(3.14) completely determine the evolution of the 3D axisymmetric Navier–Stokes equations.

Hou and Li (2008*a*) introduced the following new variables,

$$u_1 = u^\theta/r, \quad \omega_1 = \omega^\theta/r, \quad \psi_1 = \psi^\theta/r, \tag{3.15}$$

and derived the following equivalent system that governs the dynamics of u_1, ω_1 and ψ_1:

$$\partial_t u_1 + u^r \partial_r u_1 + u^z \partial_z u_1 = \nu\left(\partial_r^2 + \frac{3}{r}\partial_r + \partial_z^2\right)u_1 + 2u_1\psi_{1z}, \tag{3.16a}$$

$$\partial_t \omega_1 + u^r \partial_r \omega_1 + u^z \partial_z \omega_1 = \nu\left(\partial_r^2 + \frac{3}{r}\partial_r + \partial_z^2\right)\omega_1 + (u_1^2)_z, \tag{3.16b}$$

$$-\left(\partial_r^2 + \frac{3}{r}\partial_r + \partial_z^2\right)\psi_1 = \omega_1, \tag{3.16c}$$

where $u^r = -r\psi_{1z}$, $\quad u^z = 2\psi_1 + r\psi_{1r}$. Liu and Wang (2006) showed that if $\mathbf{u}$ is a smooth velocity field, then u^θ, ω^θ and ψ^θ must satisfy the compatibility condition $u^\theta|_{r=0} = \omega^\theta|_{r=0} = \psi^\theta|_{r=0} = 0$. Thus u_1, ψ_1 and ω_1 are well defined as long as the solution remains smooth.

3.2. An exact 1D model for 3D Navier–Stokes equations

Hou and Li (2008*a*) derived an exact 1D model along the symmetry axis by assuming the solution is more singular along the z-direction than along the r-direction (*i.e.*, the solution has an locally anisotropic scaling). Along the symmetry axis $r = 0$, we have $u^r = 0$, $u^z = 2\psi_1$. Since the solution is more singular along the z-direction, one can drop the derivatives along the r-direction to the leading order in the reformulated Navier–Stokes equations (note that $\frac{3}{r}\partial_r$ is of the same order as ∂_r^2). This gives rise to the following

1D model:

$$(u_1)_t + 2\psi_1(u_1)_z = \nu(u_1)_{zz} + 2(\psi_1)_z u_1, \tag{3.17}$$

$$(\omega_1)_t + 2\psi_1(\omega_1)_z = \nu(\omega_1)_{zz} + (u_1^2)_z, \tag{3.18}$$

$$-(\psi_1)_{zz} = \omega_1. \tag{3.19}$$

Note that the system (3.17)–(3.19) is already a closed system. Let $\tilde{u} = u_1$, $\tilde{v} = -(\psi_1)_z$, and $\tilde{\psi} = \psi_1$. By integrating (3.18) with respect to z, one can further reduce the above system to

$$(\tilde{u})_t + 2\tilde{\psi}(\tilde{u})_z = \nu(\tilde{u})_{zz} - 2\tilde{v}\tilde{u}, \tag{3.20}$$

$$(\tilde{v})_t + 2\tilde{\psi}(\tilde{v})_z = \nu(\tilde{v})_{zz} + (\tilde{u})^2 - (\tilde{v})^2 + c(t), \tag{3.21}$$

where $\tilde{v} = -(\tilde{\psi})_z$, $\tilde{v}_z = \tilde{\omega}$, and $c(t)$ is an integration constant to enforce the mean of $\tilde{v}$ equal to zero. If we assume that the solution is periodic with respect to z with period 1, the integration constant $c(t)$ is equal to $3\int_0^1 (\tilde{v})^2\,\mathrm{d}z - \int_0^1 (\tilde{u})^2\,\mathrm{d}z$.

A surprising result is that the above 1D model is exact. This is stated in the following theorem.

Theorem 3.1. Let u_1, ψ_1 and ω_1 be the solution of the 1D model (3.17)–(3.19) and define

$$u^\theta(r,z,t) = ru_1(z,t), \quad \omega^\theta(r,z,t) = r\omega_1(z,t), \quad \psi^\theta(r,z,t) = r\psi_1(z,t).$$

Then $(u^\theta(r,z,t), \omega^\theta(r,z,t), \psi^\theta(r,z,t))$ is an exact solution of the 3D Navier–Stokes equations.

Theorem 3.1 tells us that the 1D model (3.17)–(3.19) preserves some essential nonlinear structure of the 3D axisymmetric Navier–Stokes equations.

3.3. Properties of the model equation

In this section, we will study some properties of the 1D model. We first consider the properties of some further simplified models obtained from these equations. Both numerical and analytical studies are presented for these simplified models. Based on the understanding of the simplified models, we prove the global existence of the full 1D model.

The ODE model

To start with, we consider an ODE model by ignoring the convection and diffusion term:

$$(\tilde{u})_t = -2\tilde{v}\tilde{u}, \tag{3.22}$$

$$(\tilde{v})_t = (\tilde{u})^2 - (\tilde{v})^2, \tag{3.23}$$

with initial condition $\tilde{u}(0) = \tilde{u}_0$ and $\tilde{v}(0) = \tilde{v}_0$.

Clearly, if $\tilde{u}_0 = 0$, then $\tilde{u}(t) = 0$ for all $t > 0$. In this case, the equation for $\tilde{v}$ is decoupled from $\tilde{u}$ completely, and will blow up in finite time if $\tilde{v}_0 < 0$. In fact, if $\tilde{v}_0 < 0$ and $\tilde{u}_0$ is very small, then the solution can experience very large growth dynamically. The growth can be made arbitrarily large if we choose $\tilde{u}_0$ to be arbitrarily small. However, the special nonlinear structure of the ODE system has an interesting cancellation property which has a stabilizing effect on the solution for large times. This is described by the following theorem.

Theorem 3.2. Assume that $\tilde{u}_0 \neq 0$. Then the solution $(\tilde{u}(t), \tilde{v}(t))$ of the ODE system (3.22)–(3.23) exists for all times. Moreover, we have

$$\lim_{t \to +\infty} \tilde{u}(t) = 0, \quad \lim_{t \to +\infty} \tilde{v}(t) = 0. \tag{3.24}$$

Proof. Inspired by the work of Constantin, Lax and Majda (1985), we make the following change of variables: $w = \tilde{u} + i\tilde{v}$. Then the ODE system (3.22)–(3.23) is reduced to the following complex nonlinear ODE:

$$\frac{\mathrm{d}w}{\mathrm{d}t} = \mathrm{i}w^2, \quad w(0) = w_0, \tag{3.25}$$

which can be solved analytically. The solution has the form

$$w(t) = \frac{w_0}{1 - \mathrm{i}w_0 t}. \tag{3.26}$$

In terms of the original variables, we have

$$\tilde{u}(t) = \frac{\tilde{u}_0(1 + \tilde{v}_0 t) - \tilde{u}_0 \tilde{v}_0 t}{(1 + \tilde{v}_0 t)^2 + (\tilde{u}_0 t)^2}, \tag{3.27}$$

$$\tilde{v}(t) = \frac{\tilde{v}_0(1 + \tilde{v}_0 t) + \tilde{u}_0^2 t}{(1 + \tilde{v}_0 t)^2 + (\tilde{u}_0 t)^2}. \tag{3.28}$$

It is clear from (3.27)–(3.28) that the solution of the ODE system (3.22)–(3.23) exists for all times and decays to zero as $t \to +\infty$ as long as $\tilde{u}_0 \neq 0$. This completes the proof of Theorem 3.2. □

As we can see from (3.27)–(3.28), the solution can grow very fast in a very short time if $\tilde{u}_0$ is small, but $\tilde{v}_0$ is large and negative. For example, if we let $\tilde{v}_0 = -1/\epsilon$ and $\tilde{u}_0 = \epsilon$ for $\epsilon > 0$ small, we obtain at $t = \epsilon$

$$\tilde{u}(\epsilon) = 1/\epsilon^3, \quad \tilde{v}(\epsilon) = 1/\epsilon.$$

We can see that within ϵ time, $\tilde{u}$ grows from its initial value of order ϵ to $O(\epsilon^{-3})$, a factor of ϵ^{-4} amplification.

The key ingredient in obtaining the global existence in Theorem 3.2 is that the coefficient on the right-hand side of (3.22) is less than -1. For this ODE system, there are two distinguished phases. In the first phase, if $\tilde{v}$ is negative and large in magnitude, but $\tilde{u}$ is small, then $\tilde{v}$ can experience

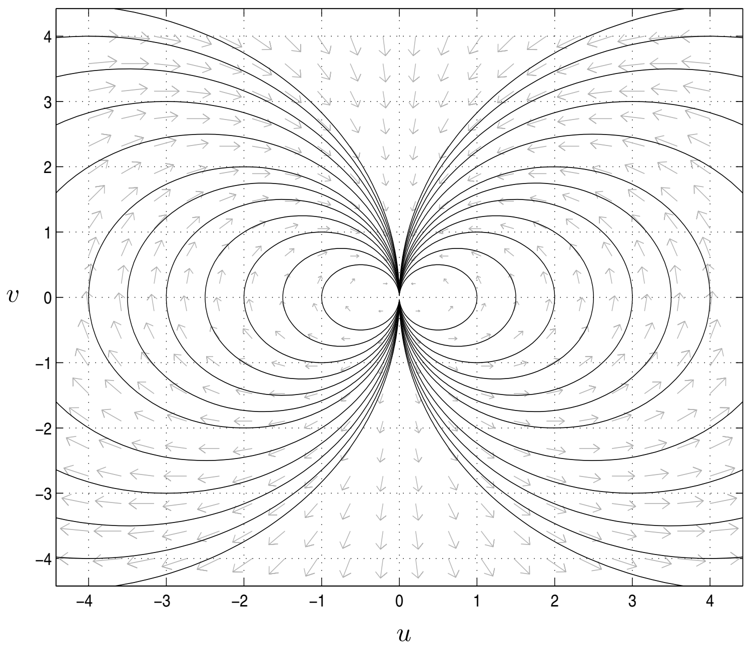

Figure 3.1. The phase diagram for the ODE system.

tremendous dynamic growth, which is essentially governed by

$$\tilde{v}_t = -\tilde{v}^2.$$

However, as $\tilde{v}$ becomes very large and negative, it will induce a rapid growth in $\tilde{u}$. The nonlinear structure of the ODE system is such that $\tilde{u}$ will eventually grow even faster than $\tilde{v}$ and force $(\tilde{u})^2 - (\tilde{v})^2 < 0$ in the second phase. From this time on, $\tilde{v}$ will increase in time and eventually become positive. Once $\tilde{v}$ becomes positive, the nonlinear term, $-\tilde{v}^2$, becomes stabilizing for $\tilde{v}$. Similarly, the nonlinear term, $-2\tilde{u}\tilde{v}$, becomes stabilizing for $\tilde{u}$. This subtle dynamic stability property of the ODE system can be best illustrated by the phase diagram in Figure 3.1.

The reaction–diffusion model

In this subsection, we consider the reaction–diffusion system:

$$(\tilde{u})_t = \nu \tilde{u}_{zz} - 2\tilde{v}\tilde{u}, \tag{3.29}$$

$$(\tilde{v})_t = \nu \tilde{v}_{zz} + (\tilde{u})^2 - (\tilde{v})^2. \tag{3.30}$$

As we can see for the corresponding ODE system, the structure of the nonlinearity plays an essential role in obtaining global existence. Intuitively, one may think that the diffusion term would help to stabilize the dynamic growth induced by the nonlinear terms. However, because the nonlinear ODE system in the absence of viscosity is very unstable, the diffusion term can actually have a destabilizing effect. Below we demonstrate this somewhat surprising fact through careful numerical experiments.

In Figures 3.2–3.4, we plot a time sequence of solutions for the above reaction–diffusion system with the following initial data:

$$\tilde{u}_0(z) = \epsilon(2 + \sin(2\pi z)), \quad \tilde{v}_0(z) = -\frac{1}{\epsilon} - \sin(2\pi z),$$

where $\epsilon = 0.001$. For this initial condition, the solution is periodic in z with period one. We use a pseudo-spectral method to discretize the coupled system (3.29)–(3.30) in space and use the simple forward Euler discretization for the nonlinear terms and the backward Euler discretization for the diffusion term. In order to resolve the nearly singular solution structure, we use $N = 32,768$ grid points with an adaptive time step satisfying

$$\Delta t_n\big(|\max\{\tilde{u}^n\}| + |\min\{\tilde{u}^n\}| + |\max\{\tilde{v}^n\}| + |\min\{\tilde{v}^n\}|\big) \leq 0.01,$$

where $\tilde{u}^n$ and $\tilde{v}^n$ are the numerical solution at time t_n and $t_n = t_{n-1}+\Delta t_{n-1}$ with the initial time stepsize $\Delta t_0 = 0.01\epsilon$. During the time iterations, the smallest time step is as small as $O(10^{-10})$.

From Figure 3.2, we can see that the magnitude of the solution $\tilde{v}$ increases rapidly by a factor of 150 within a very short time ($t = 0.00099817$). As the solution $\tilde{v}$ becomes large and negative, the solution $\tilde{u}$ increases much more rapidly than $\tilde{v}$. By time $t = 0.0010042$, $\tilde{u}$ has increased to about 2.5×10^8 from its initial condition, which is of magnitude 10^{-3}. This is a factor of 2.5×10^{11} increase. At this time, the minimum of $\tilde{v}$ has reached -2×10^8. Note that since $\tilde{u}$ has outgrown $\tilde{v}$ in magnitude, the nonlinear term, $\tilde{u}^2 - \tilde{v}^2$, on the right-hand side of the $\tilde{v}$-equation has changed sign. This causes the solution $\tilde{v}$ to split. By the time $t = 0.001004314$ (see Figure 3.3), both $\tilde{u}$ and $\tilde{v}$ have split and settled down to two relatively stable travelling wave solutions. The wave on the left will travel to the left while the wave on the right will travel to the right. Due to the periodicity in z, the two travelling waves approach each other from the right side of the domain. The ‘collision’ of these two travelling waves tends to annihilate each other. In particular, the negative part of $\tilde{v}$ is effectively eliminated during this nonlinear interaction. By the time $t = 0.00100603$ (see Figure 3.4), the solution $\tilde{v}$ becomes all positive. Once $\tilde{v}$ becomes positive, the effect of nonlinearity becomes stabilizing for both $\tilde{u}$ and $\tilde{v}$, as in the case of the ODE system. From then on, the solution decays rapidly. By $t = 0.2007$, the magnitude of $\tilde{u}$ is as small as 5.2×10^{-8}, and $\tilde{v}$ becomes almost a constant function with value close to 5. From this time on, $\tilde{u}$ is essentially decoupled from $\tilde{v}$ and will decay like $O(1/t)$.

(a)

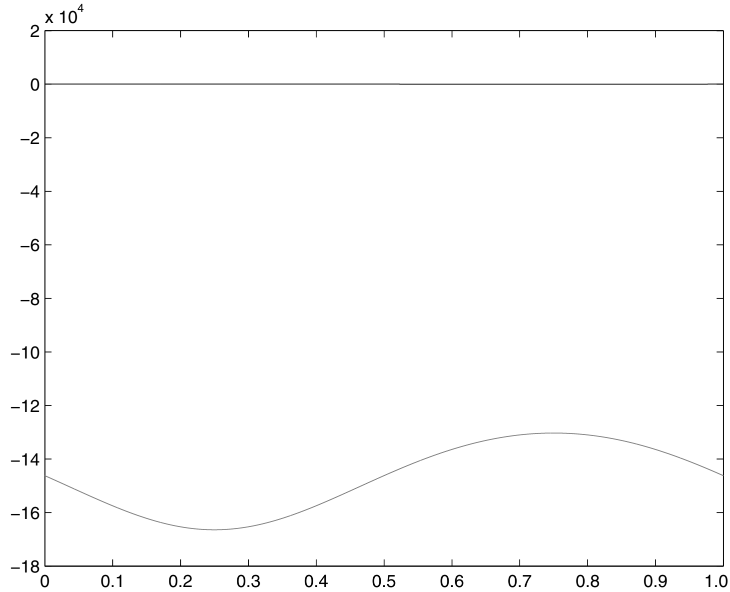

(b)

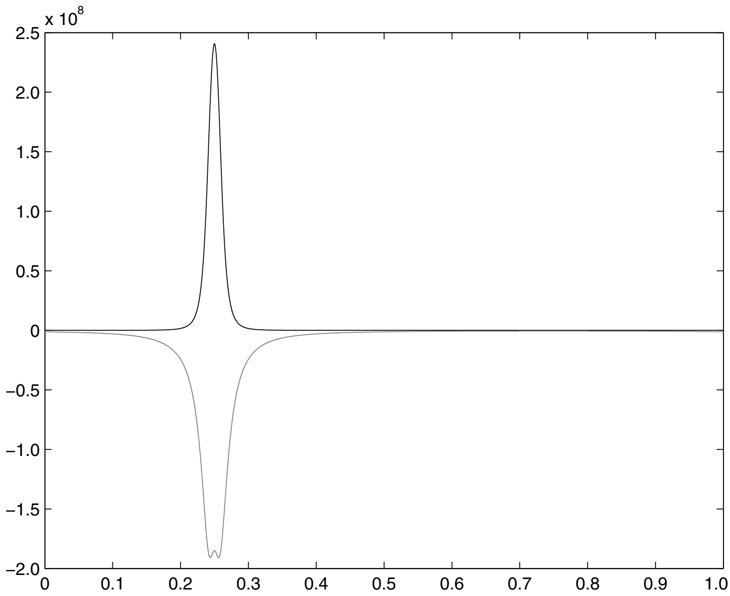

Figure 3.2. The solutions u (dark curve) and v (light curve) at
(a) $t = 0.00099817$, and (b) $t = 0.0010042$, respectively; $N = 32768$, $\nu = 1$.

(a)

(b)

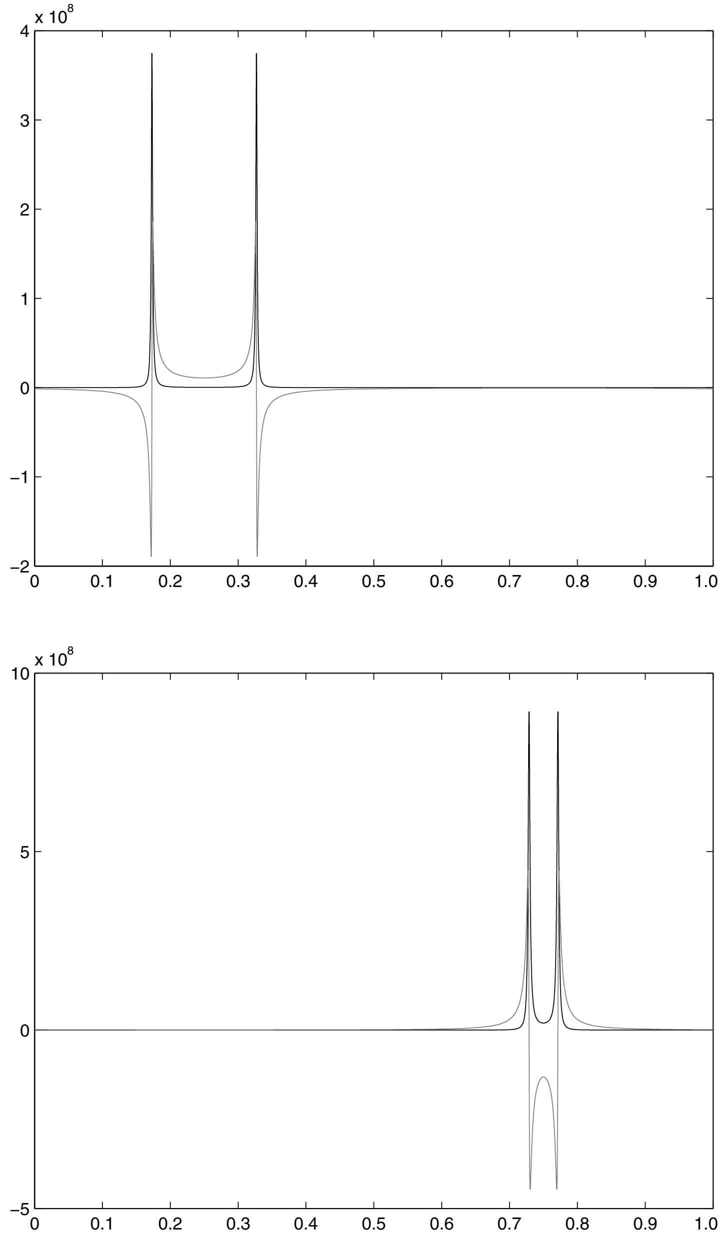

Figure 3.3. The solutions u (dark) and v (light) at (a) $t = 0.001004314$, and (b) $t = 0.001005862$, respectively; $N = 32768$, $\nu = 1$.

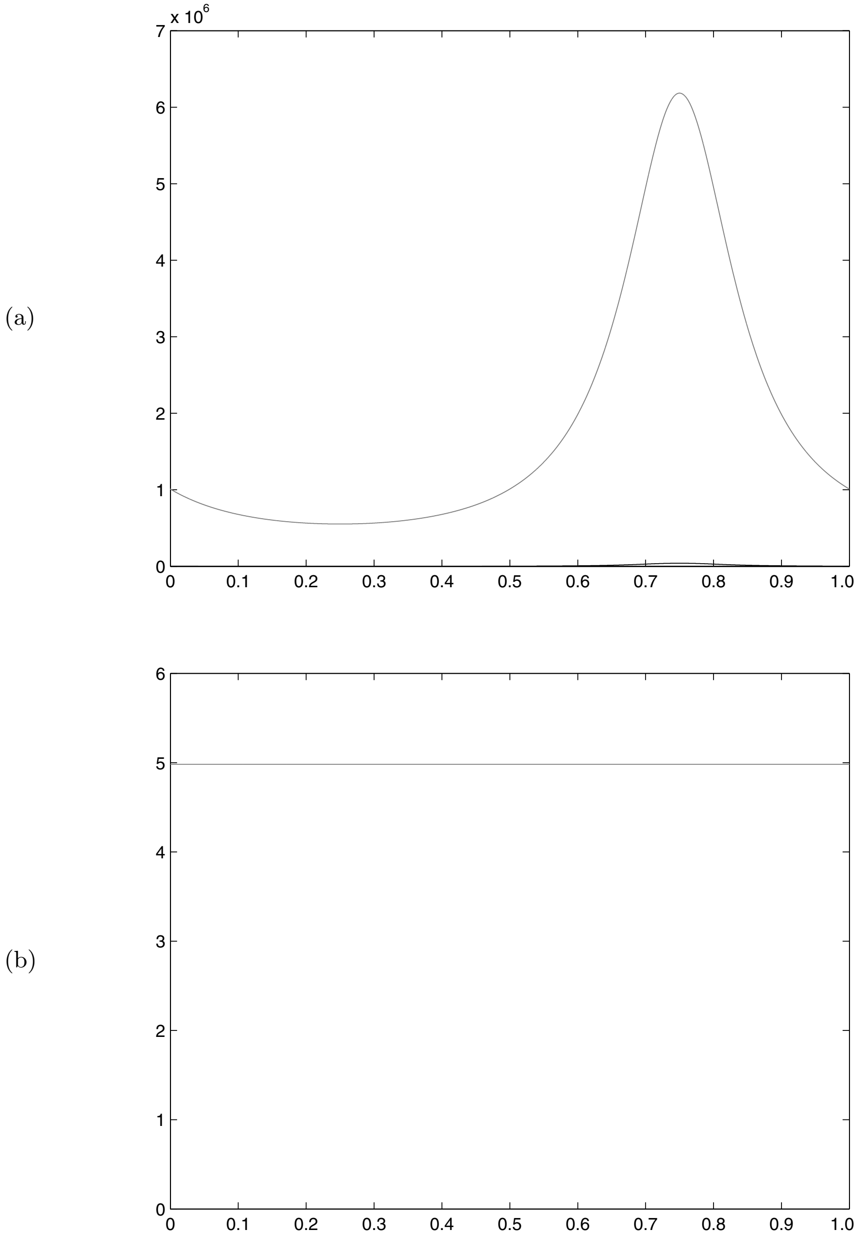

Figure 3.4. The solutions u (dark) and v (light) at (a) $t = 0.00100603$, and (b) $t = 0.2007$, respectively; $N = 32768$, $\nu = 1$. Note that at $t = 0.00100603$, the value of u becomes quite small and is very close to the x-axis. By $t = 0.2007$, the value of u is of the order 5.2×10^{-8} and is almost invisible.

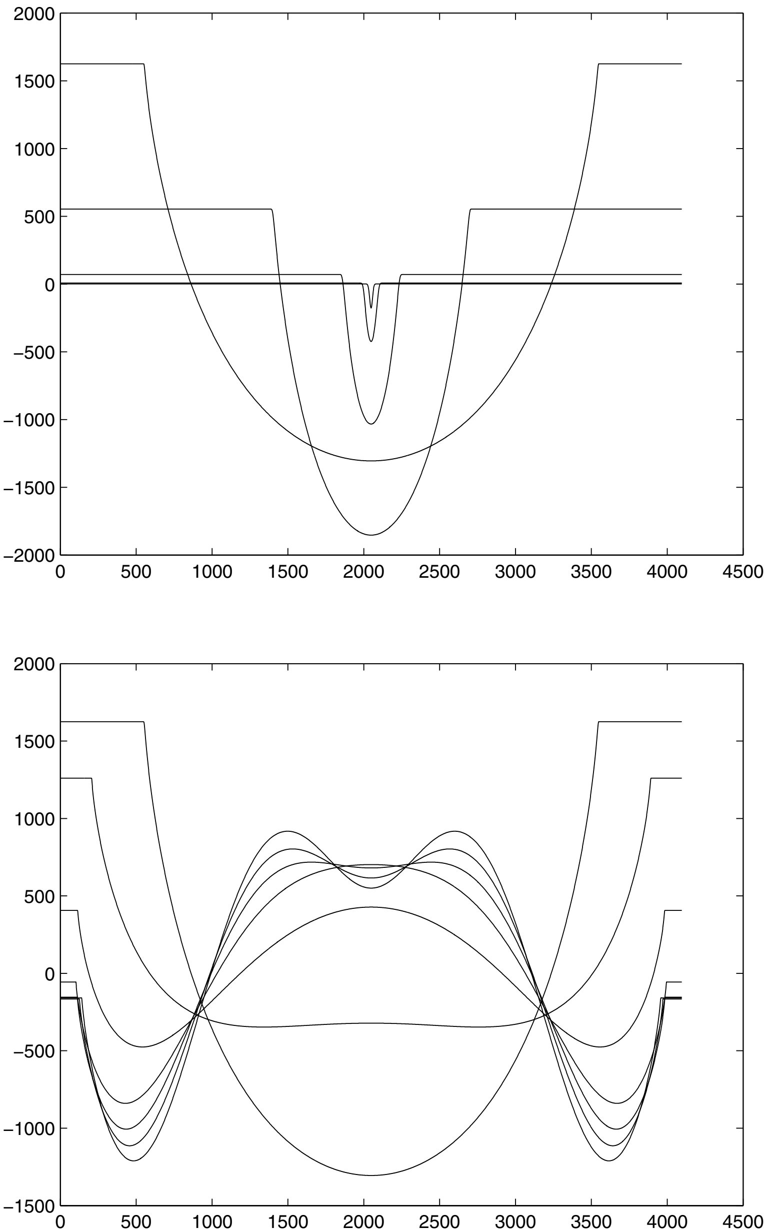

(a)

(b)

Figure 3.5. The time sequence of v in the Eulerian coordinate, $N = 4096$, $\nu = 0$. (a) $t = 0, 0.0033, 0.0048, 0.0055, 0.0059$, (b) $t = 0.0059, 0.0062, 0.0066, 0.007, 0.0074, 0.0078, 0.0081$. The solutions are plotted against the number of grid points corresponding to the range $[0, 1]$ in physical space.

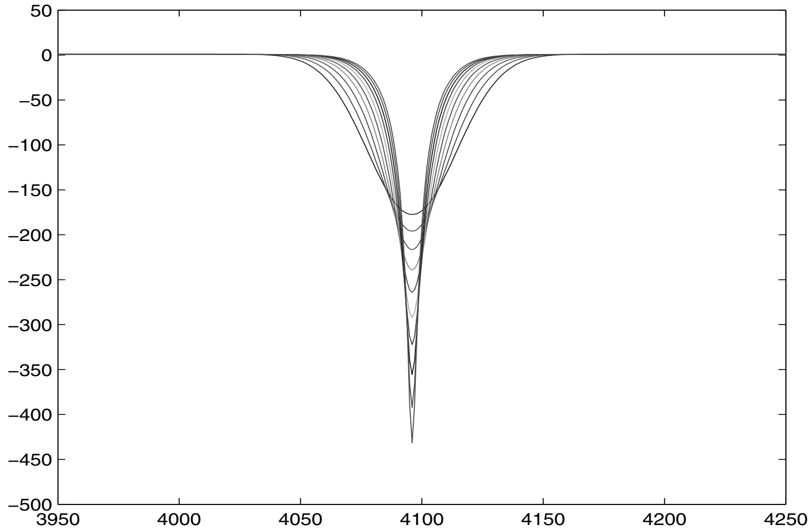

Figure 3.6. The time sequence of solution v in the Lagrangian coordinate by solving the model equation with the wrong sign, $N = 8192$, $\nu = 0$. The time sequence is from $t = 0$ to 0.0033 corresponding to a sequence of curves from the top to the bottom. The solutions are plotted against the number of grid points corresponding to the range $[0.482, 0.519]$ in physical space.

3.4. Global well-posedness of the full 1D model

We have also performed numerical studies of the full 1D model. We find that the solution behaviour of the full 1D model is completely different from the reaction–diffusion model. In particular, the convection term plays an essential role in regularizing the nearly singular behaviour of the reaction–diffusion model. In our numerical computations, we use a pseudo-spectral method to discretize in space and a second-order Runge–Kutta discretization in time with an adaptive time-stepping. The initial data are given by

$$u(\alpha, 0) = 1, \quad v(\alpha, 0) = 1 - \frac{1}{\delta} \exp^{-(x-0.5)^2/\epsilon},$$

with $\epsilon = 0.00001$ and $\delta = \sqrt{\epsilon\pi}$. In Figure 3.5, we plot a sequence of snapshots of the solution. We see that the solution experiences a similar splitting process as in the reaction–diffusion model. On the other hand, we observe that as the solution $\tilde{v}$ grows large and negative, the initial sharp profile of $\tilde{v}$ becomes defocused and smoother. This is a consequence of the incompressibility of the fluid flow. If we change the sign of the convection velocity from $2\tilde{\psi}$ to $-2\tilde{\psi}$, the profile of $\tilde{v}$ becomes focused dynamically and seems to evolve into a focusing finite-time blow-up: see Figure 3.6.

Based on our numerical studies, we become convinced that the solution of the full 1D model should be regular for all times. However, it is extremely difficult, if not impossible, to prove the global regularity of the 1D model by using an energy type of estimates. If we multiply the $\tilde{u}$-equation by $\tilde{u}$, and the $\tilde{v}$-equation by $\tilde{v}$, and integrate over z, we arrive at

$$\frac{1}{2}\frac{\mathrm{d}}{\mathrm{d}t}\int_0^1 \tilde{u}^2\,\mathrm{d}z = -3\int_0^1 (\tilde{u})^2\tilde{v}\,\mathrm{d}z - \nu\int_0^1 \tilde{u}_z^2\,\mathrm{d}z, \tag{3.31}$$

$$\frac{1}{2}\frac{\mathrm{d}}{\mathrm{d}t}\int_0^1 \tilde{v}^2\,\mathrm{d}z = \int_0^1 \tilde{u}^2\tilde{v}\,\mathrm{d}z - 3\int_0^1 (\tilde{v})^3\,\mathrm{d}z - \nu\int_0^1 \tilde{v}_z^2\,\mathrm{d}z. \tag{3.32}$$

Even for this 1D model, the energy estimate shares the some essential difficulty as the 3D Navier–Stokes equations. It is not clear how to control the nonlinear vortex-stretching-like terms by the diffusion term. On the other hand, if we assume that

$$\int_0^T \|\tilde{v}\|_{L^\infty}\,\mathrm{d}t < \infty,$$

similar to the Beale–Kato–Majda non-blow-up condition for vorticity (Beale, Kato and Majda 1984), then one can easily show that there is no blow-up before $t = T$.

In order to obtain the global regularity of the 1D model, we need to use a local estimate. The key is to obtain a pointwise estimate for a positive Lyapunov function. Convection is found to play an essential role in cancelling the destabilizing vortex stretching terms. Using this pointwise estimate, we can prove that if the initial conditions for $\tilde{u}$ and $\tilde{v}$ are in C^m with $m \geq 1$, then the solution remains in C^m for all times.

Theorem 3.3. (Hou and Li 2008*a*) Assume that $\tilde{u}(z,0)$ and $\tilde{v}(z,0)$ are in $C^m[0,1]$ with $m \geq 1$ and periodic with period 1. Then the solution $(\tilde{u},\tilde{v})$ of the 1D model will be in $C^m[0,1]$ for all times and for $\nu \geq 0$.

Proof. The key is to obtain a *pointwise* estimate *a priori* for the positive Lyapunov function $\tilde{u}_z^2 + \tilde{v}_z^2$. Differentiating (3.20)–(3.21) with respect to z, we get

$$(\tilde{u}_z)_t + 2\tilde{\psi}(\tilde{u}_z)_z - 2\tilde{v}\tilde{u}_z = -2\tilde{v}\tilde{u}_z - 2\tilde{u}\tilde{v}_z + \nu(\tilde{u}_z)_{zz}, \tag{3.33}$$

$$(\tilde{v}_z)_t + 2\tilde{\psi}(\tilde{v}_z)_z - 2\tilde{v}\tilde{v}_z = 2\tilde{u}\tilde{u}_z - 2\tilde{v}\tilde{v}_z + \nu(\tilde{v}_z)_{zz}. \tag{3.34}$$

Note that the convection term contributes to stability by *cancelling one of the nonlinear terms* on the right-hand side. This gives

$$(\tilde{u}_z)_t + 2\tilde{\psi}(\tilde{u}_z)_z = -2\tilde{u}\tilde{v}_z + \nu(\tilde{u}_z)_{zz}, \tag{3.35}$$

$$(\tilde{v}_z)_t + 2\tilde{\psi}(\tilde{v}_z)_z = 2\tilde{u}\tilde{u}_z + \nu(\tilde{v}_z)_{zz}. \tag{3.36}$$

Multiplying (3.35) by $2\tilde{u}_z$ and (3.36) by $2\tilde{v}_z$, we obtain

$$(\tilde{u}_z^2)_t + 2\tilde{\psi}(\tilde{u}_z^2)_z = -4\tilde{u}\tilde{u}_z\tilde{v}_z + 2\nu\tilde{u}_z(\tilde{u}_z)_{zz}, \tag{3.37}$$

$$(\tilde{v}_z^2)_t + 2\tilde{\psi}(\tilde{v}_z^2)_z = 4\tilde{u}\tilde{u}_z\tilde{v}_z + 2\nu\tilde{v}_z(\tilde{v}_z)_{zz}. \tag{3.38}$$

Now, we add (3.37) to (3.38). *Surprisingly, the remaining nonlinear vortex stretching terms cancel each other exactly.* We get

$$\big(\tilde{u}_z^2 + \tilde{v}_z^2\big)_t + 2\tilde{\psi}\big(\tilde{u}_z^2 + \tilde{v}_z^2\big)_z = 2\nu\big(\tilde{u}_z(\tilde{u}_z)_{zz} + \tilde{v}_z(\tilde{v}_z)_{zz}\big). \tag{3.39}$$

Further, we can rewrite equation (3.39) as follows:

$$\big(\tilde{u}_z^2 + \tilde{v}_z^2\big)_t + 2\tilde{\psi}\big(\tilde{u}_z^2 + \tilde{v}_z^2\big)_z = \nu\big(\tilde{u}_z^2 + \tilde{v}_z^2\big)_{zz} - 2\nu\big[(\tilde{u}_{zz})^2 + (\tilde{v}_{zz})^2\big]. \tag{3.40}$$

Now it is easy to see that $(\tilde{u}_z^2 + \tilde{v}_z^2)$ satisfies a *maximum principle* for all $\nu \geq 0$:

$$\|\tilde{u}_z^2 + \tilde{v}_z^2\|_{L^\infty} \leq \|(\tilde{u}_0)_z^2 + (\tilde{v}_0)_z^2\|_{L^\infty}.$$

It is worth emphasizing that the cancellation between the convection term and the vortex stretching term takes place at the inviscid level. Viscosity does not play an essential role here. Since $\tilde{v}$ has zero mean, the Poincaré inequality implies that $\|\tilde{v}\|_{L^\infty} \leq C_0$, with C_0 defined by

$$C_0 = \|\big((\tilde{u}_0)_z^2 + (\tilde{v}_0)_z^2\big)^{\frac{1}{2}}\|_{L^\infty}.$$

The boundedness of $\tilde{u}$ follows from the bound on $\tilde{v}$, that is, $\|\tilde{u}(t)\|_{L^\infty} \leq \|\tilde{u}_0\|_{L^\infty}\exp(2C_0 t)$. The higher-order regularity follows from the standard estimates. This proves Theorem 3.3. □

3.5. Construction of a family of 3D globally smooth solutions

We can use the solution from the 1D model to construct a family of globally smooth solutions for the 3D axisymmetric Navier–Stokes equations with large initial data of finite energy. We remark that a special feature of this family of globally smooth solutions is that the solution can potentially develop very large dynamic growth and it violates the smallness condition required by classical global existence results (Constantin and Foias 1988, Temam 2001).

Theorem 3.4. (Hou and Li 2008*a*) Let $\phi(r)$ be a smooth cut-off function and u_1, ω_1 and ψ_1 be the solution of the 1D model. Define

$$u^\theta(r,z,t) = ru_1(z,t)\phi(r) + \tilde{u}(r,z,t),$$

$$\omega^\theta(r,z,t) = r\omega_1(z,t)\phi(r) + \tilde{\omega}(r,z,t),$$

$$\psi^\theta(r,z,t) = r\psi_1(z,t)\phi(r) + \tilde{\psi}(r,z,t).$$

Then there exists a family of globally smooth functions $\tilde{u}$, $\tilde{\omega}$ and $\tilde{\psi}$ such that u^θ, ω^θ and ψ^θ are globally smooth solutions of the 3D Navier–Stokes equations with finite energy.

4. Stabilizing effect of convection for 3D Navier–Stokes

Hou and Lei (2009*b*) studied the stabilizing effect of the convection term in the 3D incompressible Euler or Navier–Stokes equations using a new 3D model. This model was derived from the reformulated Navier–Stokes equations. It shares many properties with the 3D Euler or Navier–Stokes equations. First of all, it has the same nonlinear vortex stretching term. Secondly, it has the same type of *a priori* energy identity. Thirdly, almost all the existing non-blow-up criteria for the 3D Euler or Navier–Stokes equations are also valid for our model. A 3D model that satisfies all these properties seems hard to find in general. But in terms of the equations for the new variables, u_1, ω_1, and ψ_1, we obtain our 3D model equations by simply dropping the convective term from the reformulated Navier–Stokes equations (3.16):

$$\partial_t u_1 = \nu\left(\partial_r^2 + \frac{3}{r}\partial_r + \partial_z^2\right)u_1 + 2u_1\psi_{1z}, \tag{4.1a}$$

$$\partial_t \omega_1 = \nu\left(\partial_r^2 + \frac{3}{r}\partial_r + \partial_z^2\right)\omega_1 + (u_1^2)_z, \tag{4.1b}$$

$$-\left(\partial_r^2 + \frac{3}{r}\partial_r + \partial_z^2\right)\psi_1 = \omega_1. \tag{4.1c}$$

Note that (4.1) is already a closed system. The main difference between our 3D model and the Navier–Stokes equations is that we neglect the convection term in our model. If we add the convection term back to our 3D model, we will recover the Navier–Stokes equations.

Below we will summarize some important properties of the model equations (4.1).

4.1. Properties of the 3D model

This 3D model shares many important properties with the axisymmetric Navier–Stokes equations. First of all, one can define an incompressible velocity field for the 3D model,

$$\mathbf{u}(t, \mathbf{x}) = u^r(t, r, z)e_r + u^\theta(t, r, z)e_\theta + u^z(t, r, z)e_z, \tag{4.2}$$

$$u^\theta = ru_1, \ u^r = -r\psi_{1z}, \quad u^z = 2\psi_1 + r\psi_{1r}, \tag{4.3}$$

where $\mathbf{x} = (x,\ y,\ z)$, $r = \sqrt{x^2+y^2}$. It is easy to check that

$$\nabla\cdot\mathbf{u} = \partial_r u^r + \partial_z u^z + \frac{u^r}{r} = 0, \tag{4.4}$$

which is the same as the original Navier–Stokes equations.

Furthermore, Hou and Lei (2009*b*) proved the following energy identity for the 3D model.

Theorem 4.1. (Energy identity (Hou and Lei 2009*b*)) The strong solution of (4.1) satisfies

$$\frac{1}{2}\frac{\mathrm{d}}{\mathrm{d}t}\int \big(|u_1|^2 + 2|D\psi_1|^2\big) r^3 \,\mathrm{d}r\,\mathrm{d}z + \nu \int \big(|Du_1|^2 + 2|D^2\psi_1|^2\big) r^3 \,\mathrm{d}r\,\mathrm{d}z = 0, \tag{4.5}$$

Here D is the first-order derivative operator defined in $\mathbb{R}^5$.

This energy identity is equivalent to that of the Navier–Stokes equations, which has the form

$$\frac{1}{2}\frac{\mathrm{d}}{\mathrm{d}t}\int \big(|u_1|^2 + |D\psi_1|^2\big) r^3 \,\mathrm{d}r\,\mathrm{d}z + \nu \int \big(|Du_1|^2 + |D^2\psi_1|^2\big) r^3 \,\mathrm{d}r\,\mathrm{d}z = 0. \tag{4.6}$$

Another result obtained by Hou and Lei is a non-blow-up criterion of the 3D model equations (4.1), which is an analogue of the Beale–Kato–Majda (BKM) result for the 3D Euler and Navier–Stokes equations. For the 3D Euler and Navier–Stokes equations, the BKM non-blow-up criterion states that the solution $\mathbf{u}$ blows up at time $T < \infty$ if and only if the accumulation of vorticity $\int_0^T \|\nabla_x \times \mathbf{u}\|_{L^\infty(\mathbb{R}^3)}\,\mathrm{d}t$ is infinite (Beale, Kato and Majda 1984). The BKM non-blow-up criterion was later improved by Kozono and Taniuchi (2000), who proved that the $\|\cdot\|_{L^\infty}$-norm can be replaced by the norm in the BMO space. This generalization is interesting because some crucial Sobolev embedding theorems can be applied to the BMO space, but not to the L^∞-space. A non-blow-up result formulated in terms of the BMO space has a broader range of applications.

Theorem 4.2. (A non-blow-up criterion of Beale–Kato–Majda type (Hou and Lei 2009*b*)) A smooth solution (u_1, ω_1, ψ_1) of the model (4.1) for $0 \le t < T$ blows up at time $t = T$ if and only if

$$\int_0^T \|\nabla \times \mathbf{u}\|_{\mathrm{BMO}(\mathbb{R}^3)}\,\mathrm{d}t = \infty, \tag{4.7}$$

where $\mathbf{u}$ is defined in (4.2)–(4.3).

There have been many results on the global regularity of the solutions of the 3D Navier–Stokes equations under some additional conditions imposed on the solution. In particular, the papers of Prodi (1959) and Serrin (1963) gave the following non-blow-up criterion for the solution of the 3D Navier–Stokes equations: *Any Leray–Hopf solution u to the 3D Navier–Stokes equations on $[0,T]$ is smooth on $[0,T]$ if $\|\mathbf{u}\|_{L^q_t L^p_x([0,T]\times\mathbb{R}^3)} < \infty$ for* *some p, q satisfying* $(3/p)+(2/q) \leq 1$, $3 < p \leq \infty$. A local version was later established by Serrin (1962) for $(3/p)+(2/q) < 1$ and by Struwe (1988) for $(3/p)+(2/q) = 1$. The highly non-trivial end-point case of $p = 3$ was recently established by Iskauriaza, Seregin and Sverak (2003).

To demonstrate the similarity between the 3D model equations (4.1) and the axisymmetric Navier–Stokes equations, Hou and Lei proved a non-blow-up criterion of the Prodi–Serrin type for their model.

Theorem 4.3. (A non-blow-up criterion of Prodi–Serrin type (Hou and Lei 2009*b*)) A weak solution (u_1, ω_1, ψ_1) of the model (4.1) is smooth on $[0,T] \times \mathbb{R}^3$ provided that

$$\|u^\theta\|_{L_t^q L_x^p([0,T]\times\mathbb{R}^3)} < \infty \tag{4.8}$$

for some p, q satisfying $\frac{3}{p} + \frac{2}{q} \leq 1$ with $3 < p \leq \infty$ and $2 \leq q < \infty$.

Finally, Hou and Lei (2009*a*) studied the local behaviour of the solutions to the 3D model equations and established an analogue of the Caffarelli–Kohn–Nirenberg partial regularity theory (Caffarelli *et al.* 1982) for their model. They proved that for any suitable weak solution of the 3D model in an open set in space-time, the one-dimensional Hausdorff measure of the associated singular set is zero. The proof of this partial regularity result is similar in spirit to that of Lin (1998), but there are some new technical difficulties associated with the 3D model. One of the difficulties is in handling the singularity induced by the cylindrical coordinates. This makes it difficult to analyse the partial regularity of the 3D model in $\mathbb{R} \times \mathbb{R}^3$. To overcome this difficulty, they performed their partial regularity analysis in $\mathbb{R} \times \mathbb{R}^5$. By working in $\mathbb{R}^5$, they avoided the difficulty associated with the coordinate singularity.

Another difficulty in obtaining our partial regularity result is that we do not have an evolution equation for the entire velocity field. We need to reformulate the model in terms of a new vector variable. This new variable can be considered as a 'generalized velocity field' in $\mathbb{R}^5$. We remark that the partial regularity theory for Navier–Stokes equations in $\mathbb{R}^5$ is still open due to the lack of certain compactness. When formulating the 3D model in $\mathbb{R} \times \mathbb{R}^5$, they found a 3D structure which has the same scaling as that of the 3D Navier–Stokes equations. This is why the partial regularity analysis can be carried out for the 3D model in $\mathbb{R} \times \mathbb{R}^5$ using a strategy similar to that of Lin (1998).

Theorem 4.4. (An analogue of Caffarelli–Kohn–Nirenberg partial regularity result (Hou and Lei 2009*a*)) For any suitable weak solution of the 3D model equations (4.1) on an open set in space-time, the one-dimensional Hausdorff measure of the associated singular set is zero.

4.2. Potential singularity formation of the 3D model

Despite the striking similarity at the theoretical level between the 3D model and the Navier–Stokes equations, the former displays a completely different behaviour from the full Navier–Stokes equations. In the next subsection, we will present numerical evidence which seems to support that the model may develop a potential finite-time singularity from smooth initial data with finite energy. Before we do that, we would like to gain some understanding at the theoretical level why the 3D model may develop a finite-time singularity. For this purpose, we consider the inviscid model by setting $\nu = 0$ in (4.1):

$$\partial_t u_1 = 2u_1\psi_{1z}, \tag{4.9a}$$

$$\partial_t \omega_1 = (u_1^2)_z, \tag{4.9b}$$

$$-\left(\partial_r^2 + \frac{3}{r}\partial_r + \partial_z^2\right)\psi_1 = \omega_1. \tag{4.9c}$$

If we let $v = \log(u_1^2)$, then we can further reduce the 3D model to the following non-local nonlinear wave equation:

$$v_{tt} = 4\big((-\Delta_5)^{-1}\mathrm{e}^v\big)_{zz}, \tag{4.10}$$

where $-\Delta_5 = -\big(\partial_r^2 + \frac{3}{r}\partial_r + \partial_z^2\big)$, and $\int \mathrm{e}^v r^3 \,\mathrm{d}r\,\mathrm{d}z \leq C_0$. Note that $(-\Delta_5)^{-1}$ is a positive operator. If we were to omit $(-\Delta_5)^{-1}$ from (4.10), we would obtain a 1D nonlinear wave equation, $v_{tt} = 4(\mathrm{e}^v)_{zz}$, or

$$v_{tt} = 4\mathrm{e}^v v_{zz} + 4\mathrm{e}^v(v_z)^2, \tag{4.11}$$

which we expect to develop a finite-time singularity.

4.3. Special blow-up solutions of the 3D model

We can construct a special class of blow-up solutions by letting $u_1 = z\tilde{u}(r,t)$, $\omega_1 = z\tilde{\omega}(r,t)$, and $\psi_1 = z\tilde{\psi}(r,t)$. Then it is easy to derive the following system for $\tilde{u}(r,t)$, $\tilde{\omega}(r,t)$, and $\tilde{\psi}(r,t)$:

$$\partial_t\tilde{u} = 2\tilde{\psi}\tilde{u} + \nu(\partial_r^2 + \frac{3}{r}\partial_r)\tilde{u}, \tag{4.12a}$$

$$\partial_t\tilde{\omega} = 2\tilde{u}^2 + \nu(\partial_r^2 + \frac{3}{r}\partial_r)\tilde{\omega}, \tag{4.12b}$$

$$-\left(\partial_r^2 + \frac{3}{r}\partial_r\right)\tilde{\psi} = \tilde{\omega}. \tag{4.12c}$$

Note that the nonlinear terms become local and quadratic. It is easy to show that if the initial data are positive, then the solution of (4.12) will remain positive for all times. Using this property, we can prove that the above system has finite-time blow-up solutions. However, such singular solutions have infinite energy unless we introduce a cut-off along the z-direction.

We remark that Constantin (1986) has constructed a family of finite-time blow-up solutions to the distorted Euler equations:

$$(\nabla \mathbf{u})_t + (\nabla \mathbf{u})^2 + \nabla\nabla p = 0, \tag{4.13}$$

where $-\Delta p = Tr((\nabla \mathbf{u})^2)$. We note that $\mathbf{u}$ is no longer divergence-free (in fact, there is no evolution equation for $\mathbf{u}$), and the model does not conserve energy. Moreover, the blow-up solution has infinite energy.

4.4. Numerical evidence for a potential finite-time singularity

In this subsection, we present numerical evidence which seems to support that the model may develop a potential finite-time singularity from smooth initial data with finite energy. By exploiting the axisymmetric geometry of the problem, we obtain a very efficient adaptive solver with an optimal complexity which provides effective local resolutions of order 4096^3. With this level of resolution, we obtain an excellent fit for the asymptotic blow-up rate of maximum axial vorticity. If we denote by ω^z the axial vorticity component along the z-direction, we find that $\|\omega^z\|_\infty(t) \approx C(T-t)^{-1}$ and the potential singularity approaches the symmetry axis (the z-axis) as $t \to T$. Moreover, our study seems to suggest that the potential singularity is locally self-similar and isotropic.

The initial condition considered in our numerical computations is given by

$$u_1(z,r,0) = (1+\sin(4\pi z))(r^2-1)^{20}(r^2-1.2)^{30}, \tag{4.14}$$

$$\psi_1(z,r,0) = 0, \tag{4.15}$$

$$\omega_1(z,r,0) = 0. \tag{4.16}$$

A second-order finite-difference discretization is used in space, and the classical fourth-order Runge–Kutta method is used to discretize in time. Since we expect that the potential singularity will appear along the symmetry axis at $r = 0$, we use the following coordinate transformation along the r-direction to achieve the adaptivity by clustering the grid points near $r = 0$:

$$r = f(\alpha) \equiv \alpha - 0.9\sin(\pi\alpha)/\pi. \tag{4.17}$$

With this change of variables, we can achieve an effective resolution up to 4096^3 for the corresponding 3D problem.

We now present numerical results which show that the solution of the viscous model becomes nearly singular. We choose the viscous coefficient to be $\nu = 0.001$ and perform a series of resolution studies using the adaptive method. We have used both uniform mesh and adaptive mesh with N_z ranging from 256 to 4096. Below we present the computational results obtained by using the adaptive mesh with the highest resolution $N_z = 4096$, $N_r = 400$, and $\Delta t = 2.5 \times 10^{-7}$. We will also perform a resolution study to demonstrate that our computations are well resolved.

From our analytical study of the 3D model, it follows by using a standard energy estimate that if u_1 is bounded, then the solution of the viscous 3D model cannot blow up in a finite time. Thus it is sufficient to monitor the growth of $\|u_1\|_\infty$ in time. We will present numerical evidence which seems to support that u_1 may develop a potential finite-time singularity for the initial condition we consider. The nature of this potential singularity and the mechanism for generating this potential singularity will be analysed in a later subsection.

In Figure 4.1, we plot the maximum of u_1 in time over the time interval $[0,\ 0.021]$ using the adaptive mesh method with $N_z = 4096$ and $N_r = 400$. The time step is chosen to be $\Delta t = 2.5\times 10^{-7}$. We can see that $\|u_1\|_\infty$ experiences a very rapid growth in time after $t = 0.02$. In Figure 4.1(b), we also plot $\log(\log(\|u_1\|_\infty))$ as a function of time. We can see clearly that $\|u_1\|_\infty$ grows much more rapidly than double exponential in time, which implies that the solution of our model may develop a finite-time singularity. We will present more careful analysis of this potentially singular behaviour later.

In Figures 4.2–4.3, we show a sequence of contour plots for u_1 from $t = 0.014$ to $t = 0.021$. At early times, we observe that the solution forms two large focusing centres of u_1 which approach each other. As this occurs, these rather localized regions are squeezed and form a thin layer parallel to the r-axis and with large gradients along the z-direction. As these regions approach each other and develop a thin layer parallel to the r-axis, the solution becomes locally z-dominant near the region where u_1 achieves its maximum. In this region, the 3D model can be approximated to the leading order by the corresponding 1D model along the z-direction. Hou and Lei (2009*b*) proved that the solution of the 1D model cannot blow up. The solution survives this potential blow-up scenario. After $t = 0.0172$, the maximum of u_1 starts to decrease. The two focusing centres move away from each other and their supports become more isotropic. As time increases, we observe that there is a strong nonlinear interaction between u_1 and $(\psi_1)_z$, which is induced by the overlap between the support of maximum of u_1 and the support of maximum of $(\psi_1)_z$. By the support of maximum of u_1, we mean the region in which u_1 is comparable to its maximum. The strong alignment between u_1 and $(\psi_1)_z$ near the support of maximum of u_1 leads to a rapid growth of the solution which may become singular in a finite time.

Another important observation is that as time increases, the position at which u_1 achieves its maximum also moves towards the symmetry axis. This suggests that the potential singularity will be along the symmetry axis at the singularity time. We note that $\lim_{r\to 0+} u_1 = 0.5 \lim_{r\to 0+} \omega^z$. Thus, the blow-up of u_1 characterizes the blow-up of the axial vorticity, ω^z.

Next, we perform a detailed study for the 3D model and push our computations very close to the potential singularity time. We use a sequence of

(a)

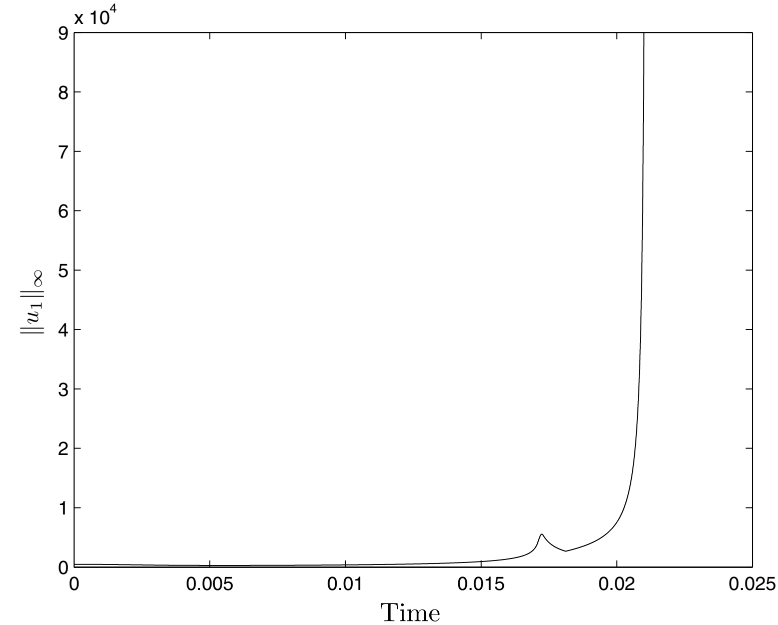

(b)

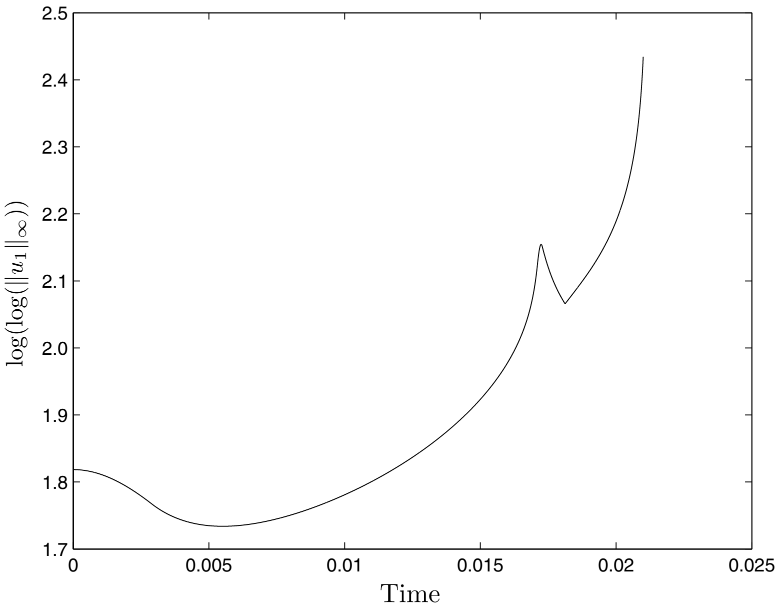

Figure 4.1. (a) $\|u_1\|_\infty$ as a function of time over the interval $[0,\ 0.021]$, (b) $\log(\log(\|u_1\|_\infty))$ as a function of time over the same interval. The solution is computed by an adaptive mesh with $N_z = 4096,\ N_r = 400,\ \Delta t = 2.5 \times 10^{-7}$, $\nu = 0.001$.

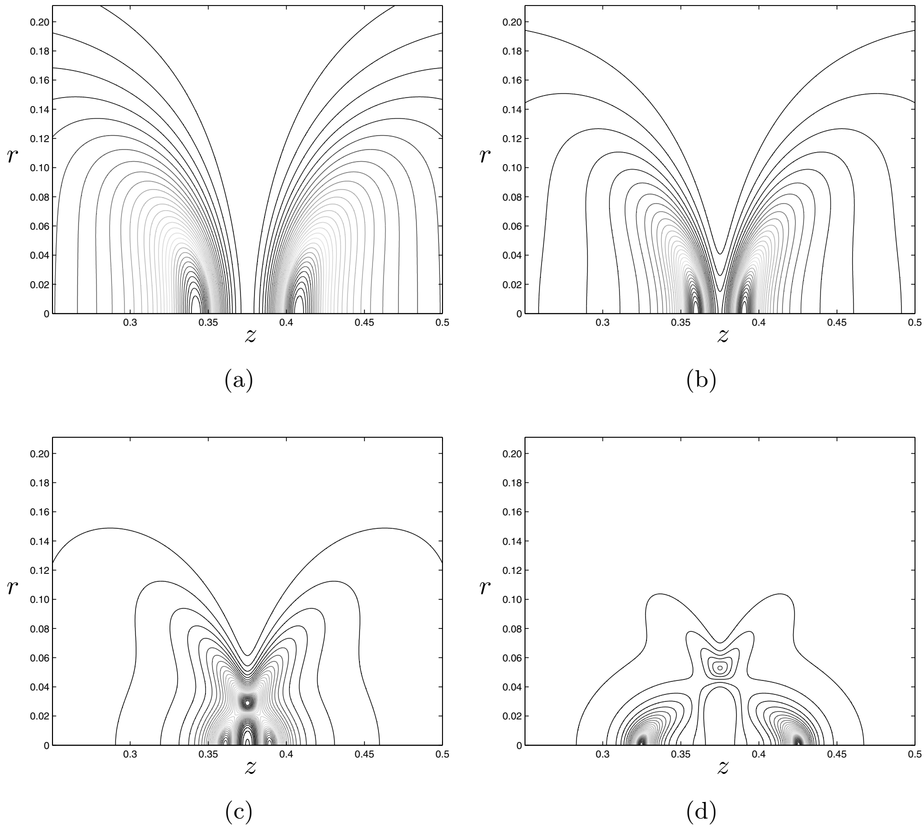

Figure 4.2. (a)–(d) The contour plots of u_1 for the viscous model at $t = 0.014$, 0.016, 0.018 and 0.02 respectively. Adaptive mesh computation with $N_z = 4096$, $N_r = 400$, $\Delta t = 2.5 \times 10^{-7}$, $\nu = 0.001$.

resolutions using both uniform and adaptive mesh. For the uniform mesh, we use resolutions for $N_z \times N_r$ ranging from 256×256 to 2048×2048 with time steps ranging from $\Delta t = 5 \times 10^{-6}$ to 5×10^{-7}. For the adaptive mesh, we use $N_z \times N_r = 2048 \times 256$, $N_z \times N_r = 3072 \times 328$ and $N_z \times N_r = 4096 \times 400$ respectively. The corresponding time steps for these computations are $\Delta t = 10^{-6}$, $\Delta t = 5 \times 10^{-7}$, and $\Delta t = 2.5 \times 10^{-7}$ respectively. With $N_z \times N_r = 4096 \times 400$, we achieve an effective resolution of 4000×4000 near the region of $r = 0$ where the solution is most singular.

To obtain further evidence for a potential finite-time singularity, we use a systematic singularity form fit procedure to obtain a good fit for the possible singularity of the solution. The procedure of our form fit is as

(a)

(b)

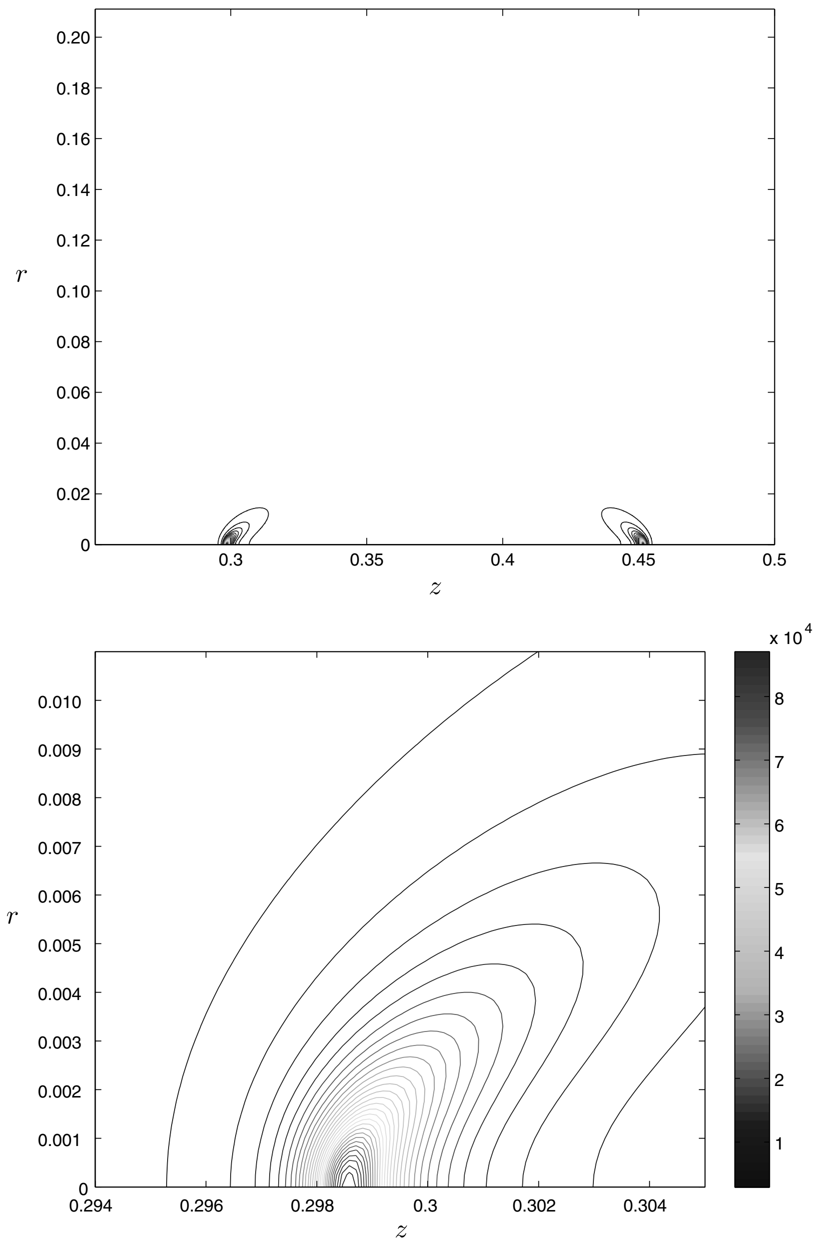

Figure 4.3. The contour of u_1 at $t = 0.021$ (a) and its close-up view (b) for the viscous model computed by the adaptive mesh with $N_z = 4096,\ N_r = 400$, $\Delta t = 2.5 \times 10^{-7}$, $\nu = 0.001$.

follows. We look for a finite-time singularity of the form

$$\|u_1\|_\infty \approx \frac{C}{(T-t)^\alpha}. \tag{4.18}$$

We have tried several ways to determine the fitting parameters T, C and α. Ultimately, we find that the best way is to study the inverse of $\|u_1\|_\infty$ as a function of time using a sequence of numerical resolutions. For each resolution, we find that the inverse of $\|u_1\|_\infty$ is almost a perfect linear function of time: see Figures 4.4 and 4.5. By using a least-squares fit of the inverse of $\|u_1\|_\infty$, we find that $\alpha = 1$ gives the best fit. The same least-squares fit also determines the potential singularity time T and the constant C. We remark that the $O(1/(T-t))$ blow-up rate of u_1, which measures the axial vorticity, is consistent with the non-blow-up criterion of Beale–Kato–Majda type.

To confirm that the above procedure indeed gives a good fit for the potential singularity, we plot $\|u_1\|_\infty^{-1}$ as a function of time in Figure 4.4(a). We can see that the agreement between the computed solution with $N_z \times N_r = 4096 \times 400$ and the fitted solution is almost perfect. In Figure 4.4(b) we plot $\|u_1\|_\infty$ computed by our adaptive method against the form fit $C/(T-t)$ with $T = 0.02109$ and $C = 8.20348$. The two curves are almost indistinguishable during the final stage of the computation from $t = 0.018$ to $t = 0.021$.

We further investigate the potential singular behaviour of the solution by using a sequence of resolutions to study the limiting behaviour of the

Table 4.1. Resolution study of parameters T and C in the asymptotic fit for the viscous model: $\|u_1\|_\infty^{-1} \approx \frac{(T-t)}{C}$ using different resolutions $h_z = 1/(2N_z)$. The resolutions we use in our adaptive computations are $N_z \times N_r = 1024 \times 128$, 2048×256, 3072×328 and 4096×400 respectively. The corresponding time steps are $\Delta t = 10^{-6}$, 5×10^{-7}, 3.625×10^{-7} and 2.5×10^{-7} respectively. The last row is obtained by extrapolating the second-order polynomial that interpolates the data obtained using $h_z = 1/4096$, $1/6144$ and $1/8192$.

h_z	T	C
1/2048	0.02114	8.409
1/4096	0.0211	8.2237
1/6144	0.021093	8.20946
1/8192	0.02109	8.20348
extrapolation to $h_z = 0$	0.021083	8.1901

(a)

(b)

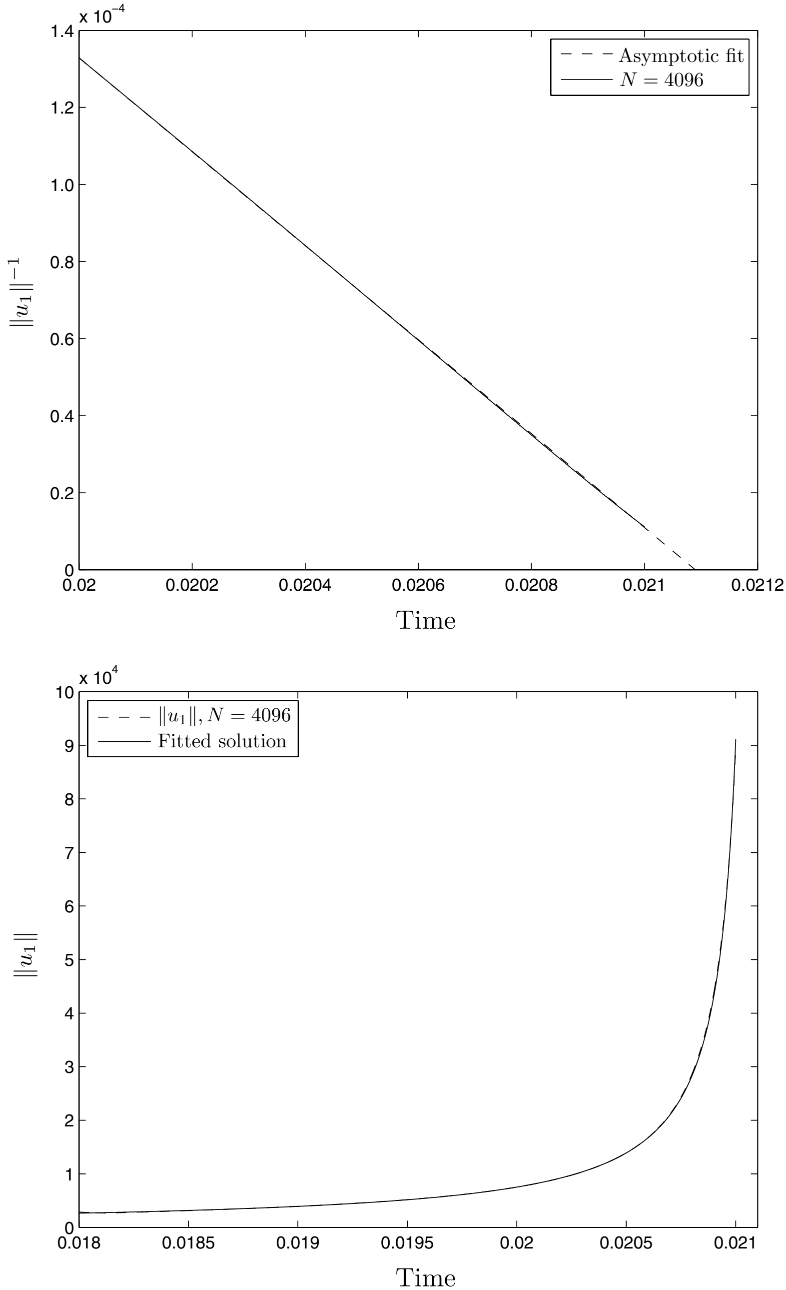

Figure 4.4. (a) The inverse of $\|u_1\|_\infty$ (solid line) versus the asymptotic fit (dashed line) for the viscous model; (b) $\|u_1\|_\infty$ (solid line) versus the asymptotic fit (dashed line). The asymptotic fit is of the form $\|u_1\|_\infty^{-1} \approx \frac{(T-t)}{C}$ with $T = 0.02109$ and $C = 8.20348$. The solution is computed by adaptive mesh with $N_z = 4096$, $N_r = 400$, $\Delta t = 2.5 \times 10^{-7}$; $\nu = 0.001$.

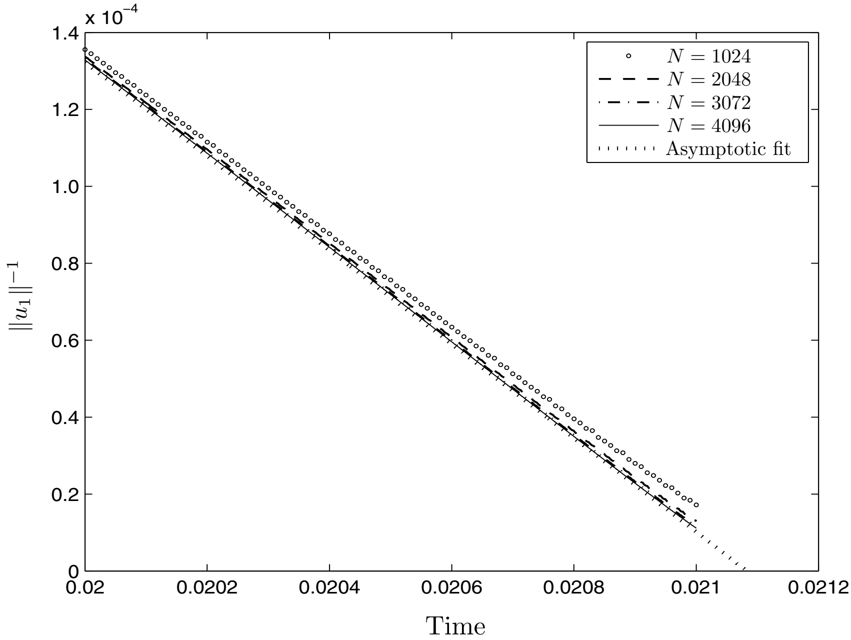

Figure 4.5. The inverse of $\|u_1\|_\infty$ in time for the viscous model. The solution is computed by adaptive mesh with $N_z = 1024$, 2048, 3072 and 4096 respectively (ordering from top to bottom in the figure), $\Delta t = 10^{-6}$, 5×10^{-7}, 3.625×10^{-7}, and 2.5×10^{-7} respectively. The last curve is the singularity fit by extrapolating the computational results obtained by $N_z = 2048$, 3072 and 4096 to infinite resolution $N_z = \infty$. The fitted curve is of the form $\|u_1\|_\infty^{-1} \approx (T - t)/C$, with $T = 0.021083$ and $C = 8.1901$; $\nu = 0.001$.

computed solution as we refine our resolutions. The space resolutions we use are $N_z \times N_r = 1024 \times 128$, 2048×256, 3072×328 and 4096×400 respectively. The corresponding time steps are $\Delta t = 10^{-6}$, 5×10^{-7}, 3.625×10^{-7} and 2.5×10^{-7} respectively. For each resolution, we obtain an optimal least-squares fit of the singularity of the form $\|u_1\|_\infty^{-1} \approx (T - t)/C$. The results are summarized in Table 4.1. Based on the fitted parameters T and C from the three largest resolutions, we construct a second-order polynomial that interpolates T and C through these three data points. We then use the polynomial to extrapolate the values of T and C to the infinite resolution limit. The extrapolated values at $h_z = 0$ are $T = 0.021083$ and $C = 8.1901$ respectively. In Figure 4.5, we plot the inverse of $\|u_1\|_\infty$ as a function of time using four different resolutions. We can see that as we refine the resolution, the computed solution converges to the extrapolated singularity limiting profile.

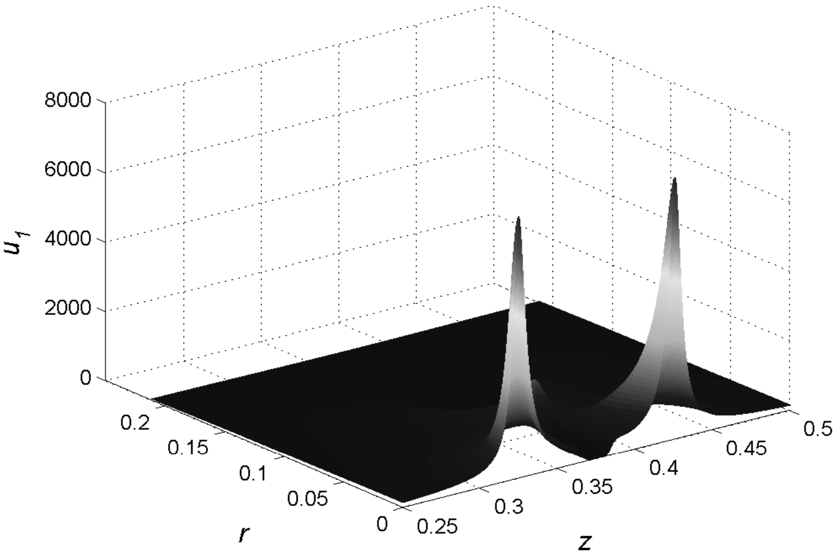

Figure 4.6. The 3D view of u_1 at $t = 0.02$ for the viscous model computed by the adaptive mesh with $N_z = 4096$, $N_r = 400$, $\Delta t = 2.5 \times 10^{-7}$, $\nu = 0.001$.

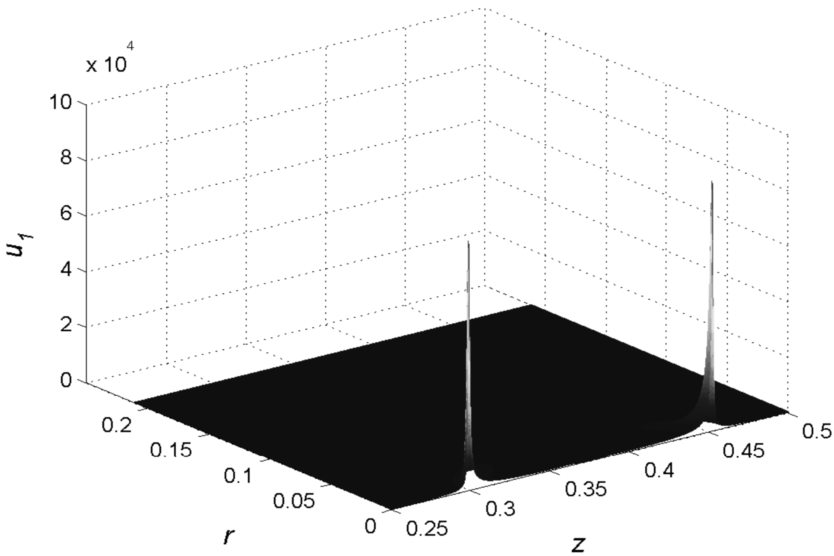

Figure 4.7. The 3D view of u_1 at $t = 0.021$ for the viscous model computed by the adaptive mesh with $N_z = 4096$, $N_r = 400$, $\Delta t = 2.5 \times 10^{-7}$, $\nu = 0.001$.

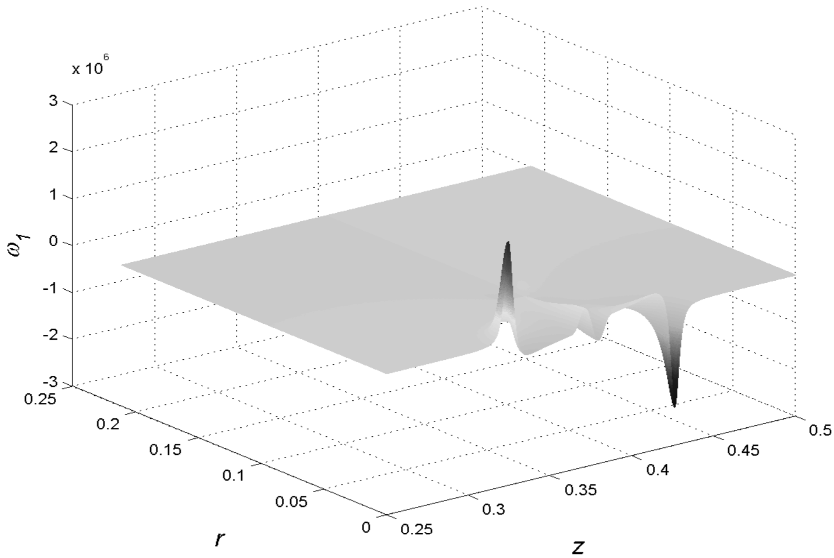

Figure 4.8. The 3D view of ω_1 at $t = 0.02$ for the viscous model computed by the adaptive mesh with $N_z = 4096,\ N_r = 400$, $\Delta t = 2.5 \times 10^{-7}$, $\nu = 0.001$.

To illustrate the nature of the nearly singular solution, we show the 3D view of u_1 as a function of r and z in Figures 4.6 and 4.7. We also show the 3D view of w_1 as a function of r and z in Figure 4.8. While u_1 is symmetric with respect to $z = 0.375$, w_1 is anti-symmetric with respect to $z = 0.375$. We can see that the support of the solution u_1 in the most singular region is isotropic and appears to be locally self-similar (Hou and Lei 2009*b*).

Resolution study

Finally, we perform a resolution study for our computations by comparing the computation obtained by three different resolutions, which are $N_z \times N_r = 2048 \times 256$, $N_z \times N_r = 3072 \times 328$, and $N_z \times N_r = 4096 \times 400$. In Figure 4.9, we plot $\|u_1\|_\infty$ as a function of time using these three resolutions $N_z \times N_r = 2048 \times 256$, $N_z \times N_r = 3072 \times 328$, and $N_z \times N_r = 4096 \times 400$ over the time interval $[0,\ 0.021]$. We can see that while the computation with $N_z = 2048$ under-resolves the solution near the end of the computation, the solution obtained by using $N_z = 3072$ gives an excellent agreement with that obtained by using $N_z = 4096$.

We also compare the solution of u_1 at $r = 0$ using three different resolutions. Using the partial regularity theory for the 3D model, any singularity of our 3D model must lie on the symmetry axis, $r = 0$. Thus it makes

(a)

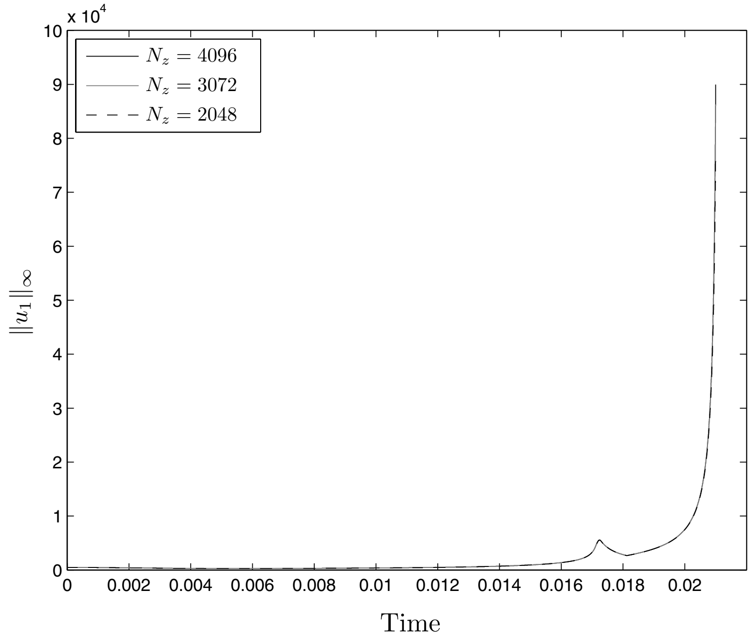

(b)

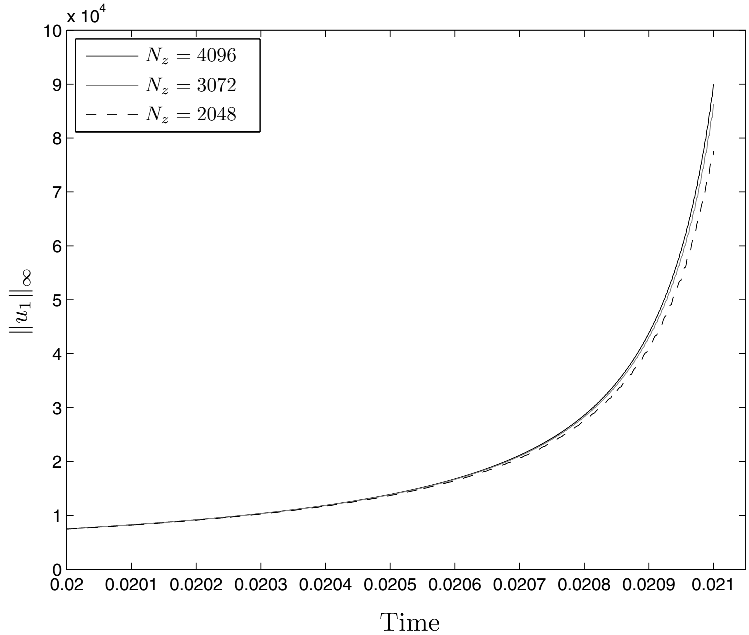

Figure 4.9. Convergence study for $\|u_1\|_\infty$ in time for the viscous model with three resolutions: $N_z \times N_r = 2048 \times 256$, $\Delta t = 5 \times 10^{-7}$ (dashed line), $N_z \times N_r = 3072 \times 328$, $\Delta t = 3.625 \times 10^{-7}$ (grey line), $N_z \times N_r = 4096 \times 400$, $\Delta t = 2.5 \times 10^{-7}$ (solid line). Figure (a) is over the time interval $[0,\ 0.021]$; (b) is a close-up view over the time interval $[0.02,\ 0.021]$; $\nu = 0.001$.

(a)

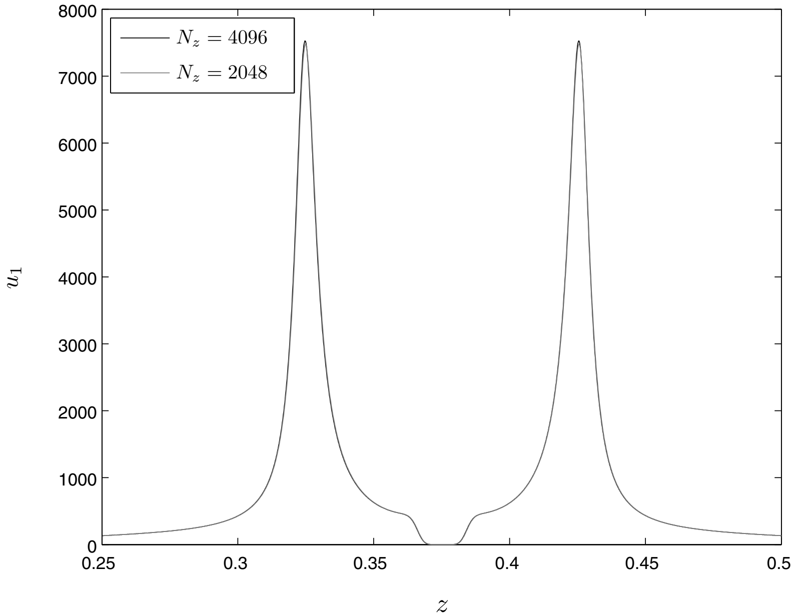

(b)

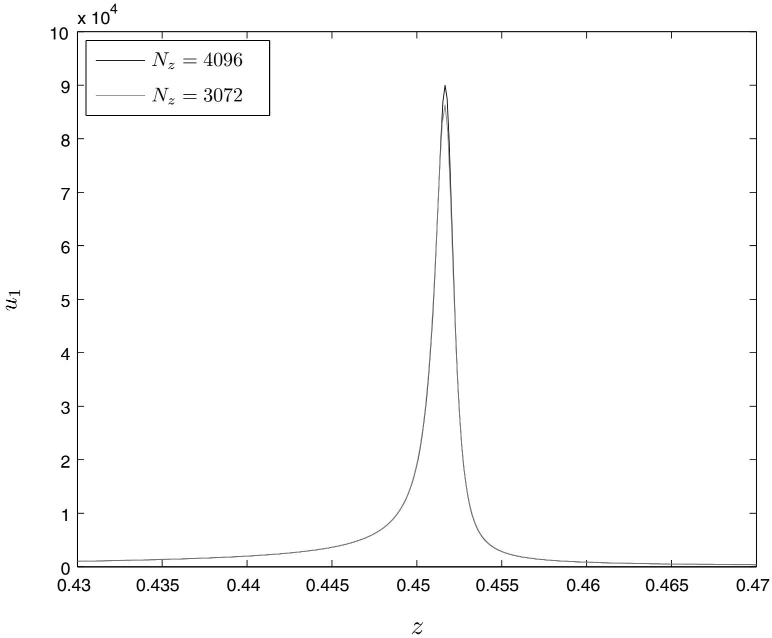

Figure 4.10. Convergence study for u_1 at $r = 0$ and $t = 0.02$ and $t = 0.021$ for the viscous model with different resolutions. Figure (a) is the comparison between $N_z \times N_r = 2048 \times 256$ (solid line) and $N_z \times N_r = 4096 \times 400$ (grey line); (b) is the comparison between $N_z \times N_r = 3072 \times 328$ (solid line) and $N_z \times N_r = 4096 \times 400$ (grey line); $\nu = 0.001$.

sense to perform a resolution study for the solution along the symmetry axis which is the most singular region of the solution. In Figure 4.10(a), we plot the solutions obtained by two resolutions using $N_z \times N_r = 2048 \times 256$ ($\Delta t = 5 \times 10^{-7}$) and $N_z \times N_r = 4096 \times 400$ ($\Delta t = 2.5 \times 10^{-7}$) on top of each other at $t = 0.02$. The two solutions are almost indistinguishable. However, the computation with $N_z \times N_r = 2048 \times 256$ is not sufficient to resolve the nearly singular behaviour of the solution at $t = 0.021$. On the other hand, the computation with $N_z \times N_r = 3072 \times 328$ ($\Delta t = 3.625 \times 10^{-7}$) gives much improved resolution. In Figure 4.10(b) we compare the solution obtained by using $N_z \times N_r = 3072 \times 328$ with that obtained by using $N_z \times N_r = 4096 \times 400$ at $t = 0.021$. We observe that the agreement of the two solutions is very good except near the points where u_1 attains its maximum.

4.5. Mechanism for a finite-time blow-up

To understand the mechanism for the potential blow-up of the viscous model, we plot the solution u_1 on top of $(\psi_1)_z$ along the symmetry axis $r = 0$ at t=0.021 in Figure 4.11. We see that there is a significant overlap between the supports of the maximum of u_1 and of the maximum of $(\psi_1)_z$. Moreover, the solution u_1 has a strong alignment with $(\psi_1)_z$ near the region of maximum of u_1. The local alignment between u_1 and $(\psi_1)_z$ induces a strong nonlinearity on the right-hand side of the u_1-equation, which has the form $2(\psi_1)_z u_1$. This strong alignment between u_1 and $(\psi_1)_z$ is the main mechanism for the potential finite-time blow-up of the 3D model. Similar alignment between u_1 and $(\psi_1)_z$ near the region of maximum u_1 is also observed for the inviscid model (Hou and Lei 2009*b*).

It is interesting to note that the position at which u_1 attains its maximum does not coincide with that at which $(\psi_1)_z$ attains its maximum. In fact, at the point where u_1 reaches its maximum, the value of $(\psi_1)_z$ is relatively small, or even negative. This misalignment between the position at which u_1 attains its maximum and the position at which $(\psi_1)_z$ attains its maximum induces a dynamic motion which pushes the two focusing centres of u_1 to move away from each other. This dynamics reinforces the local alignment between u_1 and $(\psi_1)_z$. We remark that this wave-like behaviour of the solution along the z-direction is consistent with the nonlinear non-local wave equation (4.10) that we derived for $v = \log(u_1^2)$ for the inviscid model.

As we see in the next subsection, the inclusion of the convection term forces the two focusing centres to travel towards each other. Moreover, the local alignment between u_1 and $(\psi_1)_z$ is destroyed. As a result, the solution becomes defocused and smoother along the symmetry axis. There is no evidence that the solution of the full Navier–Stokes equations would develop a finite-time singularity, at least for the time interval considered here.

(a)

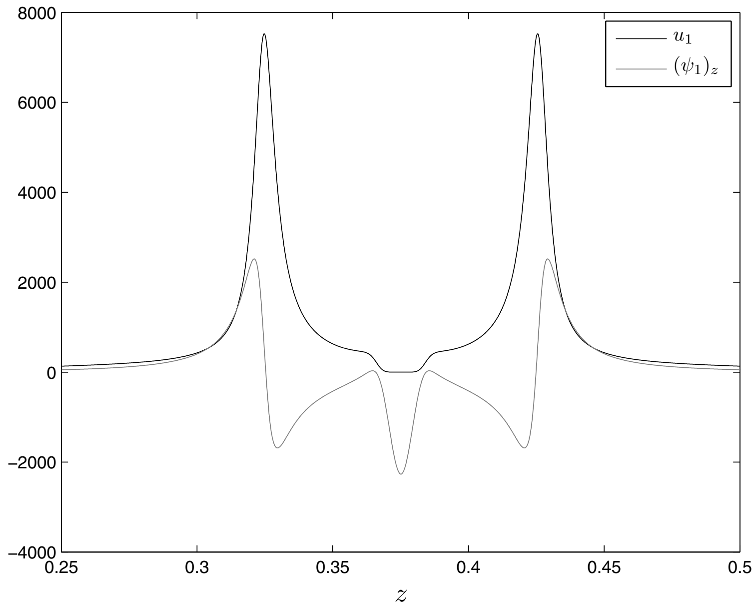

(b)

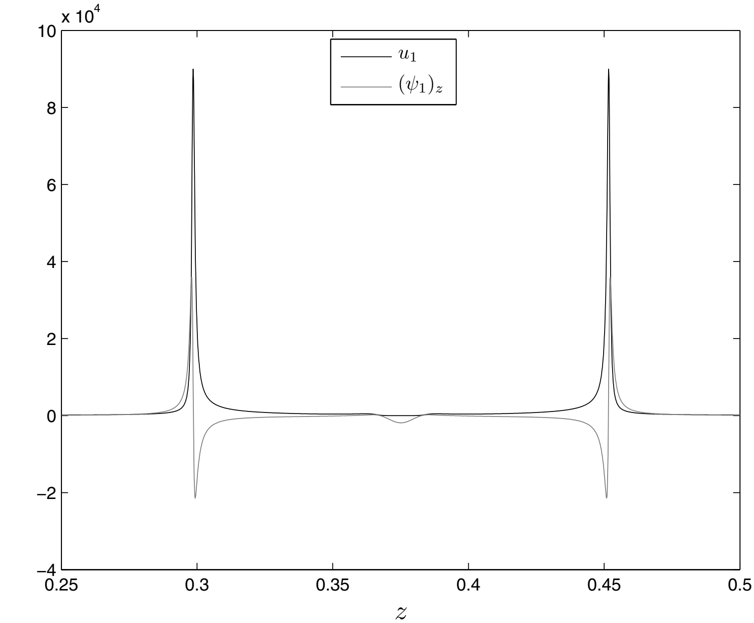

Figure 4.11. u_1 (solid line) versus $(\psi_1)_z$ (grey line) of the viscous model along the symmetry axis $r = 0$. (a) $t = 0.02$; (b) $t = 0.021$. Adaptive mesh computation with $N_z = 4096$, $N_r = 400$, $\Delta t = 2.5 \times 10^{-7}$, $\nu = 0.001$.

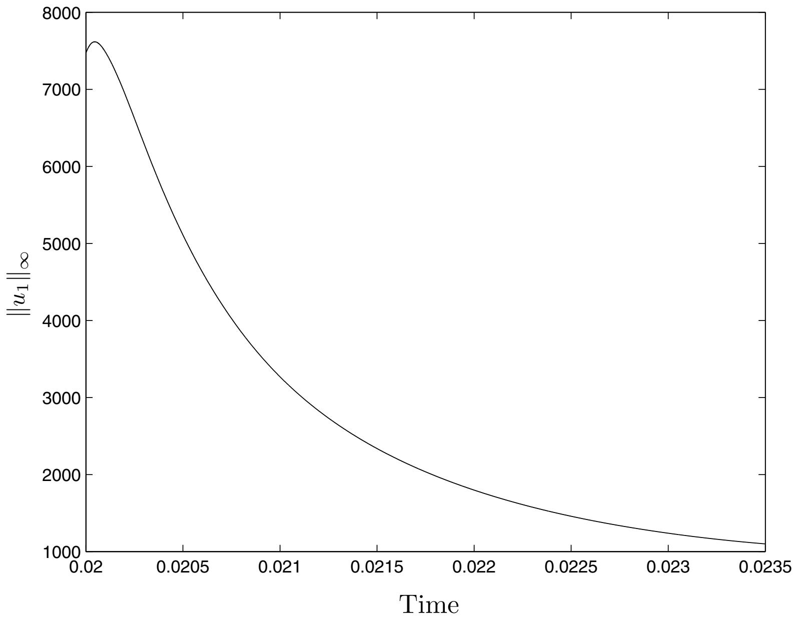

Figure 4.12. $\|u_1\|_\infty$ in time, the full Navier–Stokes computation using the solution of the 3D viscous model at $t = 0.02$ as the initial condition. Adaptive mesh computation with $N_z = 2048$, $N_r = 1024$, $\nu = 0.001$.

4.6. The stabilizing effect of the convection term

In this subsection, we show that by adding back the convection term to the 3D model, which recovers the reformulated Navier–Stokes equations, the solution behaves completely differently. The mechanism for generating the potential finite time singularity for the 3D model is destroyed. Even if we start with the nearly singular solution obtained by the 3D model at $t = 0.02$ and use it as the initial condition for the full Navier–Stokes equations, we observe that the maximum of u_1 soon decreases in time: see Figure 4.12. It is easy to see that the 3D axisymmetric Navier–Stokes equations with swirl cannot develop a finite-time singularity if u_1 is bounded. Thus the fact that $\|u_1\|_\infty$ is decreasing in time is a clear indication that the solution does not develop a finite-time singularity, at least over the time interval considered here.

We also observe that the local alignment between u_1 and $(\psi_1)_z$ near the region of maximum u_1 is destroyed by including the convection term (see Figure 4.13), as is the focusing mechanism. The solution becomes defocused (see Figure 4.14). As time evolves, the two focusing centres approach each other. This process creates a strong internal layer orthogonal to the z-axis

(a)

(b)

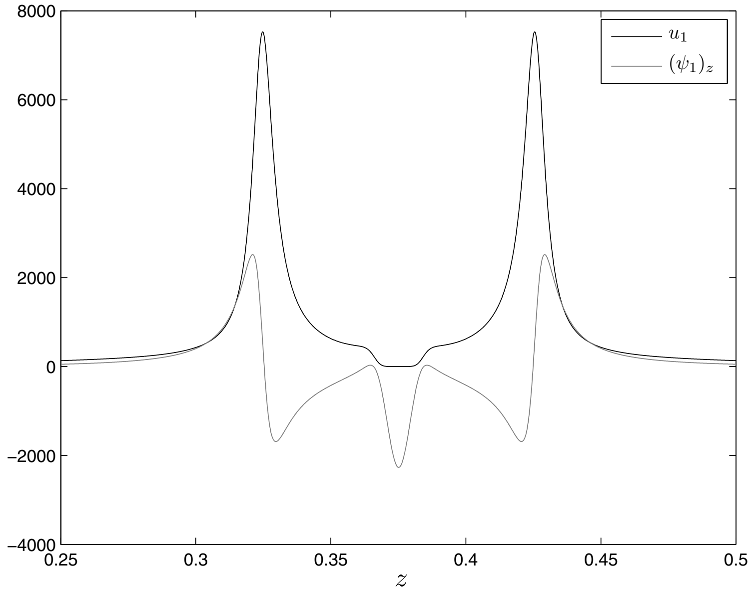

Figure 4.13. u_1 (solid line) versus $(\psi_1)_z$ (grey line) along the symmetry axis $r = 0$. Figure (a) corresponds to $t = 0.02$ (the solution from the 3D viscous model); (b) corresponds to $t = 0.021$ obtained by solving the full Navier–Stokes equations. Adaptive mesh computation with $N_z = 2048$, $N_r = 1024$, $\nu = 0.001$.

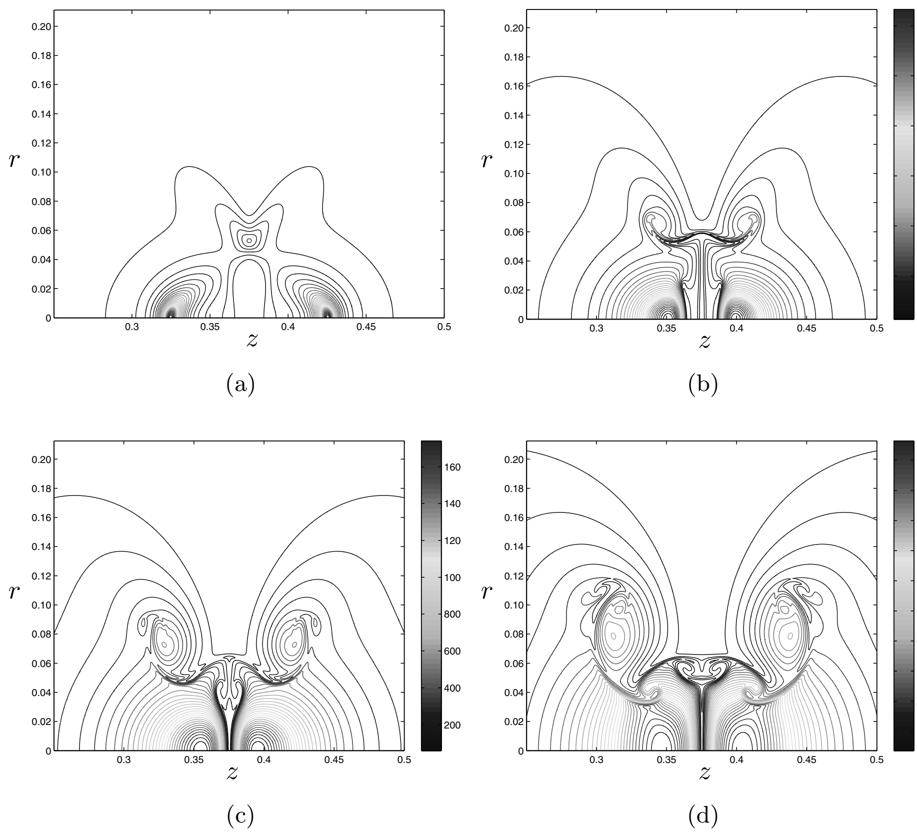

Figure 4.14. (a) The contour of u_1 at $t = 0.02$ obtained from the 3D viscous model which serves as the initial condition for the full Navier–Stokes equations. (b) The contour of u_1 at $t = 0.021$ obtained by solving the full Navier–Stokes equations. (c), (d) The contours of u_1 at $t = 0.022$ and $t = 0.0235$, respectively, by solving the full Navier–Stokes equations. Adaptive mesh computation with $N_z = 2048$, $N_r = 1024$, $\nu = 0.001$.

and forms a jet that moves away from the symmetry axis (the z-axis). The jet further generates some interesting vortex structures. This is illustrated in Figure 4.14. Since the most singular part of the solution of the Navier–Stokes equations moves away from the symmetry axis, we use a higher-resolution adaptive mesh along the r-direction with $N_r = 1024$ to better resolve the layered structure along the r-axis.

By the Caffarelli–Kohn–Nirenberg theory, the singularity of the 3D axisymmetric Navier–Stokes equations, if there is any, must be along the symmetry axis. The fact that the most singular part of the solution moves away from the symmetry axis indicates that the full Navier–Stokes equations will not form a finite-time singularity, at least not for the initial condition we consider here over the time interval for which we compute the solution. On the other hand, the solution of the 3D model with the same initial condition seems to develop a potential finite-time singularity in an earlier time. This confirms that convection plays an essential role in depleting the destabilizing effect induced by vortex stretching.

5. Concluding remarks

Our analysis and computations revealed a subtle dynamic depletion of vortex stretching. Sufficient numerical resolution is essential to capture this dynamic depletion. Our computations for the two antiparallel vortex tubes initial data showed that the velocity is bounded and that the vortex stretching term is bounded by $C\|\omega\|_{L^\infty}\log(\|\omega\|_{L^\infty})$. In Hou and Li (2008*b*), we also repeated the computation of R. Pelz using highly symmetric initial data (Pelz 1997). We found that while Pelz's vortex filament model indeed produces a finite-time self-similar singularity, the solution of the full 3D Euler equation with the same initial data gives only very modest growth dynamically. No evidence of finite-time singularities was found. Pelz's vortex filament computation was inspired by his earlier computation of the 3D Navier–Stokes equations (Boratav and Pelz 1994). However, our computation showed that the rapid growth of vorticity observed by Boratav and Pelz (1994) was due to under-resolution of his numerical solution (Hou and Li 2008*b*). The actual growth of maximum vorticity was only exponential in the time interval when the solution was still well resolved. It is natural to ask if the dynamic depletion that we observed is generic, and to consider the driving mechanism for this depletion of vortex stretching. Some recent progress has been made in analysing the dynamic depletion of vortex stretching and nonlinear stability for 3D axisymmetric flows with swirl (Hou and Li 2008*a*, Hou, Lei and Li 2008). A related study for the 2D quasi-geostrophic model can be also found in Deng, Hou, Li and Yu (2006*b*). The local geometric structure of the solution near the region of maximum vorticity and the anisotropic scaling of the support of maximum vorticity seem to play a key role in the dynamic depletion of vortex stretching.

We also studied the dynamic stability of the 3D Navier–Stokes equations via an exact 1D model. This 1D model is an exact reduction of the 3D Navier–Stokes equations along the symmetry axis for a special class of initial data. It retains some essential nonlinear features of the 3D Navier–Stokes equations. We proved the global regularity of this 1D model by using a pointwise estimate. The key was to show that a positive Lyapunov function satisfies a new maximum principle. Here convection played an essential role in cancelling the destabilizing vortex stretching terms. Using the solution of the 1D model as a building block, we constructed a family of solutions of the 3D Navier–Stokes equations which experience interesting dynamic growth but remain smooth for all times.

To gain further understanding of the stabilizing effect of convection, we constructed a new 3D model by neglecting the convection term from the reformulated Navier–Stokes equations. This 3D model shares almost all properties of the Navier–Stokes equations, including an equivalent energy identity and a partial regularity result. Our numerical results seemed to support the conclusion that the solution of the 3D model develops locally self-similar isotropic singularities. But when we added the convection term back to the 3D model, the mechanism for generating the finite-time singularity in the 3D model was destroyed.

The results presented in this paper may have some important implication to the global regularity of the 3D Navier–Stokes equations. Our studies indicate that a successful strategy in analysing the global regularity of the 3D Navier–Stokes equations need to take advantage of the stabilizing effect of the convection term in an essential way. So far most of the regularity analysis for the 3D Navier–Stokes equations has not used the stabilizing effect of the convection term. In many cases, the same results can also be obtained for our 3D model. We are currently working to prove that the 3D model develops finite-time singularities from smooth initial data with finite energy. Such a theoretical result would show convincingly that traditional energy estimates are inadequate to prove global regularity of the 3D Navier–Stokes equations. New analytical tools that exploit the local geometric structure of the solution and the stabilizing effect of convection would be needed.

We also investigated the performance of pseudo-spectral methods in computing nearly singular solutions of fluid dynamics equations. In particular, we proposed a novel pseudo-spectral method with a high (36th)-order Fourier smoothing which retains a significant portion of the Fourier modes beyond the 2/3 cut-off point. We demonstrated that the pseudo-spectral method with the high-order Fourier smoothing gives a much better performance than the pseudo-spectral method with the 2/3 de-aliasing rule. Moreover, we showed that the high-order Fourier smoothing method captures about $12 \sim 15\%$ more effective Fourier modes in each dimension than the 2/3 de-aliasing method. For the 3D Euler equations, the gain in the effective Fourier codes for the high-order Fourier smoothing method can be as large as 20% over the 2/3 de-aliasing method. Another interesting observation was that the error produced by the high-order Fourier smoothing method is highly localized near the region where the solution is most singular, while the 2/3 de-aliasing method tends to produce oscillations in the entire domain. The high-order Fourier smoothing method was found be very stable dynamically. No high-frequency instability was observed.

Acknowledgements

I would like to thank my collaborators, Drs Jian Deng, Zhen Lei, Congming Li, Ruo Li, and Xinwei Yu, who have contributed significantly to the results presented in this survey paper. We would like to thank Prof. Lin-Bo Zhang from the Institute of Computational Mathematics in Chinese Academy of Sciences (CAS) for providing us with the computing resources to perform this large-scale computational project. Additional computing resources were provided by the Center of High Performance Computing in CAS. We also thank Prof. Robert Kerr for providing us with his Fortran subroutine generating his initial data. This work was in part supported by the NSF under the NSF grant DMS-0713670.

REFERENCES

A. Babin, A. Mahalov and B. Nicolaenko (2001), '3D Navier–Stokes and Euler equations with initial data characterized by uniformly large vorticity', *Indiana Univ. Math. J.* **50**, 1–35.

J. T. Beale, T. Kato and A. Majda (1984), 'Remarks on the breakdown of smooth solutions of the 3-D Euler equations', *Comm. Math. Phys.* **96**, 61–66.

O. N. Boratav and R. B. Pelz (1994), 'Direct numerical simulation of transition to turbulence from a high-symmetry initial condition', *Phys. Fluids* **6**, 2757–2784.

J. P. Boyd (2000), *Chebyshev and Fourier Spectral Methods*, 2nd edn, Dover.

L. Caffarelli, R. Kohn and L. Nirenberg (1982), 'Partial regularity of suitable weak solutions of the Navier–Stokes equations', *Commun. Pure Appl. Math.* **35**, 771–831.

R. Caflisch (1993), 'Singularity formation for complex solutions of the 3D incompressible Euler equations', *Physica D* **67**, 1–18.

C. Cao and E. S. Titi (2007), 'Global well-posedness of the three-dimensional primitive equations of large scale ocean and atmosphere dynamics', *Ann. of Math.* **166**, 245–267.

D. Chae (2006), 'Global regularity of the 2d Boussinesq equation with partial viscous terms', *Adv. Math.* **203**, 497–513.

D. Chae and J. Lee (2002), 'On the regularity of the axisymmetric solutions of the Navier–Stokes equations', *Math. Z.* **239**, 645–671.

C. Chen, R. M. Strain, T. Tsai and H. T. Yau (2008), 'Lower bound on the blow-up rate of the axisymmetric Navier–Stokes equations', *Int. Math. Res. Not.*, article ID rnn016.

C. Chen, R. M. Strain, T. Tsai and H. T. Yau (2009), 'Lower bound on the blow-up rate of the axisymmetric Navier–Stokes equations II', to appear in *Comm. Partial Differential Equations*.

A. Chorin (1982), 'The evolution of a turbulent vortex', *Comm. Math. Phys.* **83**, 517.

A. J. Chorin and J. E. Marsden (1993), *A Mathematical Introduction to Fluid Mechanics*, 3rd edn, Springer.

P. Constantin (1986), 'Note on loss of regularity for solutions of the 3-D incompressible Euler and related equations', *Comm. Math. Phys.* **104**, 311–326.

P. Constantin (1994), 'Geometric statistics in turbulence', *SIAM Review* **36**, 73.

P. Constantin and C. Foias (1988), *Navier–Stokes Equations*, Chicago University Press.

P. Constantin, C. Fefferman and A. Majda (1996), 'Geometric constraints on potentially singular solutions for the 3-D Euler equation', *Comm. Partial Differential Equations* **21**, 559–571.

P. Constantin, P. D. Lax and A. Majda (1985), 'A simple one-dimensional model for the three-dimensional vorticity equations', *Commun. Pure Appl. Math.* **38**, 715–724.

J. Deng, T. Y. Hou and X. Yu (2005), 'Geometric properties and non-blowup of 3-D incompressible Euler flow', *Comm. Partial Differential Equations* **30**, 225–243.

J. Deng, T. Y. Hou and X. Yu (2006*a*), 'Improved geometric conditions for non-blowup of 3D incompressible Euler equation', *Comm. Partial Differential Equations* **31**, 293–306.

J. Deng, T. Y. Hou, R. Li and X. Yu (2006*b*), 'Level set dynamics and the non-blow-up of the quasi-geostrophic equation', *Methods Appl. Anal.* **13**, 157–180.

V. M. Fernandez, N. J. Zabusky and V. M. Gryanik (1995), 'Vortex intensification and collapse of the Lissajous-elliptic ring: Single and multi-filament Biot–Savart simulations and visiometrics', *J. Fluid Mech.* **299**, 289–331.

J. Goodman, T. Y. Hou and E. Tadmor (1994), 'On the stability of the unsmoothed Fourier method for hyperbolic equations', *Numer. Math.* **67**, 93–129.

R. Grauer and T. Sideris (1991), 'Numerical computation of three dimensional incompressible ideal fluids with swirl', *Phys. Rev. Lett.* **67**, 3511.

R. Grauer, C. Marliani and K. Germaschewski (1998), 'Adaptive mesh refinement for singular solutions of the incompressible Euler equations', *Phys. Rev. Lett.* **80**, 19.

T. Y. Hou and Z. Lei (2009*a*), 'On the partial regularity of a 3D model of the Navier–Stokes equations', *Comm. Math. Phys.* **287**, 589–612.

T. Y. Hou and Z. Lei (2009*b*), 'On the stabilizing effect of convection for three dimensional incompressible flows', *Commun. Pure Appl. Math.* **62**, 501–564

T. Y. Hou and C. Li (2005), 'Global well-posedness of the viscous Boussinesq equations', *Discrete Contin. Dyn. Syst.* **12**, 1–12.

T. Y. Hou and C. Li (2008*a*), 'Dynamic stability of the 3D axi-symmetric Navier–Stokes equations with swirl', *Commun. Pure Appl. Math.* **61**, 661–697.

T. Y. Hou and R. Li (2006), 'Dynamic depletion of vortex stretching and non-blowup of the 3-D incompressible Euler equations', *J. Nonlinear Sci.* **16**, 639–664.

T. Y. Hou and R. Li (2007), 'Computing nearly singular solutions using pseudo-spectral methods', *J. Comput. Phys.* **226**, 379–397.

T. Y. Hou and R. Li (2008*b*), 'Blowup or no blowup? The interplay between theory and numerics', *Physica D* **237**, 1937–1944.

T. Y. Hou, Z. Lei and C. Li (2008), 'Global regularity of the 3D axi-symmetric Navier–Stokes equations with anisotropic data', *Comm. Partial Differential Equations* **33**, 1622–1637.

L. Iskauriaza, G. Seregin and V. Sverak (2003), '$L_{3,\infty}$-solutions of Navier–Stokes equations and backward uniqueness', *Uspekhi Mat. Nauk* **58**, 3–44.

R. M. Kerr (1993), 'Evidence for a singularity of the three dimensional, incompressible Euler equations', *Phys. Fluids* **5**, 1725–1746.

R. M. Kerr (2005), 'Velocity and scaling of collapsing Euler vortices', *Phys. Fluids* **17**, 075103–114.

R. M. Kerr and F. Hussain (1989), 'Simulation of vortex reconnection', *Physica D* **37**, 474.

G. Koch, N. Nadirashvili, G. Seregin and V. Sverak (2009), 'Liouville theorems for the Navier–Stokes equations and applications', to appear in *Acta Mathematica.*

H. Kozono and Y. Taniuchi (2000), 'Bilinear estimates in BMO and Navier–Stokes equations', *Math Z.* **235**, 173–194.

O. Ladyzhenskaya (1970), *Mathematical Problems of the Dynamics of Viscous Incompressible Fluids*, Nauka, Moscow.

R. J. LeVeque (1992), *Numerical Method for Conservation Laws*, Birkhäuser.

F. H. Lin (1998), 'A new proof of the Caffarelli–Kohn–Nirenberg theorem', *Commun. Pure Appl. Math.* **51**, 241–257.

J. G. Liu and W. C. Wang (2006), 'Convergence analysis of the energy and helicity preserving scheme for axisymmetric flows', *SIAM J. Numer. Anal.* **44**, 2456–2480.

A. J. Majda and A. L. Bertozzi (2002), *Vorticity and Incompressible Flow*, Cambridge University Press.

R. B. Pelz (1997), 'Locally self-similar, finite-time collapse in a high-symmetry vortex filament model', *Phys. Rev. E* **55**, 1617–1626.

G. Prodi (1959), 'Un teorema di unicità per el equazioni di Navier–Stokes', *Ann. Mat. Pura Appl.* **48**, 173–182.

A. Pumir and E. E. Siggia (1990), 'Collapsing solutions to the 3-D Euler equations', *Phys. Fluids A* **2**, 220–241.

G. Raugel and G. Sell (1993*a*), 'Navier–Stokes equations on thin 3D domains I: Global attractors and global regularity of solutions', *J. Amer. Math. Soc.* **6**, 503–568.

G. Raugel and G. Sell (1993*b*), Navier–Stokes equations on thin 3D domains III: Global and local attractors, in *Turbulence in Fluid Flows: A Dynamical Systems Approach*, Vol. 55 of *IMA Volumes in Mathematics and its Applications*, Springer, pp. 137–163.

G. Raugel and G. Sell (1994), Navier–Stokes equations on thin 3D domains II: Global regularity of spatially periodic solutions, in *Nonlinear Partial Differential Equations and their Applications, Collège de France Seminar*, Vol. XI of *Pitman Research Notes Math, Series 299*, Longman, pp. 205–247.

J. Serrin (1962), 'On the interior regularity of weak solutions of the Navier–Stokes equations', *Arch. Ration. Mech. Anal.* **9**, 187–195.

J. Serrin (1963), The initial value problem for the Navier–Stokes equations, in *Nonlinear Problems* (R. Langer, ed.), University of Wisconsin Press, pp. 69–98.

M. J. Shelley, D. I. Meiron and S. A. Orszag (1993), 'Dynamical aspects of vortex reconnection of perturbed anti-parallel vortex tubes', *J. Fluid Mech.* **246**, 613–652.

M. Struwe (1988), 'On partial regularity results for the Navier–Stokes equations', *Commun. Pure Appl. Math.* **41**, 437–458.

R. Temam (2001), *Navier–Stokes Equations*, AMS, Providence, RI.

Online references

C. Fefferman, Clay Mathematical Institute, Millennium Open Problems:
www.claymath.org/millennium/Navier–Stokes_Equations/